UNIVERSITÀ DEGLI STUDI DI TRIESTE

XXIX CYCLE OF THE DOCTORAL COURSE IN

Scienze della Terra e Meccanica dei Fluidi

A method to characterize statistical extremes in marine biogeochemistry: the case of the Mediterranean chlorophyll

Specific subject area: **GEO/12 Oceanografia e Fisica dell'atmosfera**

Ph.D. student
Valeria Di Biagio

Ph.D. program Coordinator
Prof. Pierpaolo Omari

Thesis Supervisor
Dr. Stefano Salon

Thesis co-Supervisors
Dr. Gianpiero Cossarini
Dr. Cosimo Solidoro

ACADEMIC YEAR 2015/2016

Valeria di Biagio. *A method to characterize the statistical extremes in marine biogeochemistry: the case of the Mediterranean chlorophyll.*
Ph.D. thesis. University of Trieste

EMAIL: vdibiagio@inogs.it

Contents

Introduction

Extreme events have been widely studied in hydrology and atmospheric sciences for several decades (Delaunay [1988], Katz [1999], Luterbacher et al. [2004], Allan and Soden [2008], Tramblay et al. [2014]). The study of the extremes in ocean has been concentrated mainly on the sea level (Zhang and Sheng [2015]), especially in relationship to hydrology (Walsh et al. [2012]), but recently there has been interest also in extreme wave height (Hansom et al. [2014]) and current speed (Green and Stigebrandt [2003]). However, extreme events in properties like sea surface temperature or chlorophyll concentration have received relatively little attention in the past years, despite the related heavy impacts on the **marine ecosystems** functions and services (Crisci et al. [2011], [Hobday et al., 2016]), with cascading effects at larger scales on the biogeochemical cycles.

Considering the carbon cycle as a representative example, it is estimated that the oceans sequester about 30% of the carbon released by the human activities each year ([Le Quéré et al., 2015]), mostly as the result of the biological carbon pump mechanism ([Passow and Carlson, 2012]). Since the process is driven by multiple and concomitant biotic interactions, correlated with the specific ecosystems and involved plankton species, the biological response to extreme conditions and global changes like the mean increasing temperature and the ocean acidification is hard to be predicted ([Legendre et al., 2015]).

Marine biogeochemistry itself is a relatively young science, that tackles the high complexity of the physical and biological interconnections of the marine system and the general scarcity and difficulty of measurements of data over great part of the world oceans, mainly in the deeper layers. Nevertheless, monitoring and modeling the marine ecosystems and how they can be affected by the extreme events is of primary importance to understand the global Earth System dynamics and, possibly, to promote effectual decisions among the policy makers.

The study conducted in this PhD thesis, focused on the **marine biogeochemical extremes**, joins such emerging field of research, potentially in expansion due to the growing interest arising from the global change debate and the related issues of the environmental protection and the sustainable use of the marine resources.

The **approach** of the present work to the biogeochemical extremes is

methodological and the aim is to characterize and classify them in the open-sea, on a basin scale. The method here proposed is applied to the surface chlorophyll as a representative biological variable of the marine ecosystem, in the Mediterranean Sea as the basin of reference. Nevertheless, this case study is used as an example, to highlight the characteristics and the capabilities of the method itself, whose validity is more general. In fact, the same procedure can be applied to other biogeochemical variables (e.g. the nutrients), as well as to the chlorophyll at other depths or integrated over the water column, in the same basin or in others.

It is important to stress that the term "**extreme**" in the present work is used in a **statistical** sense. In fact, the extremes are in the first stage defined as the **values of the biogeochemical variable** under study that are **higher than a reference percentile threshold** ([Gohin et al., 2008], [EEA, 2015]), computed on the time series of data in the fixed point. In regards to the present case study, the chlorophyll extremes here treated are not related to Harmful Algal Blooms (HAB, [Anderson et al., 2002]), or other "red tides" phenomena ([Okaichi, 2004]), that are instead referred to some specific kinds of phytoplankton producing toxins, with oxygen depletion and fish mortality as possible consequences. The concept of chlorophyll extremes in the present work remains statistical by definition, even if some considerations on the impact of the extremes on the ecosystem are made in the specific characterization of these events.

One of the novel issues of the proposed method is the reformulation of the definition of the extremes. The spatial extension of the extremes, that is scarcely treated in literature, is here considered in addition to the temporal feature, that is the one usually considered. In fact, an "extreme event" is identified as a set of points near in space with extremes at the same time (i.e. with chlorophyll values higher than the thresholds). In this way, the previous (local) definition is extended to define spatio-temporal volumes, as **macro-events** of extreme values that cover an extended area for a certain time duration.

Thus, the **metrics** necessary to characterize and classify the biogeochemical extremes, initially introduced at the local stage (as in Hauri et al. [2013], Hobday et al. [2016]), is then further developed to describe the macro-events shape and strenght. The set of scalar indexes referred to the macro-events constitutes a reference for similar statistical studies, also dedicated to evaluate and quantify possible climatological differences between the present state and future scenarios.

As regards the domain of study, the choice of the **Mediterranean Sea** as the example of application area is far from being restrictive, despite it is a marginal sea. In fact, due to the complicated morphology of the Mediterranean region and the cohesistance of various climate types, the Mediterranean Sea is widely considered a laboratory basin for oceanographic, environmental and climatic studies ([Bethoux et al., 1999]). Moreover, it is an hot-spot for the

worldwide marine biodiversity ([Coll et al., 2010]). Lastly, the temperature and salinity properties of the water masses outflowing from the basin to the Atlantic Ocean influence the thermoaline circulation on the global scale. In particular, the effects of the recent trends detected in temperature and salinity (and, potentially, in the biogeochemical variables) on the functioning of the Atlantic Ocean are still under investigation ([Schroeder et al., 2016]).

Considering the specific example of application, i.e. the phytoplankton chlorophyll, literature offers several case studies of intense phytoplankton blooms occurring in coastal areas, e.g. in connection with river floods (Oubelkheir et al. [2014]) and with strong mixing due to rainfalls and cyclones (Maneesha et al. [2011]). Nevertheless, in the present work the extremes are investigated in the **open sea** domain, that is indirectly affected by the coastal dynamics, e.g. the riverine influence.

In general, a systematic study of the extremes statistics (Ghil et al. [2011]) requires long sampling times at high frequency. However, in the present case of investigation on the basin scale, the use of **numerical models** is necessary. Remote sensing observations are in fact limited by the cloud coverage, whereas in situ-mesasurements do not provide the suitable spatial and temporal sampling at the basin scale and can lack in standardization. On the contrary, numerical models provide biogeochemical data with continuity at high frequency in time and space. Moreover, models can account for the vertical processes of mixing and nutrients transport related to the surface chlorophyll, allowing a more complete reconstruction of the dynamics of the extremes. Finally, they can also yield scenario simulations, in a perspective of climate change that affects the occurrence and the severity of extreme events (Field [2012]). Currently, new studies have been dedicated to investigate marine biogeochemical extremes on the regional scale using coupled physical - biogeochemical models to assess the present state of the ecosystems and to make predictions for the future (Hauri et al. [2013]).

To characterize the extreme events in the Mediterranean biogeochemistry, in the present study a **coupled model** composed by an hydrodynamic part, the MIT general circulation model (MITgcm[1]), and a biogeochemical part, the Biogeochemical Flux Model (BFM[2]), simulated the physics and the biogeochemistry of the basin for the period 1979-2012. The same MITgcm configuration has been already used in other simulations of the Mediterranean Sea ([Harzallah et al., 2016],[Llasses et al., 2016]). In this study an overall amount of about 150 thousand core-hours on the Tier-1 system GALILEO and on the BigData infrastucture PICO at Cineca, assigned through three ISCRA C projects ("BIOMEDCO" , "BIOMEDXT" and "BLOMEDXT"), were used to implement the coupling, to run the simulation and to analyze the output data (8 terabyte).

[1] `http://mitgcm.org`

[2] `http://bfm-community.eu/`

The complete description of the coupling of the MITgcm-BFM model used for this study is included in the recently published paper "Development of BFMCOUPLER (v1.0), the coupling scheme that links the MITgcm and BFM models for ocean biogeochemistry simulations" (Cossarini et al. [2017a]). Moreover, preliminary results of this study were presented during 2016, at the 8th International Workshop on Modeling the Ocean (IWMO[3]), obtaining the achievement of the Outstanding Young Scientist Award of the poster session, and at the 41st CIESM Congress[4].

The **content** of the thesis is structured as follows. A general overview of the main physical and biogeochemical features of the Mediterranean ecosystem, focused on the phytoplankton chlorophyll as the case study, is the object of chapt. 1. The components and the coupling of the numerical model are then described, together with its initial and boundary conditions and external forcings in chapt. 2, whereas the corroboration of the coupled model is provided in appendix A. The focus on the extremes of chlorophyll is in chapt. 3, where the method to identify these events is described, starting from the definitions of local and macro extreme events. Then, the macro extreme events are characterized and classified by the set of scalar indexes properly introduced. The overall results obtained applying the proposed method to the model-derived Mediterranean surface chlorophyll are shown in chapt. 4. The following chapt. 5 illustrates some representative macro-events detected in the simulation, reconstructing their main physical and biological dynamics and comparing the results with the available data. The last section provides a general discussion about the proposed method, the main results and the possible future developments of this work.

[3] `https://events.unibo.it/iwmo2016`

[4] `http://ciesm.org/marine/congresses/Kiel.htm`

Chapter 1

Phytoplankton chlorophyll in the Mediterranean ecosystem

The chlorophyll concentration is the main signature of the phytoplankton presence in the oceans and in the other aquatic systems. In order to provide an overview of the fundamental phytoplankton features and dynamics in the Mediterranean Sea, at first in the sec. 1.1 some preliminary definitions related to the ecosystems are given, clarifying some basic concepts and the terminology used in the present study. Then, the general physical and chemical properties of the Mediterranean Sea are illustrated in the sec. 1.2, stressing the processes and the peculiarities that significatively affect the plankton. The mean state of the phytoplankton chlorophyll in the Mediterranean Sea is finally described in the sec. 1.3, together with the primary production.

1.1 The ecosystem structure: general definitions

A first definition of **ecosystem** is formulated in Tansley [1935], where it is identified as the union of two components: the *habitat*, i.e. the set of the physical and inorganic factors that characterize the environment, and the *biome*, i.e. the set of all the organisms present in the ecological unit. The biome is subjected to continuos processes of change, with an evolution depending on both *autogenic factors* (self adaptation) and *allogenic factors* (external events, e.g. the anthropogenic activities).

The ecosystem can be studied with a **biogeochemical approach**, in which the state variables are bulk quantities quantifying the chemical, physical, geological and biological processes, including a multiplicity of transformations cycles of matter and energy. Other approaches, more biologically oriented, are based on species traits and focus on the interactions among organisms that inhabit the ecosystem.

The main process driving the dynamics and functioning of the ecosystem is the channeling of the solar energy in the biogeochemical cycles. Following

the energy cycling terminology borrowed from the language of economics ([Thienemann, 1926]), the autotrophic organisms are called *producers*, since they produce complex organic compounds, where the solar energy is stored in molecules based on carbon, from simple inorganic substances (*primary production*). Altough part of the energy is released in catabolic processes, a significant portion is retained and can be used in turn by the *consumer* organisms that feed on the primary producers.

A hierarchical structure for the energy fluxes and the productivities rates involving the different trophic levels of the aquatic ecosystems is suggested for the first time in Lindeman [1942], as the succession of the rates of incident solar radiation, photosynthetic production by phytoplankton, primary consumption, primary predation and so on. Moreover, *decomposer* organisms constitutes a different class, separated from the consumers, already in Lindeman [1941], where the study of the food cycle outlines a complex structure more similar to a web than a cycle, with the bacteria occupying the central position.

The view of the trophic dynamics characterizing the ecosystem historically shifted from the *food chain*, i.e. a linear structure from relative large phytoplankton species to fishes via the zooplankton, to the *food web*, i.e. a complex structure of multiple interactions among the organisms, that includes also the microbial loop, composed of small phytoplankton, bacteria, protozoa and viruses ([Azam et al., 1983]).

The carbon fixed in photosynthesis is delivered towards larger organisms through the predatory processes, or it can leave the euphotic zone in the form of particulate sinking at a significant rate, or it can be released through a multitude of processes to the pool of Dissolved Organic Carbon (DOC) [Thingstad and Rassoulzadegan, 1999]. This organic material can be in turn, at least partially, re-incorporated in the food web by the microbial loop, or exported from the euphotic zone, by diffusion or transport downwards during downwelling events ([Miquel et al., 1994]).

Marine biogeochemistry does not involve only the energy-carbon dynamics, but also the **cycling of** several **macro-nutrients**, like phosphates, nitrates, silicates, that are compounds necessary for the cellular functioning, growth and duplication. Therefore, the physical processes involving the transport of the macro-nutrients considerably influence the marine ecosystems and they are described in the following sections.

1.2 Physical and chemical framework

The habitat of the Mediterranean Sea ecosystem is here described at first from the point of view of the basin morphology and its general circulation, then highlighting explicitly the specific features that affect the plankton dynamics.

1.2.1 The Mediterranean Sea morphology and circulation

The Mediterranean Sea is a mid-latitude semi-enclosed sea often regarded as a "laboratory basin" for oceanographic studies, due to the variety of oceanic processes exhibited, e.g. thermohaline circulation, deep water formation, water exchange through the straits, upwelling.

The Mediterranean Sea is connected to the Atlantic Ocean through the **Gibraltar Strait** (300 m depth at the shallower point) and to the Black Sea through the Dardanelles Strait (maximum depth equal to 100 m) and the Bosphorus Strait (65 m depth on average). Its surface amounts to 2.5×10^6 km^2 (without the Black Sea) and its mean depth is about 1500m.

The basin is characterized by a rough bathymetry (fig. 1.1) with a narrow continental shelf (<200 m) and a steep continental slope. It is composed of **two sub-basins**, the western and the eastern one, separated by the **Sicily Strait** (430 m depth). The two sub-basins display peculiar bathymetric depressions characterised by great depths: the Algero-Provencal basin (maximum depth of 2900 m) and the Tyrrhenian Sea (3900 m) in the western part and the Ionian abyssal plain (4200 m), the Hellenic trench (5000 m), the Rhodes depression (4200 m) and the Herodotus abyssal plain (3000 m) in the eastern one.

The picture of the **general circulation** is complex, and composed of three predominant and interacting spatial scales: basin scale, sub-basin scale, and mesoscale. Complexity and scales arise from the strong topographic and coastal influences, from the internal dynamical processes and from the multiple driving forces, i.e. wind stress and buoyancy fluxes at the surface due to freshwater and heat fluxes.

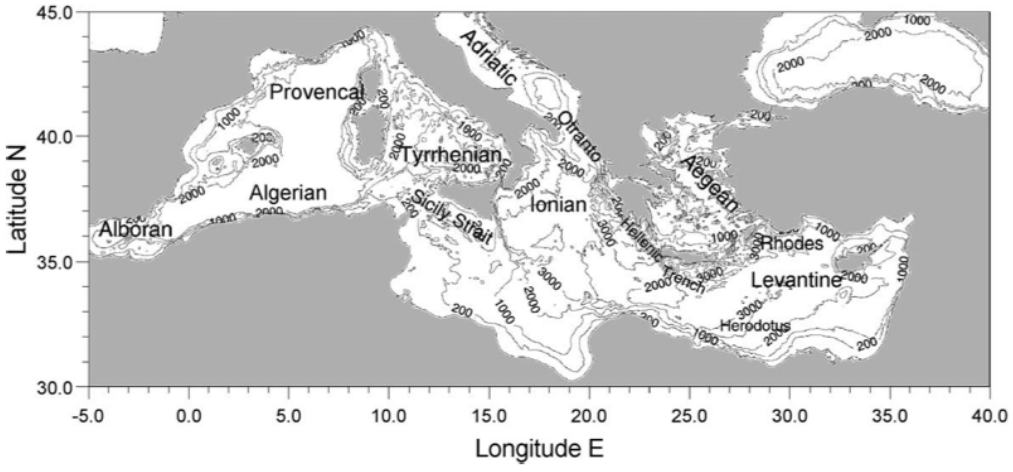

Figure 1.1. Mediterranean Sea geography showing the names of the major sub-regions and the bottom topography, with depth contours indicated in meters (figure taken from Manca et al. [2004]).

The negative heat and fresh water budgets characterizing the Mediterranean Sea, corresponding to a net loss of about 5 W m^{-2} and 0.7 m y^{-1} respectively [Pinardi et al., 2015], are balanced at multidecadal time scales by entering heat and water from the Gibraltar Strait. Following an **inverse estuarine** [Stommel and Farmer, 1953] circulation scheme, the fresher *Atlantic Water* (AW) enters the Mediterranean Sea at surface, in replacement of the evaporated water, while the outflow is composed of a mixture of intermediate and deep waters dwelling in the basin.

As the AW flows eastward, its physical properties rapidly change due to the high evaporation rate, that produces an increase of salinity and gives rise to the *Modified Atlantic Water* (MAW). In the Levantine Sea the MAW becomes even saltier and denser, due to the continental dry winds and a further increase of the evaporation rates, and it sinks down to the intermediate layer (100-500 m), forming the *Levantine Intermediate Water* (LIW) [Lascaratos, 1993]. The LIW then flows across the Strait of Sicily into the western basin and, together with a part of the *Western Mediterranean Deep Water* (WMDW) formed in the Gulf of Lion by deep convection, which occupies the bottom layer, outflows at the Gibraltar Strait ([Stommel et al., 1973], [Gascard and Richez, 1985], [Garcia Lafuente et al., 2007]).

As concerns the vertical structure of the water masses, under the 0-100 m layer characterized by the fresher Modified Atlantic Water (MAW) and the underlying LIW layer, the water masses in the deep layer are distinct between the western and eastern parts of the basin, due to the shallowness of the Gibraltar and the Sicily Strait. In addition to the Gulf of Lion site of **deep water formation** belonging to the western sub-basin, the *Eastern Mediterranean Deep Waters* (EMDW) are formed mainly in the Southern Adriatic Sea. However, other sites for the deep water formation are the Rhodes gyre (Levantine Deep Water, LDW, [Gertmann et al., 1994]) and the Sea of Crete (CDW, [Tsimplis et al., 1999]); in this regard, in the late 1980s and early 1990s the event known as the *Eastern Mediterranean Transient* (EMT, [Roether et al., 1996], [Roether et al., 2007]) showed for the first time the contribution of the Aegean Sea to the Eastern Mediterranean deep waters. The water mass formation rates and variability are dominated by event-like periods where the intermediate and deep waters are formed for 2-3 years at higher rates ([Pinardi et al., 2015]). The largest deep water formation events of the past twenty years occurred separately in the two Mediterranean sub-basins: the first coincided with the EMT and the second with the *Western Mediterranean Transient* (WMT), occurred in the consecutive winters of years 2004-2005 and 2005-2006 ([Smith et al., 2008], [Schroeder et al., 2010], [Schroeder et al., 2016]), when large amounts of anomalously warm, salty and dense deep water masses were produced and successively spread eastward, toward the Tyrrenian Sea, and westward, toward the Atlantic Ocean.

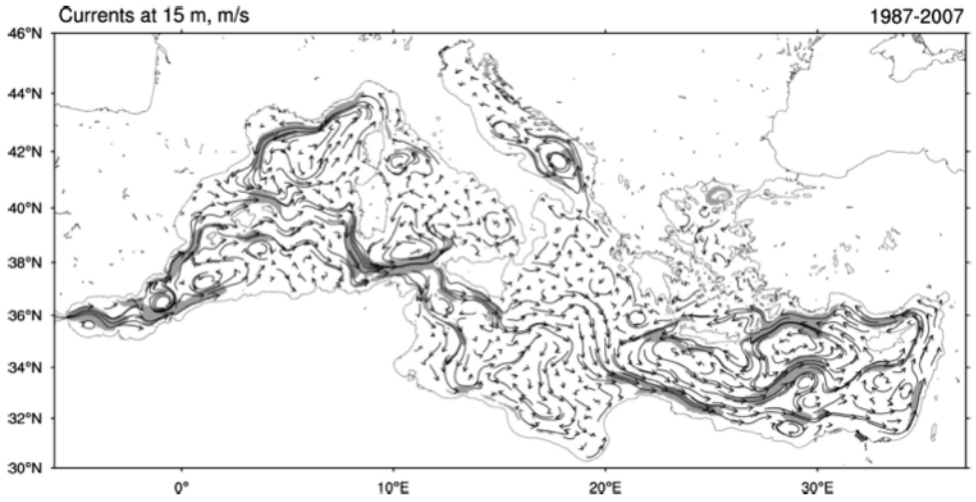

Figure 1.2. The 1987-2007 time-mean circulation at 15 m depth (from reanalysis) with gray areas indicating velocity amplitudes greater than 0.1 m s−1 (figure taken from Pinardi et al. [2015]).

Different **circulation structures** are present in the Mediterranean Sea: free and boundary currents, jets which bifurcate, meander and grow and shed ring vortices, permanent and recurrent sub-basin scale cyclonic and anticyclonic gyres and small but energetic mesoscale eddies (fig. 1.2). Some of these latter, due to this specific persistency in time, may be also called gyres, like the Ierapetra and Pelops gyres [Larnicol et al., 2002]. The large scale basin circulation is generally characterized in the northern regions by cyclonic gyres and in its southern parts by anticyclonic gyres and eddy-dominated flow fields, with the exception of the Tyrrhenian and the northern Ionian Sea. The time-mean Tyrrhenian Sea circulation is dominated by cyclonic gyres of different intensity and intermittency. The northern Ionian Sea upper layer circulation reversed in sign in 1987 (from cyclonic to anticyclonic, as described by data-validated simulations in Pinardi et al. [1997], Korres et al. [2000]), in 1997 (to cyclonic, as shown by altimetry data [Pujol and Larnicol, 2005], [Demirov and Pinardi, 2007]), in 2006 (to anticyclonic, [Gačić et al., 2010], [Bessières et al., 2013]), and for three times in more rapid succession in 2011-2013 [Gačić et al., 2014], according the so called *Northern Ionian reversal phenomenon*. The driving mechanisms behind this reversal are currently under debate and involve variations in the wind stress curl over the basin ([Korres et al., 2000]), the baroclinic dynamics in the Adriatic-Ionian System ([Gačić et al., 2010]) and the baroclinic dynamics driven by thermoaline properties at the eastern boundary of this latter ([Theocharis et al., 2014], [Reale et al., 2016]).

1.2.2 Physical factors affecting the plankton dynamics

Many physical processes and features, related to the morphology and circulation of the Mediterranean Sea illustated in the previous paragraph, affect in different extent the ecosystem biome and, in particular, the phytoplankton.

Starting from the **bathymetry**, the shallowness of the straits separating the two sub-basins generally prevents the mixing of the deep water masses, so that the two deep-sea environments are permanently separated. Aside the topographic depressions of great depths, where nutrient-rich deep-water masses can be stored for long time [Manca et al., 2004], the Mediterranean deep layers are efficiently oxygenated as a consequence of the deep water formation occurring separately in both the two sub-basins ([Hopkins, 1978]).

The dynamics of the marine circulation regulates the horizontal and vertical transport of the biogeochemical variables (e.g. nutrients, plankton). In particular, along the **anti-estuarine circulation** described in sec. 1.2.1, unlike the salinity, the nutrient concentration decreases, so that at the Gibraltar Strait the relatively nutrient-poor AW enters the basin and the nutrient-rich intermediate and deep waters flow out. The total flux of macro-nutrients is negative, with a net export to the Atlantic Ocean estimated equal to 139 and 4.8 Gmol yr$-$1 for nitrate and phosphate, respectively [Huertas et al., 2012]. A similar exchange dynamics is observed at the Sicily Strait and this explains the decreasing trophic activity observed moving eastward across the basin. The net export of the nutrients is compensated for by the **Atmospheric and Terrestrial Inputs (ATIs)**, constituted by atmospheric depositions and rivers discharge, respectively [Ribera d'Alcalà et al., 2003].

Along the vertical direction, a lot of processes contribute to modify the biogeochemical water properties. According to the classical theory of the phytoplankton spring bloom [Mann and Lazier, 2006], the winter wind-driven turbulence and the water cooling break down the summer **stratification** of the water column, allowing the **vertical mixing** and replenishing the surface waters of nutrients coming from the deeper layers; in spring, after the thinning of the mixed layer and the increase of the available sunlight, the phytoplankton perform the photosynthesis in the euphotic zone, whose depth depends on the water turbidity. In addition to the bloom signature, high values of chlorophyll are associated to the Deep Chlorophyll Maximum (DCM) feature, typical of the vertical stratified water columns (see sec. 1.3).

In the Mediterranean Sea the spring bloom process is recognizable only in some regions (e.g. North Western Mediterranean, as illustrated more in detail in sec. 1.3), whereas in other areas the differences between the mixing and the stratification periods are less evident (e.g. Levantine Sea), also in light of other processes superimposed to the general mechanism.

Among them, the presence of **cyclonic and anticyclonic dynamics** contribute to reduce (increase) the stratification and facilitate (prevent) the mixing. In particular, the Gulf of Lion Gyre, the South Adriatic Gyre and the

Rhodes Gyre, associated with strong convective events during winter, show a major vertical transport of nutrients and higher values of biomass detected with respect to the surrounding areas [Siokou-Frangou et al., 2010].

Also the **coastal upwelling** produce a rise of deep waters, rich of nutrients, and consequently an increase of the productivity in the area interessed, e.g. in the southern coast of Sicily ([Bonanno et al., 2014]). However, the nutrient concentrations found in these Mediterranean areas are generally lower than those found in other upwelling systems, maybe due to the very short duration of the upwelling events and to the low concentration of nutrients in the subsurface waters [Siokou-Frangou et al., 2010].

Moreover, other mesoscale and submesoscale processes, like active **frontal regions** (e.g. the North Balearic-Catalan Front, [Estrada et al., 1999]) or sites of formation of **energetic filaments**, due to the strong input of potential vorticity induced by coastal topography and wind stress ([Bignami et al., 2008]), can substantially modify the spatio-temporal distribution of the biogeochemical variables, creating physical boundaries between water masses and modulating the seasonal evolution, e.g. through sporadic events (as in Efrati et al. [2013]).

Finally, among the main events related to the decadal **variability of the Mediterranean circulation**, the EMT and the Northern Ionian reversal, causing changes in the physical and biogeochemical properties of the seawater flowing in the different areas of the basin, had great impact on the Mediterranean ecosystems and their biodiversity, e.g. revealed by variations in the species abundance and by the presence of allochtonous organisms in the Adriatic Sea of either Atlantic/Western Mediterranean or Levantine/tropical origin ([Conversi et al., 2009], [Civitarese et al., 2010]). Moreover, strong modifications in the abyssal ecosystems and even in the carbon cycle are expected as consequences of the more recent WMT ([Schroeder et al., 2016]). Correct simulations of these climate shifts in the physics and biogeochemistry of the Mediterranean Sea represent currently a challenge for the climate modeling community ([Schroeder et al., 2016]).

1.2.3 Nutrients distribution

Among the chemical features of the Mediterranean Sea, the distribution of nutrients, necessary for the functioning and the growth of the organisms, is one of the main factors influencing the plankton dynamics.

The molar ratios between the nutrient concentrations, i.e. in the stocks, deviate in many areas of the Mediterranean Sea from the Redfield values [Redfield, 1934] defined as C:Si:N:P equal to 106:16:15:1, considered a general characteristic of intermediate waters. In particular, moving eastward, the **N:P** ratio increases from the values 20-24 in the Western Mediterranean Sea ([Bethoux et al., 1998], [Segura-Noguera et al., 2016], [Lazzari et al., 2016]) to 24-36 in the Eastern Mediterrenean Sea ([Civitarese et al., 1998],[Kress and Herut, 2001], [Lazzari et al., 2016] among others). These high ratios are still

difficult to explain and have been the object of different hypotheses ([Krom et al., 1991],[Krom et al., 2010], [Van Cappellen et al., 2014].

The external inputs of nitrates and phosphates by the **ATIs** generally display anomalous high N:P ratios with respect to the Redfieldian one and are considered the natural candidates to explain the high values of molar ratios in the stocks (together with negligible denitrification, in the eastern sub-basin). Markaki et al. [2010] estimates an eastward increasing gradient in the N:P ratio associated to the atmospheric deposition, from 20-24:1 in the western sub-basin to 28:1 in the eastern one, including also the organic form. Also the river loads exhibit N:P ratios higher than Redfield values, especially after the reduction of the phosphorus utilization in land (started from the 1980s). The most of the Mediterranean rivers have limited shelves, so that they transfer the nutrient loads directly in the open sea, and overall the major contributions come from the Po river in the Northern Adriatic Sea and the Rhone in the Gulf of Lion ([Ludwig et al., 2009]).

In the surface layer, the main patterns observed in the Mediterranean Sea are an east-west gradient for the phosphate and a north-south gradient for nitrate ([Lazzari et al., 2016]).

Also the **Si:N** ratio displays a decreasing west-east gradient across the Mediterranean Sea, with values lower than 1.0 in the western sub-basin and higher than 1.3 in the eastern one, suggesting an important role of the diatoms (composed by silica in their frustule cell wall) in the vertical export of matter [Ribera d'Alcalà et al., 2003]; however, balancing the silicon budget in the Mediterranean Sea with the currently available data is still an open issue.

The phytoplankton growth in the Mediterranean Sea is usually **nutrient limited**, with the limitation mainly due to the lack of phosphate, except in the Alboran Sea, where the nitrogen limitation is important [Lazzari et al., 2016]. Moreover, the depth of the nutricline (defined as the layer in which the concentration of nutrients increase sharply) displays a zonal gradient across the Mediterranean Sea, with higher values in the eastern sub-basin, making the winter raise of nutrients more efficient in the western sub-basin than in the eastern one [Lazzari et al., 2012].

Atmosphere and rivers make also contribution of **carbon**, whose total amounts are estimated equal to about 0.35×10^{12} mol y^{-1} ([Markaki et al., 2010]) and 0.8×10^{12} mol y^{-1} ([Ludwig et al., 1996]), respectively. Moreover, the net input of dissolved organic carbon from the Atlantic Ocean through the Gibraltar Strait is estimated approximately equal to 0.3×10^{12} mol y^{-1} ([Dafner et al., 2001a]), whereas the one from the Black Sea is considered negligible ([Siokou-Frangou et al., 2010]). Therefore, the global external input of carbon in the Mediterranean Sea is estimated at about $1.5\times10^{1}2$ mol y^{-1}.

1.3 Mediterranean chlorophyll and primary production

The Mediterranean Sea is not only a fertile ground for oceanographic studies, but also an hot spot for the marine biodiversity. About 17000 species of marine organisms were estimated for the Mediterranean Sea [Coll et al., 2010], corresponding to about the 7% of the worldwide marine species, according to the World Register of Marine Species (WoRMS, `http://www.marinespecies.org`). Considering that the volume of the Mediterranean Sea is only about the 0.32% of the worldwide ocean volume, this amount is outstanding and can be explained by the long tradition of biological reports, its multifaceted geological history and the variety of climatic and hydrologic conditions affecting the basin ([Bianchi and Morri, 2000]). In the plankton group, the Mediterranean Sea biome is largely dominated by small autotrophs, microeterotrophs and egg-carrying copepod species [Siokou-Frangou et al., 2010]. Phytoplankton and zooplankton, in turn, show great diversity and variability in the basin, mainly comparing the western and the eastern sub-basins and looking at the areas of deep convection, fronts and gyres. In these latter, in particular, there are evidences that the intermittent supply of nutrients leads to an alternation of communities dominated by diatoms and small-sized microbial ones.

Focusing on the phytoplankton, that is at the base of the marine food web, the **chlorophyll concentration** is considered the proxy variable for its biomass. The status of the Mediterranean chlorophyll has been monitored in the last decades using remote sensing and in situ measurements, e.g. at fixed stations (like the DYFAMED, in the Ligurian Sea [Marty and Chiavérini, 2010]), and in several cruises. Currently, the monitoring and forecasting of the marine biogeochemical variables, in addition to the physical ones, is provided as a service by globally integrated European programs (e.g. Copernicus, `http://copernicus.eu/main/marine-monitoring`).

In the last decades, starting from the Longhurst classification of the Mediterranean Sea as a single bio-province ([Longhurst, 1998]), subsequent analyses have highlighted a more complex scenario, with noticeable differences among the sub-domains and multiple regimes.

In fact, the horizontal variability of the surface chlorophyll exhibits eastward and southward decreasing **gradients** (excluding the relatively higher values detected along the Algerian coast) in both the two sub-basins, well documented by in situ measurements ([Ignatiades et al., 2009]), satellite data ([Bosc et al., 2004]) and decadal simulations of coupled models ([Lazzari et al., 2012]). Moreover, despite high chlorophyll values are detected rarely in the most part of the basin, there are some exceptions: large **blooms** are identified in the Liguro-Provencal Sea, in the Alboran Sea and near the coasts, especially in proximity of the river mouths. As outlined in the sec. 1.2.2, the main drivers for these kinds of phytoplankton blooms are identified by the wind-induced deep convection, the mesoscale dynamics and the riverine supply of nutrients,

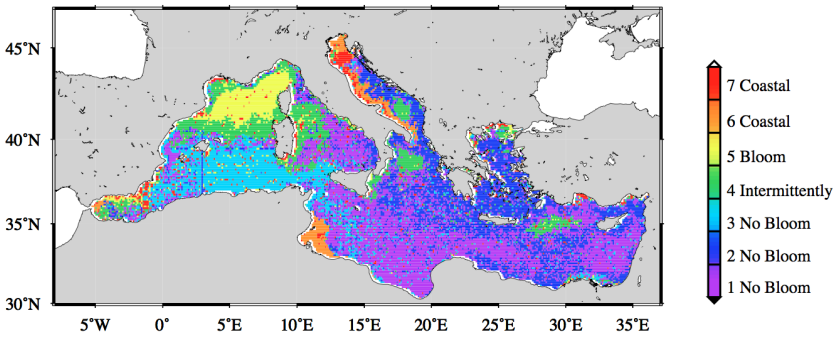

Figure 1.3. Spatial distribution of the Mediterranean trophic regimes (figure taken from D'Ortenzio and Ribera D'Alcalà [2009]).

respectively. In particular, in the Gulf of Lion area the signature of deep convection events occurring in the late winter period is represented by the so-called *blue holes* detected by remote sensing ([Barale, 2003]), i.e. a pattern of very low winter values of surface chlorophyll located in the deep water formation area. This lack of chlorophyll is ascribed to the light limitation due to the vertical displacement, before the restoration of the stratification ([Morel and André, 1991]). The years in which this feature is more pronounced are associated to subsequent massive spring blooms ([Barale et al., 2008]).

The overall Mediterranean chlorophyll variability has to be ascribed in the greatest part to the **seasonal cycle**, that represent about the 80% of the total variance ([Colella et al., 2016]). From a phenologic point of view, starting from satellite data, D'Ortenzio and Ribera D'Alcalà [2009] identified four principal trophic regimes in the Mediterranean Sea: blooming, non-blooming, intemittent and coastal (fig. 1.3). The blooming regime, located in the North Western Mediterranean Sea, is characterized by a sharp peak of chlorophyll in the late winter-early spring. The seasonal signal of the coastal one, mainly in the Northern and Western Adriatic Sea and in the Gulf of Gabes, instead displays the maximum values in late summer-early autumn. Most part of the basin follows a non-blooming regime, with a bimodal dynamics, with quite uniform values in fall-winter (higher) and late spring-summer (lower). Lastly, the intermittent blooming case is related to the South Adriatic Sea, North Ionian Sea, the Rhodes Gyre area, the Western Tyrrenian Sea and some regions at the boundaries of the North Western Mediterranean Sea and of the Alboran Sea. This regime presents a maximum of chlorophyll in the February-March months and a significant rise in October, but with differences between maxima and minima smaller than the ones of the blooming one. It is considered as the result of a typical autumnal bloom of temperate regions followed by vertical transport associated to cyclonic or mesoscale dynamics. Furthermore, the interannual variability of these regimes ([Mayot et al., 2016]) was referred to a correspondent variability in the forcing factors: the deep convection events, frontal dynamics, exchanges with the Atlantic Ocean and the Black Sea and

the river run-off.

Superimposed to the seasonal cycle, positive and negative **trends** in the chlorophyll values were estimated for different Mediterranean sub-regions on a decadal scale ([Colella et al., 2016]). In particular, positive trends were recognized around the Balearic Islands, in the Ligurian-Provencal basin, in the Rhodes Gyre, and off the Nile River delta. Negative trends were instead detected in the North Adriatic Sea (ascribed to a decrease in the Po River runoff since 2003), off the Rhone River mouth and in the North Western Aegean Sea.

Finally, considering in situ measurements of the vertical profiles of chlorophyll, two main kinds of dynamics can be identified ([Lavigne et al., 2015]): a typical midlatitude dynamics (i.e. in the North Western Mediterranean Sea, in agreement with D'Ortenzio and Ribera D'Alcalà [2009]), showing high surface chlorophyll profiles in March and April, and a subtropical dynamics (most of the remaining basin) characterized by a permanent **Deep Chlorophyll Maximum** (DCM) from spring to autumn superimposed to a large variety of vertical shapes during the winter. Moreover, the depth of the DCM is subject to a general eastward deepening (from about 50 m of depth in the Alboran Sea to the 100 m of the Levantine Sea, as in Crise et al. [1999]), with an high seasonal variability, especially in the Ionian and in the Levantine Sea.

In addition, the Mediterranean Sea is globally considered an *oligotrophic* sea, i.e. its **integrated net primary production** is lower than 100 $gC \cdot m^{-2} \cdot y^{-1}$). However, the estimated primary production presents a considerable heterogeneity, reflecting some spatial features of the chlorophyll distribution across the basin. Overall, the integrated net primary production from in situ data for the whole Mediterranean Sea was estimated about equal to 80-90 $gC \cdot m^{-2} \cdot y^{-1}$, with values larger in the western sub-basin with respect to the eastern one. Estimations from satellite data confirm this general pattern, but with generally higher values ([Colella, 2007], [Bosc et al., 2004]). The zonal gradient in the primary productivity was directly detected also by the early-summer MINOR cruise ([Moutin and Raimbault, 2002]) and confirmed in other studies referred to spring data. Single sub-regions, i.e. the Alboran Sea and the North Western Mediterranean Sea, displaying values above 100 $gC \cdot m^{-2} \cdot y^{-1}$, are consequently classified as *mesotrophic*.

More details about available in situ measurements, satellite and model mean results are included in tab. A.2 in appendix, as a reference for the corroboration of the model implemented for this study. However, the integrated net primary production is also characterized by high intra-annual varibilities, especially in very dynamic areas like the Alboran Sea ([Macías et al., 2009]) and also by important inter-annual variabilities, related to the mixed layer depth dynamics ([Estrada, 1996]). In connection to this, the contribution of the subsurface and deep chlorophyll maxima to the production is substantial ([Lazzari et al., 2012]) and estimated equal up to the 30% of the total production ([Estrada et al., 1985]).

Chapter 2

The MITgcm-BFM coupled model

The use of a numerical model is a necessary requirement to study the extreme events in the marine biogeochemistry over a selected basin area. In fact, only a numerical model can provide data at high frequency in space and time with continuity in the investigated domain.

Moreover, as emerged from the previous chapter, physics and biology are strictly connected on the vertical direction. Several physical mechanisms can lead to vertical velocity and mixing able to bring the nutrients from the bottom layers, where they are abundant, toward the euphotic zone, making them available for the photosynthesis and reoxygenating the deeper layers. Therefore, in this study a 3D hydrodynamic-biogeochemical model was implemented to describe accurately these processes, that are at the basis of the dynamics of the ecosystem and also of the extremes of its biogeochemical variables.

In particular, as widely observed, the peaks in the signals of the phytoplankton chlorophyll develop in very few days. Over a multi-decadal time scale, the investigation of chlorophyll extremes would call for an output frequency of the order of 1 day for both the physical and the biological variables. On the other hand, the use of an online coupling allows to retain higher frequencies of the physics in the computation of the biogeochemical reactions. It is noteworthy to specify that feedbacks of the biology on the physics (on a local scale, e.g. the variation of the sea temperature due to the shading of phytplankton) are neglected.

In this chapter the physical (MITgcm) and biogeochemical (BFM) components of the coupled model are described in sec. 2.1 and 2.2, respectively. The coupling procedure is then illustrated in sec. 2.3, with initial conditions, boundary conditions and biogeochemical forcings presented in sec. 2.4. Finally, although the corroboration of the coupled model is in appendix A, in the last section the overall model performances are briefly discussed.

2.1 The MITgcm model

The MITgcm, the general circulation model developed by the Massachusetts Institute of Technology (`https://mitgcm.org/`), is a numerical model that solves the Navier-Stokes equations on the sphere for complex geometries.

The code, written in FORTRAN 77, is designed to simulate both the atmosphere and the ocean. MITgcm can be used in hydrostatic, quasi-hydrostatic or non hydrostatic configuration and with different physical parametrizations, so it is suitable to study fluid phenomena on wide spatial scales. The spatial discretization is realized using the finite volumes methods, applied to an Arakawa-C grid with partially filled cells, for a better representation of the topography.

In the present study, the hydrostatic form of the semi-compressible Boussinesq approximation for the equations of the ocean motion is used:

$$\frac{D\vec{\mathbf{v}}_h}{Dt} + f\hat{\mathbf{k}} \times \vec{\mathbf{v}}_h + \frac{1}{\rho_c}\nabla_h p' = \vec{\mathbf{F}}_h \tag{2.1}$$

$$\frac{g\rho'}{\rho_c} + \frac{1}{\rho_c}\frac{\partial p'}{\partial z} = 0 \tag{2.2}$$

$$\nabla_h \cdot \vec{\mathbf{v}}_h + \frac{\partial w}{\partial z} = 0 \tag{2.3}$$

$$\rho' = \rho(T, S, p_0(z)) - \rho_c \tag{2.4}$$

$$\frac{DT}{Dt} = \mathcal{Q}_T \tag{2.5}$$

$$\frac{DS}{Dt} = \mathcal{Q}_S \tag{2.6}$$

$$\tag{2.7}$$

where $\vec{\mathbf{v}}_h = (u, v, 0)$ is the horizontal velocity, w is the vertical velocity, f is the Coriolis parameter, ρ_c is a constant reference density, p' is the pressure term, T is the potential temperature and S the salinity. The right hand side terms $\vec{\mathbf{F}}_h$, Q_T and Q_S correspond to forcing and dissipation terms, including the diffusion.

The chosen configuration employs an horizontal curvilinear grid with a resolution of 1/12° in both zonal and meridional directions, 75 not equally spaced vertical levels and it is forced by the external 3-hour fields downscaled from the ERA-Interim reanalysis (`https://www.medcordex.eu/`) for the period 1979-2012 on the Mediterranean region, entering in the model as heat and freshwater fluxes, wind stress and runoff, managed by the external forcing (EXF) package of the MITgcm. The timestep of the model is equal to 150 seconds.

2.2 The BFM model

The BFM model [Vichi et al., 2015], developed by a consortium of scientific institutes (`http://bfm-community.eu/`), is a numerical model that simulates the dynamics of the major biogeochemical properties of the marine ecosystems. This model includes the cycles of nitrogen, phosphorus, silica, carbon, and oxygen in the water dissolved phase, in the plankton and in the detritus compartment. The plankton dynamics is parameterized by considering the plankton functional groups of the producers (phytoplankton), consumers (zooplankton), and decomposers (bacteria). The functional classifications are further partitioned into functional subgroups to create a planktonic food web, as depicted in fig. 2.1.

The code, written in FORTRAN 90, solves a set of ordinary differential equations describing the time rate of change of all the components of the biogeochemical variables included in the model, expressed as concentrations C. The chlorophyll variable used in the next chapters is the model-derived quantity obtained as the sum of the chlorophyll component of the four subgroups (i.e. picophytoplankton, flagellates, diatoms, large phytoplankton) belonging to the phytoplankton functional group (green box in the fig. 2.1). The four phytoplankton subgroups are analysed separately in the examples illustrated in chapt. 5.

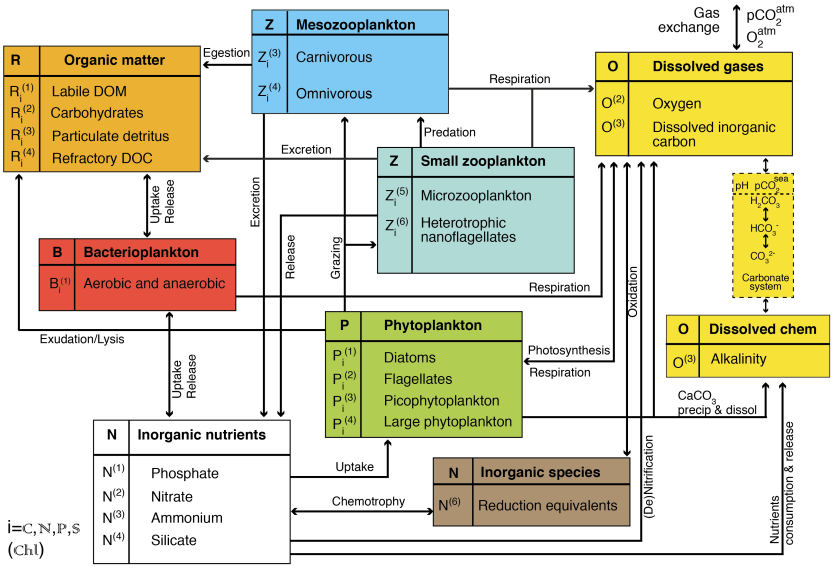

Figure 2.1. BFM model scheme, with functional groups, connected by nutrients and mass flows, and boundary fluxes with other external components.

2.3 The coupling

Through the coupling procedure, the evolution of the physical variables describing the ocean dynamics, together with various external forcings (solar radiation, nutrient discharge by rivers etc.) influences directly the evolution of plankton organisms, oxygen and nutrient concentrations.

The coupled model solves three kind of equations, that govern the physical dynamics of the sea, the transport of the tracers and the relationship among the biogeochemical variables. Since in this study no feedback is foreseen from the biogeochemical part to the hydrodynamic one, the integration of the hydrodynamic properties $(\vec{u}, S, T)$ is decoupled from the one of the biogeochemical tracer concentrations $(C_i, i = 1, 2, ...51)$.

The total rate of change of the $i-th$ tracer concentration is in turn divided in two contributions:

$$\frac{DC_i}{dt} = \left(\frac{DC_i}{dt}\right)_{TRP} + \left(\frac{DC_i}{dt}\right)_{BIO} , \tag{2.8}$$

due to the transport processes and to biogeochemical reactions, respectively. The previous equation can be rewritten as:

$$\begin{aligned} \frac{\partial C_i}{\partial t} = -\vec{\mathbf{v}} \cdot \nabla C_i + \nabla_h (K_h \nabla_h C_i) + \frac{\partial}{\partial z}\left(K_v \frac{\partial C_i}{\partial z}\right) + \\ + w_{BIO} \frac{\partial C_i}{\partial z} + \mathbf{R}(T, S, \rho, PAR, \mathbf{C}) \end{aligned} \tag{2.9}$$

where the term of transport is explicitly expressed as advection (first addend on the right hand side) and horizontal and vertical diffusion (second and third addend, respectively), whereas the biogeochemical term as possible sinking process affecting the tracer (fourth addend, present only for phytoplankton and detritus) and reactions involving different tracers (fifth addend). In the equation, $\vec{\mathbf{v}}$ is the 3D velocity, K_h and K_v the horizontal and vertical diffusivities, respectively, w_{BIO} the vertical sinking velocity, PAR the Photosintetically Active Radiation and $\mathbf{C}$ the set of the biogeochemical concentrations.

The transport terms are computed within the MITgcm by a native package (PTRACER), whereas the biogeochemical reactions are computed by the BFM model. The coupling between MITgcm and BFM allows to solve the eq. 2.9, managing efficiently the shared memory and the flow of information among the different components. Practically, it is achieved ([Cossarini et al., 2017a])) upgrading the package of the MITgcm for the geochemistry (GCHEM), in which the total derivative of the tracers is stored, and inserting the additional package **BFMCOUPLER**, that handles the memory and the core routines of the BFM (see fig 2.2). In fact, the BFM is called by the MITgcm as an external library. The total derivative of the tracer concentration defined in the eq. (2.8) is then integrated in time within the MITgcm code, according to a

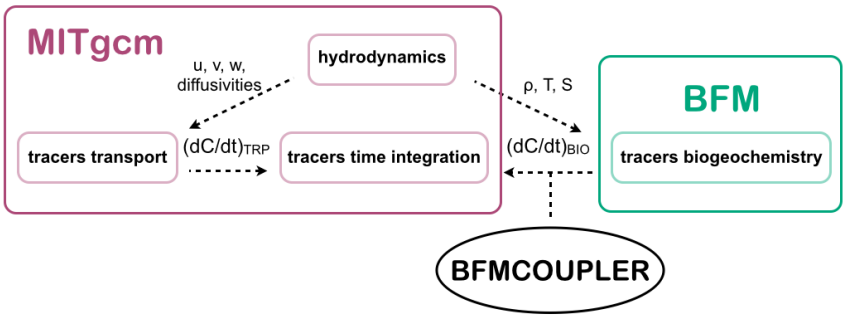

Figure 2.2. Scheme of the coupled MITgcm-BFM model, with the main variables exchanged by the components. The transport contribution to the biogeochemical tracers derivatives is computed using the velocities and diffusivities coming from the hydrodynamic core. The reaction term is insted computed within the BFM model, accounting for salinity, temperature and density, and then passed back to the MITgcm by the BFMcoupler.

direct integration scheme:

$$C_i^{n+1} = C_i^n + \left[\left(\frac{DC_i}{dt} \right)_{TRP}^n + \left(\frac{DC_i}{dt} \right)_{BIO}^n \right] \Delta t \ . \tag{2.10}$$

The BFMCOUPLER accounts also for the sinking of detritus and phytoplankton (fourth term of eq. 2.9) and for other two processes not included in the two single models, i.e. the attenuation of the PAR along the water column and the biogeochemical surface forcing as dry deposition.

In particular, the PAR profile is computed at each cell centre ($PAR|_z$) according to the Lambert-Beer formulation for the light exponential decay with depth, the shading of phytoplankton and a background extinction factor built a priori to incorporate the contributions of unparametrized processes (e.g. the pattern distribution of yellow substances):

$$PAR|_z = PAR|_0 \cdot exp \left[- \int_0^z \left(K_{ext} + \sum_j Chl_j(z) \cdot K_{P_j} \right) dz \right] \ , \tag{2.11}$$

where $PAR|_0$ is the PAR at the sea surface, Chl_j is the chlorophyll concentration of the $j-th$ phytoplankton functional type, related to the K_{P_j} extinction factor, and K_{ext} is the background extinction factor. In the configuration adopted for this study, both $PAR|_0$ and K_{ext} were pre-computed and read at runtime in the BFMCOUPLER package. $PAR|_0$ was derived from the shortwave radiation, following the standard bulk formula ([Britton and Dodd, 1976]):

$$PAR|_0 = Q_s \cdot conv \cdot pfrac \ , \tag{2.12}$$

in which Q_s is the shortwave radiation, coming from the ERA-Interim reanalysis, $conv$ is a conversion factor of $4.6 \mu Ein/m^2/s \ (W/m^2)^{-1}$, and $pfrac$ is the fraction of the radiation in the visible band, equal to 0.4. The background

extinction factor is derived from satellite observations [Lazzari et al., 2012], where the original data, with a sampling of 13 days, were interpolated on the MITgcm grid and smoothed by a simple moving average of order 3: since the temporal developing of the extremes is of order some days, in this way we damped down possible perturbations of strong light variation of the same order of magnitude on the extremes signals.

The presence of the parametrized background extinction factor is actually a limitation to a fully online coupling. Nevertheless, previous studies ([Lazzari et al., 2012]) have showed that light extinction factors formulated using standard water absorption and plankton self-shading can not reproduce adequately the observed light attenuation along the water column and the differences of depth of the DCM in the Mediterranean sub-basins. Therefore, this kind of parametrization is necessary.

On the other hand, $PAR|_0$ at the surface is pre-computed because the shortwave radiation is not used directly as a forcing field in the MITgcm. The shortwave radiation is in fact a component of the heat flux, reconstructed from the ERA-Interim reanalysis data and used as a forcing field (as already mentioned in 2.1).

The biogeochemical surface forcing (atmospheric and riverine) managed by the coupler is described in the last part of the sec. 2.4.

Finally, since the time scales of the hydrodynamic and the biogeochemical processes are different, in order to increase the computational performances without losing the high frequencies of variability ensured by the online coupling, the MITgcm **LONGSTEP** package was activated. According to it, the computation of the tracers derivatives was made only after every $LSn = 5$ timesteps of the hydrodynamic integration (i.e. 750 seconds), considering the dynamic fields involved in the computation as temporal averages over the LSn timesteps. The improvement in the coupled model performance when this package is activated is evident in the tab. 2.1, referred to the execution times of 1 day simulated by the coupled model.

Exec. times (s)	**TOT**	**I/O**	**TRP**	**BFM**	**MPI**
no LONGSTEP	983	425	286	22	118
LSn=5 LONGSTEP	576	446	69	-	50

Table 2.1. Execution times of the whole simulation (first column of results) and of its main subroutines grouped by type (input/output, transport, biogeochemical reactions, MPI parallel subroutines, respectively), before and after the LONGSTEP activation. In the second case, the profiling of the biogeochemical reactions are included in the transport term. Times are referred to 1 simulated day, by 228 processors and the test was performed on a cluster-ivy bridge core machine.

2.4 Initial and boundary conditions and biogeochemical forcings

The **initial conditions** for temperature and salinity fields are taken from Rixen et al. [2005]. The initial values for the biogeochemical tracers of the model come from Crise et al. [2003], in which fields from the MEDAR/MEDATLAS 2002 dataset ([Manca et al., 2004]) were used. According to that procedure, a vertical profile was assigned to dissolved oxygen, nitrate, phosphate and silicate to (eleven) different sub-regions of the Mediterranean Sea (see fig. 2.3 for the nitrate concentration at surface, as an example). The discontinuities between adjacent sub-regions were managed by a smoothing algorithm. The other biogeochemical state variables (plankton functional groups and their elements ratio) were homogeneously initialized in the first 200 m (as proxy for the euphotic layer) according to the standard BFM values and with lower values in the deeper layers. For the present work, all the biogeochemical profiles were interpolated from the 72 vertical levels used in Crise et al. [2003] to the 75 MITgcm levels.

For what concerns the boundaries, the Mediterranean Sea is considered in open connection only with the Atlantic Ocean through the Gibraltar Strait, whereas the Marmara Sea and the Black Sea are not included in the domain. As already mentioned in sec. 1.2.2, while the exchanges of water masses at the Gibraltar Strait manage to compensate the negative heat and fresh water budgets, the amount of nutrients flowing in the surface layer from the Atlantic Ocean is considerably smaller than the one flowing out in the bottom layer.

The **boundary conditions** at the Gibraltar Strait were handled by the relaxed boundary conditions (RBCS) package of the MITgcm, that allows to relax fields in a 3D location through a "sponge layer". According to it, the

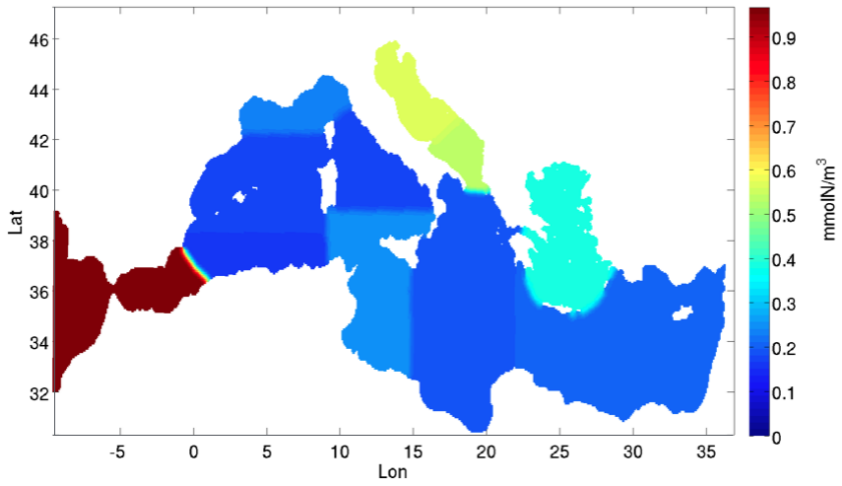

Figure 2.3. Initial conditions at the surface in the Mediterranean Sea domain for the nitrate concentration.

derivative of a generic tracer P (i.e. T, S, C_i) is modified so that:

$$\left(\frac{dP}{dt}\right)_{modified} = \frac{dP}{dt} - \frac{M_{rbc}}{\tau_P}(P - P_{rbc}) \ , \tag{2.13}$$

where M_{rbc} is a 3D mask with values between 0 and 1, τ_P is the time scale of relaxation, and P_{rbc} the relaxed field. In the present case, M_{rbc} has values different from 0 only out of the Gibraltar strait (i.e. in the Atlantic part of the domain), and all the vertical levels for a fixed horizontal grid point have the same mask value. The relaxed fields are climatological monthly records and τ_P is equal to 2 days.

The relaxed fields for salinity and temperature come from Levitus [1982]. The relaxed profiles for alkalinity and dissolved inorganic carbon were obtained by the interpolation on the 75 MITgcm levels of the data profiles published by Huertas et al. [2009] and Dafner et al. [2001b].

The vertical profiles for dissolved oxygen, phosphate, nitrate and silicate were obtained interpolating the profiles reconstructed by the WORLD OCEAN ATLAS 2013 dataset (`https://www.nodc.noaa.gov/OC5/woa13/`). The boundary conditions for the other biogeochemical variables were assumed equal to their initial conditions.

Finally, since the loss of nutrients at Gibraltar is dynamically compensated by the natural and antrophogenical sources over the Mediterranean area, estimating the **biogeochemical forcing** is a substantial factor for the configuration of the coupled model. Two kinds of biogeochemical contributions were considered for this study: the atmospheric and the riverine ones. The two different sources were preprocessed separately and then combined in one overall contribute of external biogeochemical forcing, managed by the BFMCOUPLER.

For the atmospheric part, dry deposition of phosphate and nitrate on the surface cells was considered as molar mass rate entering in the cells, at runtime diluted in the corresponding water volumes and in the later timesteps transported by the water currents. Data of molar mass rate come from Ribera d'Alcalà et al. [2003] and are (constant) mean values for the Western and the Eastern Mediterranean Sea: for the nitrate 1.51×10^{-6} mmol/m^2/s in the western sub-basin and 6.59×10^{-7} mmol/m^2/s in the eastern one, for the phosphate 1.92×10^{-8} mmol/m^2/s in the western sub-basin and 1.11×10^{-8} mmol/m^2/s in the eastern one.

The rivers provide in the model both runoff of freshwater and discharge of nutrients, dissolved inorganic carbon and alkalinity. While the runoff contribution is handled by the EXF package of the MITgcm, the biogeochemical one is instead considered as an input in the surface cells, similar to the atmospheric depositions. The original mass rate data ([Ludwig et al., 2009]) are referred to the monthly variability of 38 major and 191 minor rivers flowing in the Mediterranean area, including the Dardanelles, parametrized as a river. These data were mapped on the curvilinear grid used in this study, over the

positions of the rivers included in the runoff files. One of the major rivers, the Simav, was excluded from the dataset, since it flows into the Marmara Sea. Moreover, the biogeochemical supply of the Nile was splitted in equal parts between the two (Damietta and Rosetta) distributaries, whereas the combined input from Semani/Vjose (in the South Adriatic Sea) was assigned to the two single rivers, with weights 0.25 and 0.75, respectively, according to runoff data.

2.5 Remarks on the coupled model performances

An extended and rigorous validation of the MITgcm-BFM model is not an objective of this study. Rather, we checked if the model results are consistent with the climatological representation of the main physical variables, the nutrients, the chlorophyll and the primary production in the Mediterranean Sea.

To the best of our knowledge, at present there are not suitable datasets available to corroborate the biogeochemical extreme events (defined in sec. 3.2) on the Mediterranean Sea for a multidecadal simulation. On one hand, the time series obtained by in situ data (fixed stations or cruises) do not provide an adequate spatial sampling on the Mediterranean scale and often range over limited time periods. On the other hand, remote sensing data, due to the cloud coverage, can not be used to analyse the dynamics of extreme events. Indeed, to detect and reconstruct these events in the spatio-temporal domain we should use satellite products without missing data, i.e. where missing data are replaced by interpolated ones. Nevertheless, interpolated data are often based on climatological datasets and can introduce spurious signals that may compromise the onset and the developing of the extreme signals.

Thus, the coupled model was corroborated with in situ and satellite data and compared with other models in relation to the mean state of the main physical and biogeochemical variables, as reported in detail in **appendix A**.

As general remarks, the analysed physical variables (i.e. salinity and temperature) and the mixed layer dynamics, corroborated with the available data, showed that the MITgcm part of the coupled model is able to reproduce the physical processes driving the marine biogeochemistry in the Mediterranean Sea.

Further, the climatological means of nutrients (nitrate and phosphate), chlorophyll (at surface and in the vertical sections) and integrated net primary production indicated that the main biological features of the basin, like spatial gradients, productivity and DCM, are well simulated by the coupled model. In fact, the differences recognized between the MITgcm-BFM model and the observations or other models (mainly in the Tyrrenian Sea, Ionian Sea and Levantine Sea) are within the range of variability of the climatology.

Therefore, we assumed that the performances of the coupled model are adequate to allow the study on the extreme signals of chlorophyll on a modeling basis, as presented in the next chapter.

Chapter 3

Chlorophyll extremes: data and methods

In this chapter the investigation method for the surface chlorophyll extremes is developed. Extremes are identified for the open sea daily surface chlorophyll during the cold semester derived by the online MITgcm-BFM simulation over the period 1994-2012.

The method of identification and characterization of the extreme events of chlorophyll is formulated with a statistical approach, based on the definition of the 99th percentile as the reference threshold computed on the data.

At first (sec. 3.2.1), the extremes are defined at each grid point (local extremes), starting from the chlorophyll time series over the simulated period, and characterized by a local metrics. Then (sec. 3.2.2), the local extremes are reprocessed in space and time to identify macro extreme events of chlorophyll, as spatio-temporal volumes developing over the Mediterranean domain. Suitable indexes are finally introduced to describe the macro-events shape and strength (sec. 3.3), and to provide a standard to classify the extreme events.

3.1 The surface chlorophyll time series

The input data for the investigation of extremes are the daily time series of the surface chlorophyll concentration, computed as the sum of the 4 phytoplankton chlorophyll (sec. 2.2) and averaged on the first 10 m, in each horizontal grid point.

Fig. 3.1 shows the time series of the surface chlorophyll concentration in two points, belonging to the North West Mediterranean Sea and to the Levantine Sea. The dashed lines indicate the 99th percentile computed on the time period, according to the procedure that will be introduced in sec. 3.2.1.

As expected from the well known zonal gradient of surface chlorophyll across the basin (sec. 1.3), the values of chlorophyll in the Levantine Sea are considerably lower than the ones in the North Western Mediterranean Sea, with the only exception of the 2012, in which the highest values are

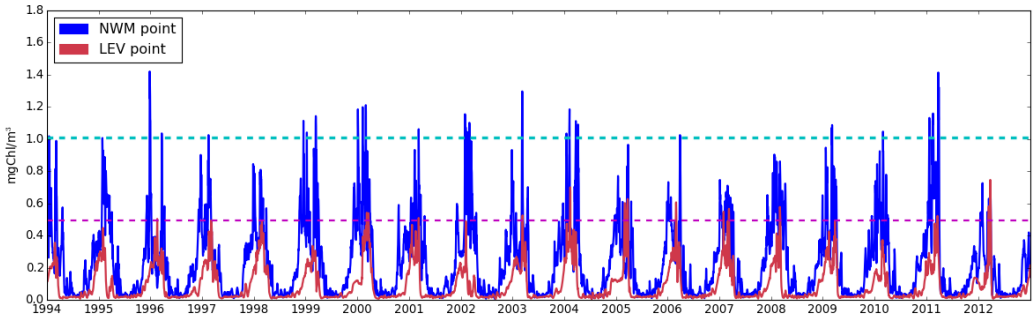

Figure 3.1. Model-derived surface chlorophyll concentration time series, from 1994 to 2012, in two single grid point belonging to the North Western Mediterranean Sea (blue series) and to the Levantine Sea (red series). The dashed lines indicate the 99th percentile of the data at those grid points (cyan and magenta lines, respectively).

comparable. Moreover, in the Levantine Sea the peaks of chlorophyll exhibit a temporal delay of about 1 month with respect to the northwestern time series. This characteristic reflects the different temporal dynamics of the mixed layer deepening and rising in the two areas. In fact, the mixed layer depth dynamics occurs in the North Western Mediterranenean Sea about 1 month in advance with respect to the Levantine Sea (as depicted in fig. A.4(a), in appendix).

More in general, the heterogeneity of the time series of surface chlorophyll features (i.e. their mean values, variability, phenology) in all the points of the domain reflects the variety of physical and biological processes happening in the basin.

The method of investigation of the chlorophyll extremes in the Mediterranean Sea was developed accounting for the spatio-temporal peculiarities of the surface chlorophyll over the domain. In fact, the extremes were at first defined locally and only at a later stage processed to evaluate their spatial extent on the whole Mediterranean region.

Moreover, the study was conducted only for the grid points with depth higher than 200 m, identified as the "open sea".

Defining the open sea domain with this vertical limit allows to neglect both the coastal points, that are directly affected by the river discharge of biogeochemical quantities, and the points where the interactions with the sea bottom occur within the euphotic layer. On the other hand, it is worth noting that the northern part of the Adriatic Sea, that is a region with high concentrations of surface chlorophyll, is consequently excluded from the analysis due to its shallowness.

The analysis consider only the cold semester since the peaks of chlorophyll are from January to May.

3.2 The definition of the extremes: local and macro-events

3.2.1 Local extremes

At each horizontal grid point, the extremes of chlorophyll concentration are defined as the **Peaks Over the 99th percentile Threshold (POTs) of the surface chlorophyll daily time series**. The 99th percentile is computed on the data of the grid point time series.

As an example, the 99th percentile thresholds for the time series referred to the two single grid points belonging to the North Western Mediterranean Sea and to the Levantine Sea (fig. 3.1), indicated by the dashed lines, are clearly different. In particular, the North Western Mediterranean point displays a 99th percentile higher with respect to the Levantine one.

Fixing a grid point (x, y), some quantities can be introduced to define the properties of the chlorophyll extremes in that point.

The $j-th$ POT (with the occurrence index $j \in J|_{(x,y)} = \{1, ..., N_{POTs|_{(x,y)}}\}$) happened at the t_j day is characterized by the value $C_j \equiv chl(x, y, t_j)$ of chlorophyll concentration and by the *intensity* (I_j) above the threshold, defined as the difference of the chlorophyll concentration and the threshold computed for the time series at the grid point ($p99$), i.e.:

$$I_j|_{(x,y)} = C_j|_{(x,y)} - p99|_{(x,y)} \ , \tag{3.1}$$

as sketched in fig. 3.2. By construction, $N_{POTs|_{(x,y)}}$ is determined by the 1% of the total number of days of simulation (in our case $N_{POTs|_{(x,y)}}$=70).

Moreover, POTs that are consecutive in time can be gathered together to define single local extremes, i.e. the set of the POTs indexes $J|_{(x,y)}$, can be decomposed in subsets $J^l|_{(x,y)}$ of consecutive POTs.

The $l-th$ local extreme, with $l \in L|_{(x,y)} = \{1, ..., N_{l|(x,y)}\}$, has a *duration* Δt_{J^l} defined as the interval of days included in the local extreme. The limit case of a local extreme including only 1 day of POT occurrence corresponds to a duration equal to 1 day. On the other hand, we assume that local extremes of chlorophyll with longer duration have in general more significant impacts on the ecosystem processes.

The overall mass of chlorophyll $M^{J^l}_{chl}$ supplied by one local extreme in the grid point is instead defined as the sum of the chlorophyll concentration multiplied by the volume V_c of the surface cells[1] over all the POTs occurrences within the local extreme, i.e.:

$$M^{J^l}_{chl}(x, y) = \sum_{j \in J^l|_{(x,y)}} C_j \times V_c(x, y) \ . \tag{3.2}$$

[1]By assumption, the volume of a surface cell is equal to the product of the cell area times the depth of the first vertical layer, approximately equal to 1 m, i.e. $V_c = a_c(x, y) \times 1m$.

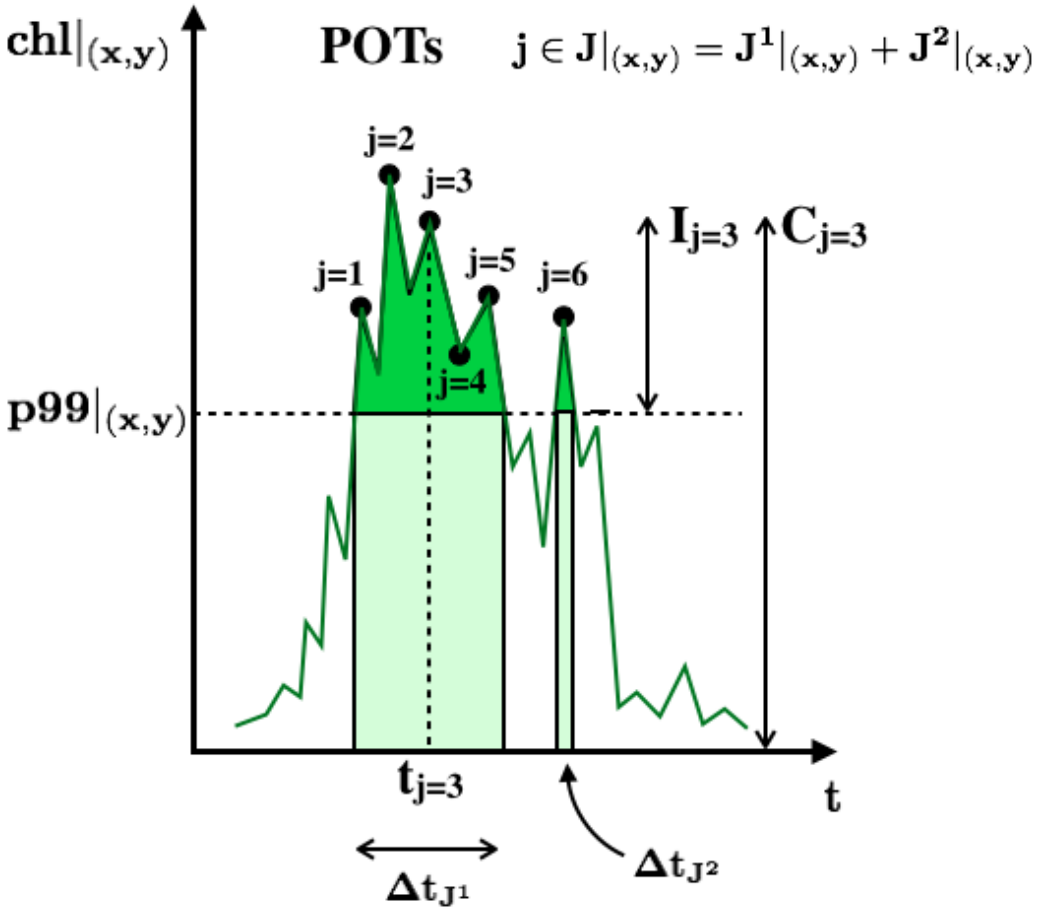

Figure 3.2. Schematics of the local metrics of the chlorophyll extremes. The horizontal dashed line indicates the 99th percentile threshold computed at the grid point. The daily chlorophyll values above the threshold are represented by the POTs (black circles), in the number of 6, as an example, grouped in two local extremes, with POTs indexes $J^1|_{(x,y)} = \{1, 2, ..., 5\}$ and $J^2|_{(x,y)} = \{6\}$, respectively. The value of chlorophyll concentration C_j and the intensity I_j related to one POT, as well as the duration of the two local extremes, defined in the text, are also shown.

The overall intensity of chlorophyll above the threshold $I^{J^l}_{chl}$, expressed in mass units, has a definition similar to eq. (3.2), but referred to I_j rather than C_j, i.e.:

$$I^{J^l}_{chl}(x,y) = \sum_{j \in J^l|_{(x,y)}} I_j \times V_c(x,y) \ . \tag{3.3}$$

Although these two quantities are computed as discrete sums rather than integrals, in order to visualize them in a simplified way (in the unit volume), in fig. (3.2) the total intensity is represented by the dark green area and the total mass by the sum of the dark and shaded green areas. In fact, the shaded green area represents the total mass (by unit volume) supplied by the 99th threshold of chlorophyll, defined as the scalar quantity $p99|_{(x,y)}$ times the total number of POTs occurrences $N_{POTs|_{(x,y)}}$.

Mapping the 99th percentile thresholds computed at each grid point of the domain on the whole basin (fig. 3.3), it can be noticed that grid points that are near in space exhibit small differences in their threshold values and also that some patterns are recognizable in different Mediterranean regions. In particular, referring to the partition of the Mediterranean Sea in the subdomains displayed in fig. 3.4, the thresholds in the North Western Mediterranean Sea, in the Alboran Sea and in the North Ionian Sea show an intra-variability in each subdomain that is lower than the inter-variability among the subdomains. Therefore, the subdomain of occurrence is considered one of the keys to characterize the extreme events.

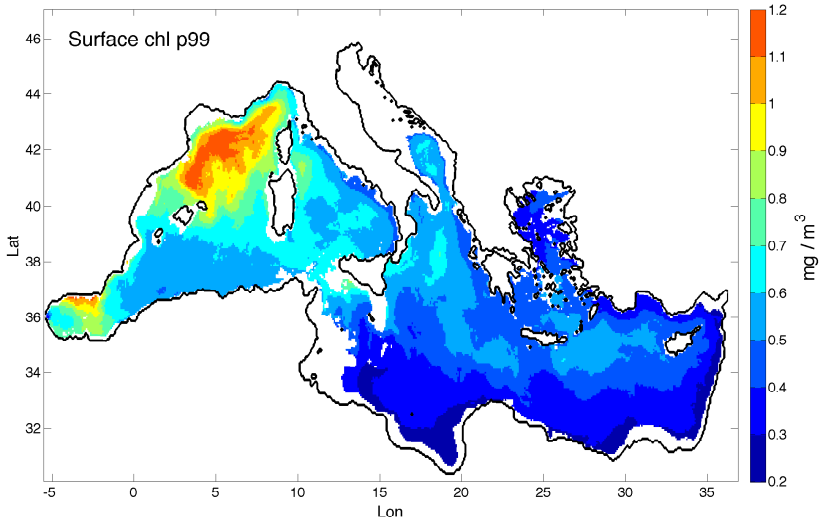

Figure 3.3. Map of the model-derived 99th percentile thresholds of the surface chlorophyll in the Mediterranean open sea domain (1994-2012). Isolated grid points with depth higher than 200m belonging to the Northern Adriatic Sea and to the Gulf of Corinth (Greek inlet) are masked.

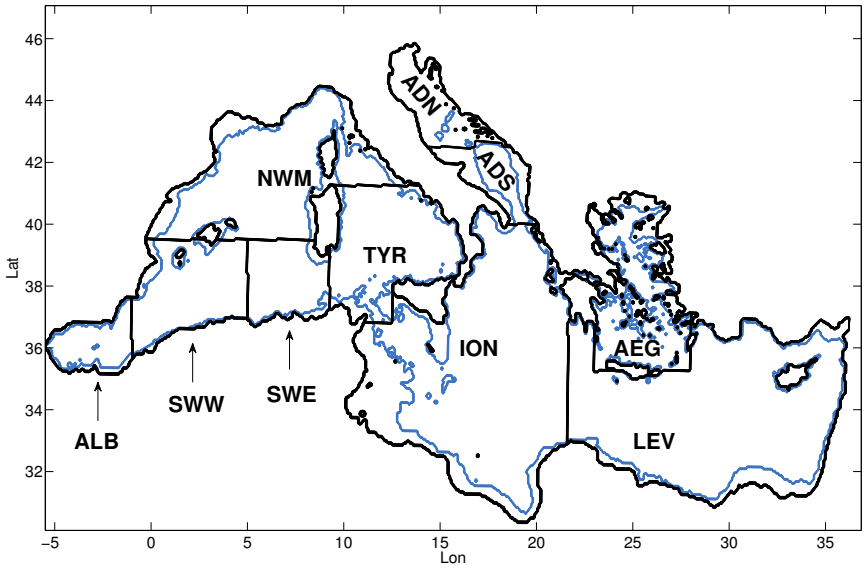

Figure 3.4. Mediterranean subdomains as reference, partially modified by [Lazzari et al., 2012]. Acronyms: ALB = Alboran Sea, SWW = western side of the South Western Mediterranean Sea, SWE = eastern side of the South Western Mediterranean Sea, NWM = North Western Mediterranean Sea, TYR = Tyrrenian Sea , ION = Ionian Sea, LEV = Levantine Sea, ADN= Northern Adriatic Sea, ADS = Southern Adriatic Sea and AEG = Aegean Sea. The contours of the 200m of depth areas (open sea) are indicated by the blue line. Considering the open sea constraint, the isolated points belonging to the ADN subdomain were excluded from the analysis.

3.2.2 Macro extreme events

The spatial and temporal occurrence of all the local POTs computed in the previous step can be remapped on a binary 3D matrix, representing the (2D map x day) flags of the extremes, equal to 1 for the (x, y, t) points of POTs occurrence and 0 for the points without POTs occurrence.

Macro extreme events (hereafter: macro-events) are then defined as **sets of POTs events that are "connected"** (mathematically: "the closest neighbours") **in space and/or in time**.

In this way, macro-events of chlorophyll are represented by spatio-temporal volumes, in which the spatial contiguity of the points with chlorophyll values above their own threshold at the same time is a further request, added to the temporal contiguity typical of the local extremes defined in sec. 3.2.1.

In fig. 3.5 an example of a macro-event of chlorophyll reconstructed applying this definition is represented in the spatio-temporal domain. It is a winter event occurred in the Western Mediterranean Sea from the 16th February to the 12th March 1994. As general interpretation of the macro-event, fig. 3.6

displays the maps of the surface chlorophyll (left column) and of the surface nitrate (right column), in selected days during the period of development of the macro-event. In the middle panels, the red patterns represent the evolution of the macro-event superimposed to the surface velocity field. The daily area of the macro-event actually includes points with noticeably high chlorophyll values in the region (by comparison of the first two columns). Nevertheless, it contains also those points with chlorophyll values that are lower on the same absolute scale, yet higher than the local 99th percentile thresholds (not appearing in the maps, but ensured by the procedure). Moreover, the macro-event patches appear to be advected by the velocity field and to follow both the convection weakening (see plots in consecutive middle panels) and the patches of high nutrient concentrations (by comparison of each middle panel with the right panel referred to the day before).

3.3 Metrics of the macro-events

Each macro-event (Ev) represented by a spatio-temporal volume is associated to a set of days in which there is at least 1 POT in a grid point of the macro-

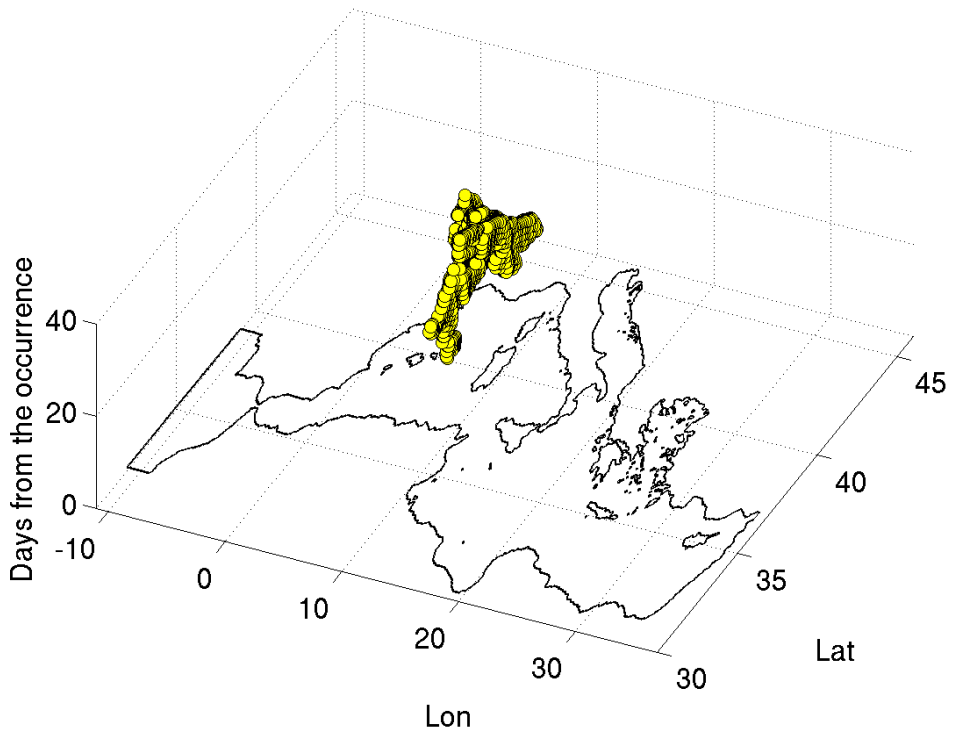

Figure 3.5. Spatio-temporal representation of a macro-event occurred in the Western Mediterranean Sea during winter (from the 16th February to the 12th March 1994). Each yellow dot flags the spatio-temporal occurrence of a POT.

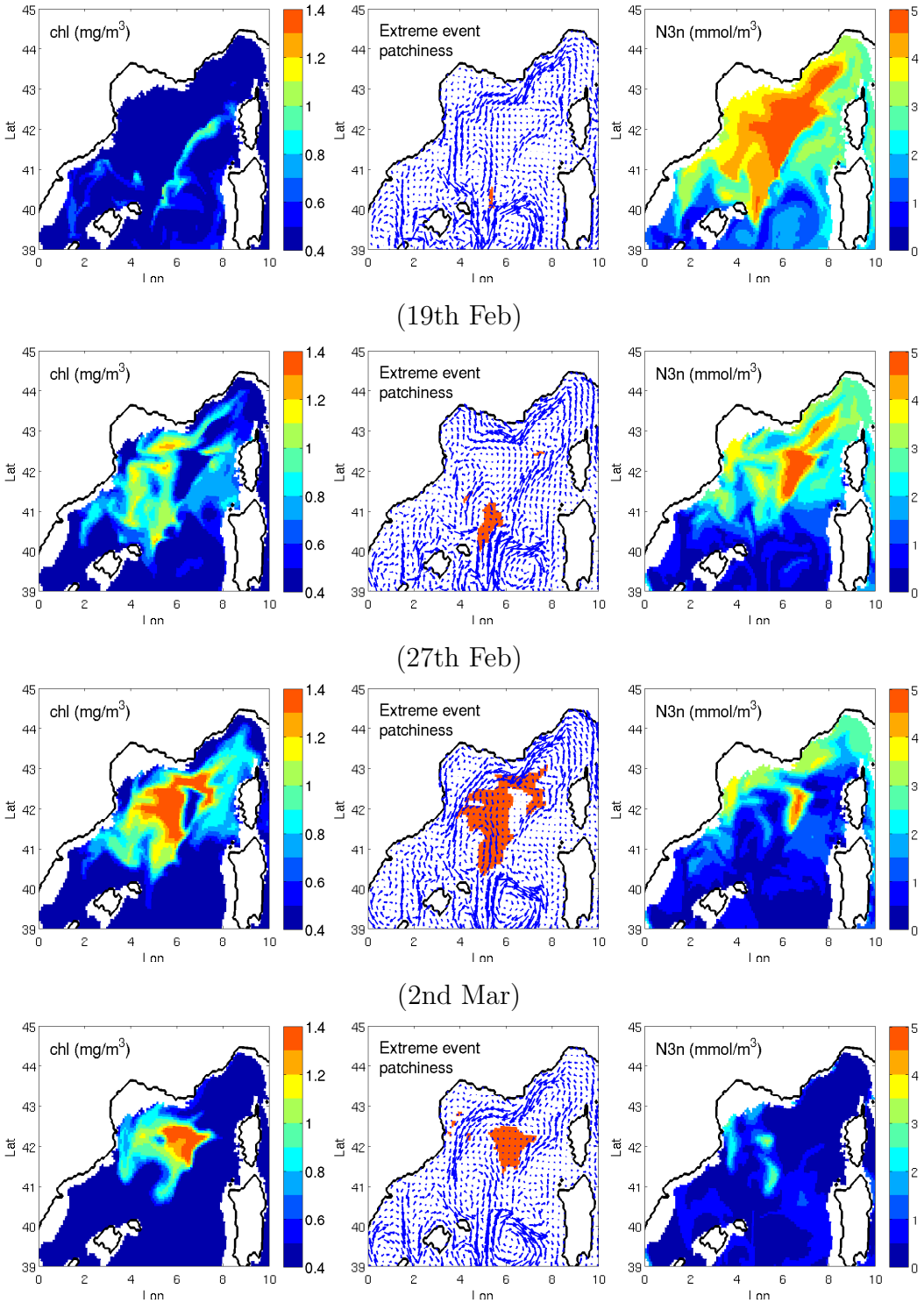

Figure 3.6. Maps of the surface chlorophyll (first column), daily portion of the area A of the macro-event superimposed to the surface velocity field, (second one) and surface nitrate (third one), for some single days of development of the macro-event depicted in fig. 3.5, happened in the Western Mediterranean Sea from the 16th February to the 12th March 1994. Surface chlorophyll and nitrate are averaged in the first 10 m of depth, whereas the horizontal velocity field (scaled by a factor 1.5) is referred to the depth of 5 m.

event volume. The set of all the indexes of POTs belonging to the macro-event is defined as J^{Ev}.

In each grid point, J^{Ev} selects a certain number of local extremes, each one with POTs indexes in $J^l|_{(x,y)}$ (see sec. 3.2.1), belonging to the macro-event. To simplify the following argumentation, hereafter only the case with 1 local extreme per grid point included in the macro-event is considered and this local extreme is defined as $J^l \subseteq J^{Ev}$, i.e. the subscript $|_{(x,y)}$ is implied. However, the extension to the general case of more than 1 local extreme per grid point selected by the macro-event can be easily obtained adding the sum over all the $l \in L$.

Assuming these definitions, for each macro-event different indexes can be introduced, as spatio-temporal coordinates, shape parameters (with a simplified sketch in fig. 3.6) and strength indexes (fig. 3.7-3.8):

Coordinates

1. the *year* is the year in which the macro-event is entirely contained, provided it occurs in the Jan-May period;

2. the *occurrence* is the first day when at least one POT belonging to the macro-event occurs;

3. the *sub-region* is identified by the Mediterranean subdomain(s) covered by the macro-event, where the reference subdomains are indicated in fig. 3.4;

4. the pair (*lon,lat*) of spatial coordinates are referred to the local maximum of chlorophyll reached in the macro-event.

Shape parameters

1. the *area* A is the union of all the grid cells housing the local extremes included in the macro-event, i.e. $A = \{(x, y) : J^l \subseteq J^{Ev}\}$, and it is labeled by the sum of these cells areas, measured in km^2;

2. the *duration* T is the union of all times in which there are POTs included in the macro-event, i.e. $T = \{t_j : j \in J^{Ev}\}$, and it is labeled by the maximum temporal difference between two POTs of the macro-event, measured in *day*;

3. the *width* W is the sum of the cell area a_c times the overall duration of the local extremes included in the event over the grid points referred to A:

$$W = \sum_{\substack{(x,y)\in A \\ J^l \subseteq J^{Ev}}} a_c(x, y)\Delta t_{J^l} \ . \tag{3.4}$$

   The width is measured in units of $km^2 \times day$;

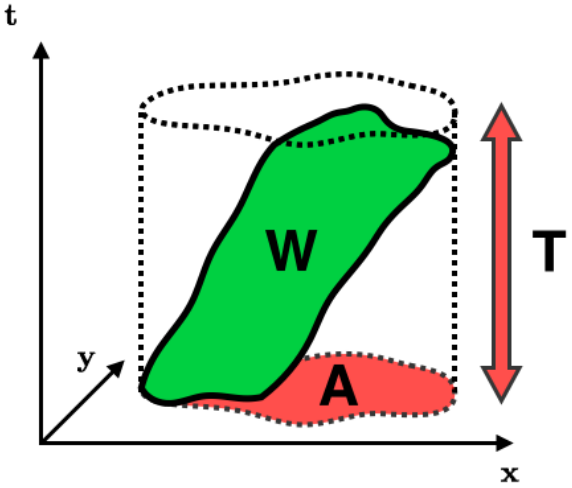

Figure 3.6. Schematics of the main shape parameters of one macro-event represented in the (x, y, t) space. The area, duration and width of the event, defined in the text, are indicated by the letters A, T and W, respectively.

4. the *uniformity* U is the ratio between the width W and the spatio-temporal volume of the prism with A as base and T as height:

$$U = \frac{W}{A \times T} \ , \tag{3.5}$$

i.e. it represents the percentage of the prism that is occupied by the event. This index quantifies how much (on average) the event is persistent on the single grid point belonging to A.

Strength indexes

The values of chlorophyll and the intensities of all the local POTs (defined in the sec. 3.2.1) can be remapped on the respective 3D (2D map x day) matrixes, in direct correspondence with the 3D matrix of POTs occurrence.

Thus, the following indexes can be defined for each macro-event:

1. the *severity* S is the sum of the mass of chlorophyll in the grid point supplied by the local extremes included in the macro-event over the grid points referred to the area A:

$$S = \sum_{\substack{(x,y)\in A \\ J^l \subseteq J^{Ev}}} M_{chl}^{J^l}(x, y) \equiv \sum_{(x,y)\in A} M_{chl}(x, y) \ . \tag{3.6}$$

The severity is therefore the result of a spatial sum of amounts already summed in time (M_{chl}) and hereafter its (mass) unit is expressed in kg. The severity is represented in a simplified way in fig. 3.7(a) as the shaded green shape. In the same figure, also the locus of points of the 99th percentile threshold for all the grid points ($P99$) is shown.

2. the *excess* E is defined, likewise the severity, as the sum of the intensity of chlorophyll above the threshold in the grid point supplied by the local extremes included in the macro-event over the grid points referred to A:

$$E = \sum_{\substack{(x,y)\in A \\ J^l \subseteq J^{Ev}}} I_{chl}^{J^l}(x,y) \equiv \sum_{(x,y)\in A} I_{chl}(x,y) \ . \tag{3.7}$$

   The excess is sketched in fig. 3.7(b) as the dark green shape above the $P99$ locus of points and it is expressed in kg;

3. the *mean severity* $<S>$ can be obtained dividing the severity by the width W of the macro-event. Its units are $kg/km^2/day$;

4. the *anomaly* is the ratio between the excess and the severity:

$$AN = \frac{E}{S} \ , \tag{3.8}$$

   and it represents the percentage of the excess in the severity of the macro-event. The anomaly index is sketched in fig. 3.8 for two macro-events with same severity but different $P99$. In particular, since the $P99$ of the second macro-event is lower, this macro-event has a higher value of the anomaly with respect to the first one.

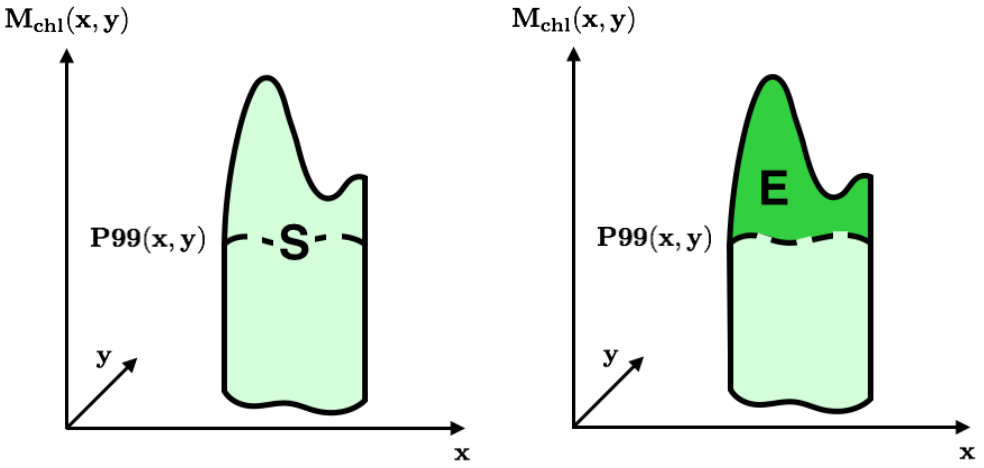

(a) (b)

Figure 3.7. Severity (a) and excess (b) conceptual schemes. Each (x, y) grid point included in the area A has a certain M_{chl} value of chlorophyll, already summed in time (referred to the vertical axis). The severity as the sum of all the M_{chl} values over the cells belonging to A is indicated by the whole shaded green shape (a), whereas the excess is the part of this volume that is above the $P99$ locus of points (dashed curved line) and it is represented by the dark green shape (b).

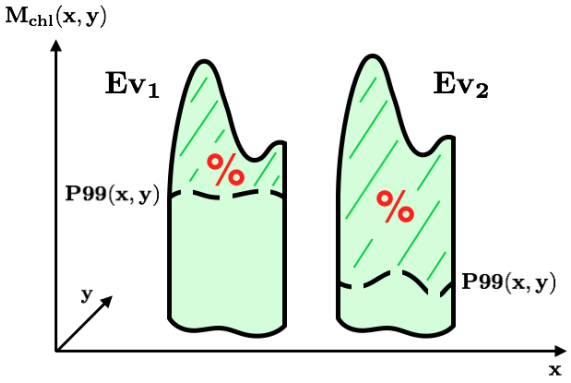

Figure 3.8. Schematics of the anomaly index, expressed as the percentage of the excess with respect to the severity, for two different macro-events with the same severity (overall green shapes), but different $P99$ locuses of points (dashed curved lines).

As an example, the macro-event in fig. 3.5 is characterized by the indexes listed in tab. 3.1, grouped by indexes of spatio-temporal coordinates, shape parameters and strength.

From the **marine ecosystem** point of view, the indexes mainly related to the **impact** of the extreme chlorophyll events on it are the mean severity, the anomaly and the uniformity.

In fact, $< S >$ provides the mean amount of biomass supplied by the macro-event to the first meter of depth in 1 day over a unit area of 1 km^2. It can be used as an indicator of eutrophication and of food availability for secondary production.

AN is instead the amount of chlorophyll anomalously high with respect to the capacity of the ecosystem itself, where the capacity is defined as the mean mass of chlorophyll supplied by the mean P99 of the points included in the macro-event to the first meter of depth in 1 day over the unit area.

Finally, the uniformity index U is a factor related to the effective persistence of the macro-event on the area A. Fixing the value of the impact indexes ($< S >$ and AN) and of the A and T shape parameters, macro-events with higher U affect the single unit of A by the impact indexes for longer times, with heavier ecological consequences on the ecosystem unit.

In the perspective of the **classification** of the extreme events of chlorophyll occurred in the Mediterranean Sea in the simulated period (chapt. 4), these three indexes will be therefore used as the main criteria to identify the most significant macro-events.

As regards the macro-event in fig. 3.5 and tab. 3.1, it is characterized by a mean severity of 1.27 $kg/km^2/day$ in the first meter of depth and the 13% of this amount is anomalous with respect to the local capacity of the system. Overall, the macro-event occurred in the North Western Mediterranean Sea and in the western side of the South Western Mediterranean Sea, involving an area equal to about one-fourth of the total North Western Mediterranean Sea itself. Even if the overall duration of the macro-event is 25 days, each unit area was actually affected only for about 3 days ($U \times T \approx 3$ $days$). This means that the macro-event spreads out in space and time with an articulated shape, as effectively emerged by fig. 3.5 and fig. 3.6.

		Ev 1
Coordinates	**Year**	1994
	Occurrence	16th Feb
	Sub-region	NWM-SWW
	(Lon, Lat)	(6°3', 42°18')
Shape	**Area** A (km^2)	6.12×10^4
	Duration T (day)	25
	Width W $(km^2 \times day)$	2.15×10^5
	Uniformity U	0.14
Strength	**Severity** S (kg)	2.72×10^5
	Excess E (kg)	3.61×10^4
	Mean Severity $< S >$ $(kg/km^2/day)$	1.27
	Anomaly AN	0.13

Table 3.1. Table of the metrics, grouped by spatio-temporal coordinates, shape parameters and strength indexes, defined in the text, for the macro-event in fig. 3.5, denominated for simplicity as the Event 1.

Chapter 4

Model-derived macro-events in the Mediterranean Sea

According to the method illustrated in the previous chapter, the local extremes of chlorophyll and, consequently, the macro-events, can be identified in the same way in all the regions of the Mediterranean Sea. Nevertheless, the values of the indexes defined in the sec. 3.3 allow to recognize the most significant macro-events, from the point of view of their shape parameters and strength.

In this chapter, the macro-events features and occurrence in the simulated period are described at first at the basin scale (sec. 4.1.1) and then in 4 representative subdomains of the Mediterranean Sea: the North Western Mediterranean Sea, the Southern Adriatic Sea, the Ionian Sea and the Levantine Sea (sec. 4.1.2).

Afterward, the macro-events of chlorophyll are classified in light of their impact on the ecosystem, related to the very high and/or anomalous biomass production supplied by the macro-events (sec. 4.2). The classification is made using the median values of the distributions of mean severity and anomaly on the basin scale as a reference point.

4.1 Characterization of the macro-events

The method illustrated in the secs. 3.2.1-3.2.2 was applied to the MITgcm-BFM model-derived surface chlorophyll in the Mediterranean open sea (1994-2012) and the macro-events were identified in the winter-spring period.

Then, a **filter** of minimum size for the macro-events equal to 100 spatio-temporal points was used to remove isolated events.

This size ideally corresponds to the shape obtained as: 5 grid points × 5 grid points × 4 days, i.e. about 35 km × 35 km × 4 day[1]. The selected time range can be explained considering that the total number of days in the 1994-2012 period (equal to 6940) determines at each grid point an occurrence

[1] 5 grid points × 5 grid points = 25 unit areas, with 1 unit area ≈ 50 km^2

of POTs (on average) equal to 4 days per year. About the horizontal scales, the length of 35 km corresponds to about one third of the diameter of the smallest gyres in the basin (O(100) km) and to about three times the mean Rossby radius estimated in the Mediterranean Sea (about 12 km, [Robinson et al., 2001]). Thus, the method allows to recognize the dynamics of the macro-events from the basin scale down to the mesoscale. However, the same spatio-temporal size can be arranged in different shapes[2] and the actual shape parameters of the macro-events (area A and duration T) are discussed later in the sec. (4.1.1).

After the filter, an overall amount of **933 macro-events** of surface chlorophyll were identified over the analysed period. Their characteristics, distribution and trends are evaluated in this section, both at the basin and at the sub-basin scale.

4.1.1 The basin scale

The macro-events occurred in the Mediterranean Sea in 1994-2012 have the **spatial distribution** shown in fig. 4.1, with positions tagged by the local maxima of chlorophyll within the macro-events. On the whole, their density is higher in the northern part of the basin and, in particular, in the northern part of the Alboran Sea and of the Ionian Sea, in the North Western Mediterranean Sea, in the Southern Adriatic Sea and in the Rhodes Gyre sub-region. The

[2]The two limit shapes are in principle identified by 5×5×4=100 unit areas × 1 day and 1 unit area × 100 days.

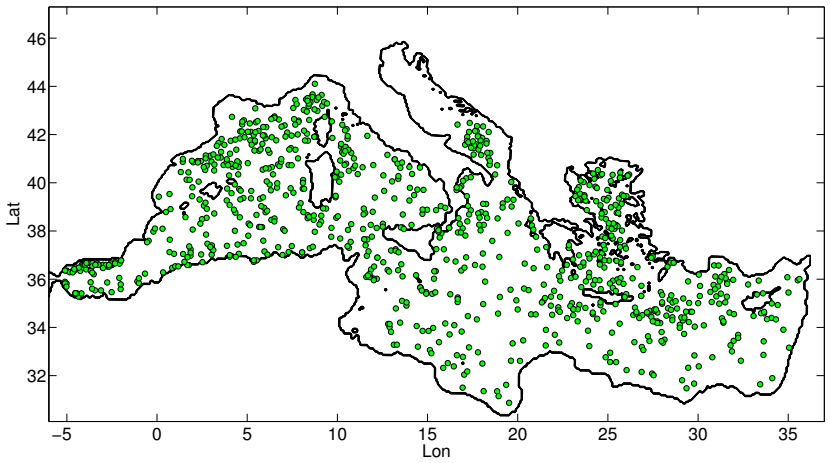

Figure 4.1. Spatial distribution of all the winter-spring macro-events occurred in the Mediterranean Sea simulated in 1994-2012. Each macro-event is represented by the (lon, lat) coordinates referred to the its spatio-temporal point with the maximum of chlorophyll concentration.

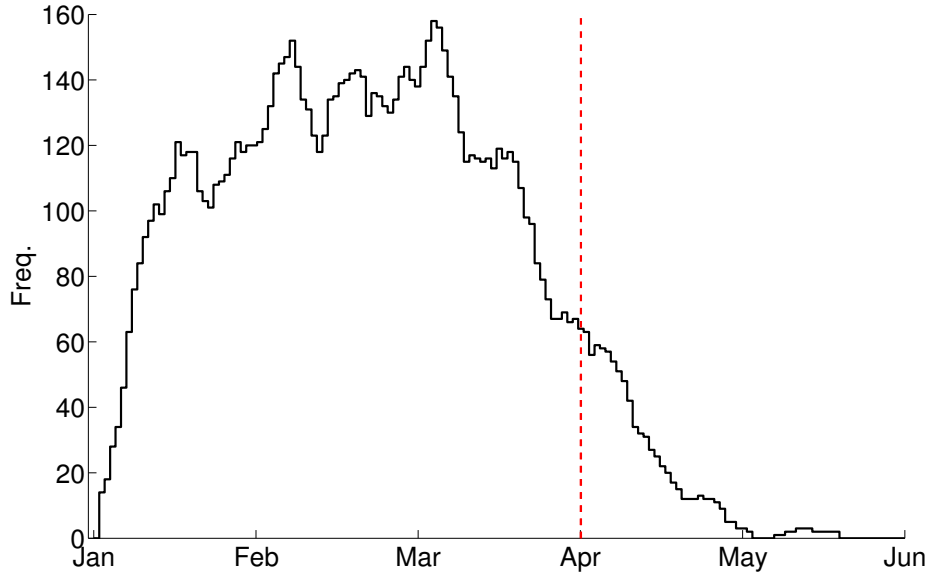

Figure 4.2. Frequency histogram of the totality of days of all the macro-events happened in the Mediterranean Sea within the Jan-May period of the time range 1994-2012. The red dashed line delimits the JFM winter period.

patterns of local maxima clearly reflect the ones of the 99th percentile thresholds (fig. 3.3).

As regards the **time development** of the macro-events in the considered months, we can consider the whole duration of each macro-event and find that the life cycle (the totality of days) is included within the January-February-March season (JFM) with the 92% of probability (see fig. 4.2 for the frequency distribution). In particular, the macro-events of chlorophyll are recognized mainly in the first halves of February and March.

The **shape parameters** of the macro-events are displayed in fig. (4.3), where each dot represents the area A and the duration T of the macro-event, in connection with the uniformity index U.

The median values of area and duration of the macro-events on the basin scale are equal to 5×10^3 km^2 and 9 days, respectively[3]. However, the 89% of the macro-events have an area smaller than 100×10^3 km^2 and a duration shorter than 20 days.

The minimum of the A index at the basin scale is associated to macro-events located near the Ionian Islands, with areas equal to about 700 km^2, (about 14 unit areas), and an overall duration of about 16 days. This means that we do not observe macro-events with 1 unit area for more than 100 days. On the

[3]As references for the areas (with the open sea constraint), the Southern Adriatic Sea has an area equal to about 33×10^3 km^2, whereas the whole basin (open sea) to 1996 km^2 $\times 10^3$ km^2.

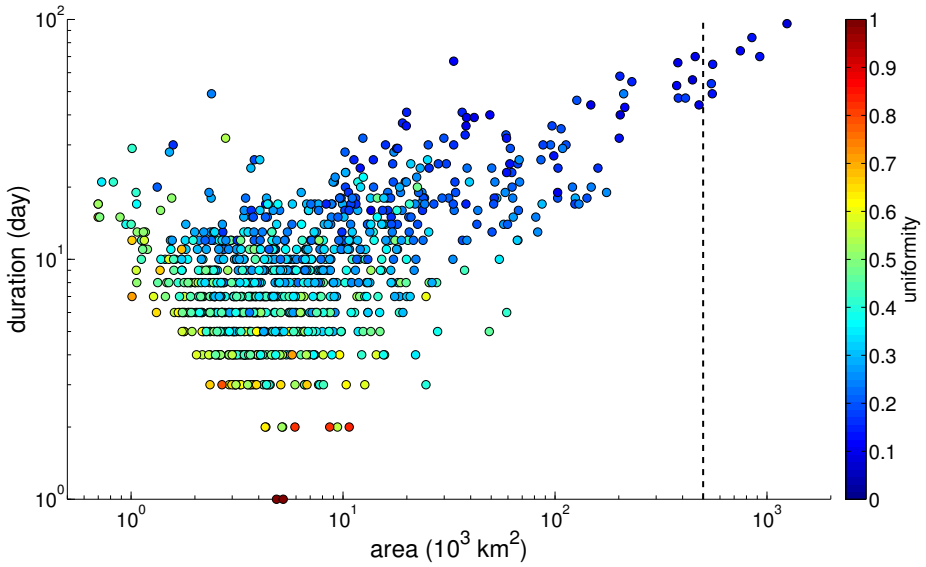

Figure 4.3. Distribution of area A and duration T shape parameters for all the macro-events occurred in the Mediterranean Sea in the winter-spring 1994-2012 simulated period. The macro-events are represented by the dots, coloured as a function of their uniformity index. The black dashed line delimits areas equal to $500 \times 10^3\ km^2$.

other hand, two macro-events (in the Northern Ionian Sea and in the Rhodes Gyre region) of only 1 day passed the filter, because their area is larger than the lowest limit fixed by the spatio-temporal size of the filter (about $4.9 \times 10^3 km^2$).

Nevertheless, there are seven macro-events with areas larger than $500 \times 10^3\ km^2$ (indicated in fig. 4.3 by the dashed line), corresponding to a coverage larger than the 25% of the Mediterranean Sea, with duration longer than 40 days. Due to their spatial dimensions, these macro-events can not be ascribed to a prevalent subdomain, but are considered on the basin scale. Three of them affected mainly the Western Mediterranean Sea in 1995, 2003 and 2004, whereas the others occurred in the Eastern Mediterranean Sea in 2000, 2005, 2006 and 2012. Since the uniformity index of these events is lower than the 20%, these macro-events are not associated with high persistency on the single grid points involved. Consequently, their potentially high impact on the basin scale, associated to their large coverage, has to be actually scaled down if we consider a local perspective.

On the other hand, higher values of the uniformity index are associated to smaller and shorter macro-events, that appear as more compact spatio-temporal shapes.

Tab. 4.1 shows the percentile statistics of the uniformity index, together with the ones for the mean severity and the anomaly.

The macro-events on average are characterized by a **uniformity** index equal

	P25	P50	P75	P95	Y-B
U	0.262	0.355	0.448	0.585	0.000
<S> $(kg/km^2/day)$	0.494	0.608	0.774	1.132	0.186
AN	0.046	0.068	0.099	0.151	0.170

Table 4.1. Percentiles statistics (25th, 50th, 75th and 95th percentiles, indicated by the P prefix, and Yule-Bowley asymmetry index, indicated by $Y - B$) for the uniformity, mean severity and anomaly indexes.

to 36%, with a distribution that is symmetric (evaluated by the Yule-Bowley asymmetry index) within the range 9% - 100% (not shown). This means that there is a wide variety of possible shapes associated to the Mediterranean macro-events. A uniformity index equal to 1 is referred to macro-events that persist in the same area for all their duration. Conversely, lower values of uniformity are related to macro-event shapes more articulated in branches spreading within the spatio-temporal volume.

The **mean severity** distribution has a median value equal to about 0.6 $kg/km^2/day$, whereas the median of the **anomaly** distribution is about 7%. The Yule-Bowley asymmetry index is equal to about 0.2 in both cases. Since the two distributions exhibit a positive asymmetry, this means that in the totality of the basin-scale macro-events, there are relatively few macro-events with very high mean severity and very anomalous, respectively.

Considering the **tails** of the distributions of uniformity, mean severity and anomaly, referred to the values higher than the 95th percentile thresholds of the single distributions, the shape parameters of the 47 macro-events ascribed to these tails are represented in fig. 4.4.

The macro-events in the tail of the uniformity distribution exhibit an inverse proportionality between area A and duration T, for macro-events that are small (areas smaller than 25×10^3 km^2) and short (durations shorter than 17 days), with respect to the whole distribution.

The macro-events in the tail of the anomaly distribution have durations at least equal to 5 days, but up to 84 days, and cover areas in the whole range of variability (including also some of the areas higher than 500×10^3 km^2), spreading out a region of the T vs A plane that is complementary to the one of the macro-events with very high uniformity. In fact, only the 4% (2 cases out of 47) of the macro-events with very high anomaly have also high uniformity, i.e. macro-events very anomalous are typically not uniform. The macro-events with very high anomaly are associated to amounts of chlorophyll that are atypical for the capacity of the involved areas and their main feature emerging from this plot is the (relatively) long duration. This result is ascribed to the persistance of the forcing conditions and/or of the internal ecosystem processes

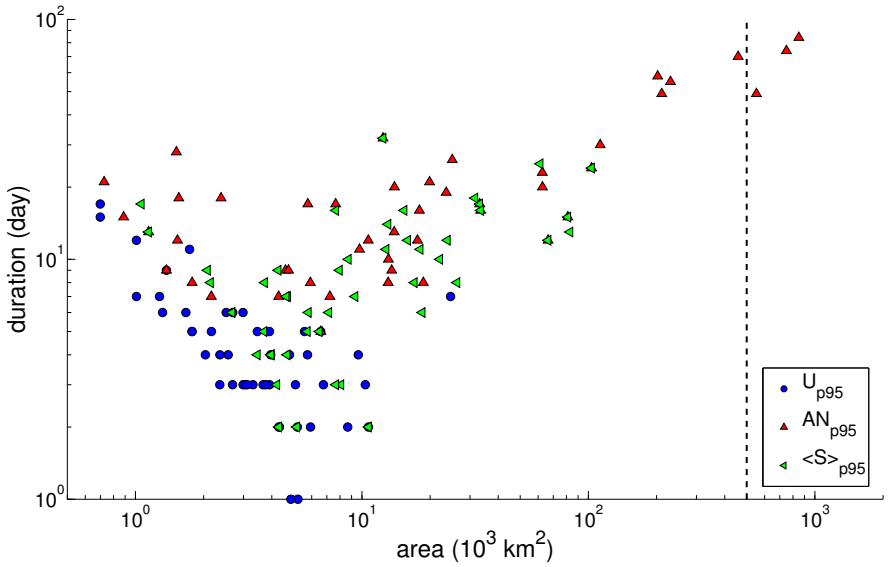

Figure 4.4. Distribution of area A and duration T shape parameters for the macro-events with uniformity (blue circles), anomaly (red upward-vertex triangles) and mean severity (green leftward-vertex triangles) higher than the 95th percentile threshold of the corresponding distributions. The black dashed line delimits areas equal to 500×10^3 km^2.

that promote and maintain these macro-events.

On the other hand, the macro-events with very high mean severity have areas between 1 and 100×10^3 km^2 and duration shorter than 1 month, i.e. spatio-temporal dimensions that are intermediate on the basin reference. They are localized mainly in the Mediterranean regions with the highest values of the 99th percentile threshold (fig. 3.3), without the inclusion of large neighbouring areas with lower thresholds (whose effect would decrease the value of the mean severity index). On the other hand, the range of duration of 1 month allows in principle different kinds of processes of development and manteinance of the macro-events. Only the 4% of the macro-events with high mean severity has also high uniformity and the 15% of them (7 cases of 47) are also very anomalous, i.e. the most severe events are typically not uniform but sometimes very anomalous.

The **annual maps of spatio-temporal occurrence** of the macro-events of chlorophyll are represented in figs. 4.5-4.6. The coloured regions correspond to areas affected by at least one macro-event, with the colorbar representing the number of macro-events in each point. The annual maximum number of macro-events in each point is 6. The coverage of the Mediterranean Sea is not homogeneous and it is evident that the macro-events have larger spatial extent in some years (2003, 2004 and 2012). Overall, the macro-events of chlorophyll appear as events irregularly scattered over the Mediterrean domain.

The information contained in these maps is summarized in tab. 4.2, con-

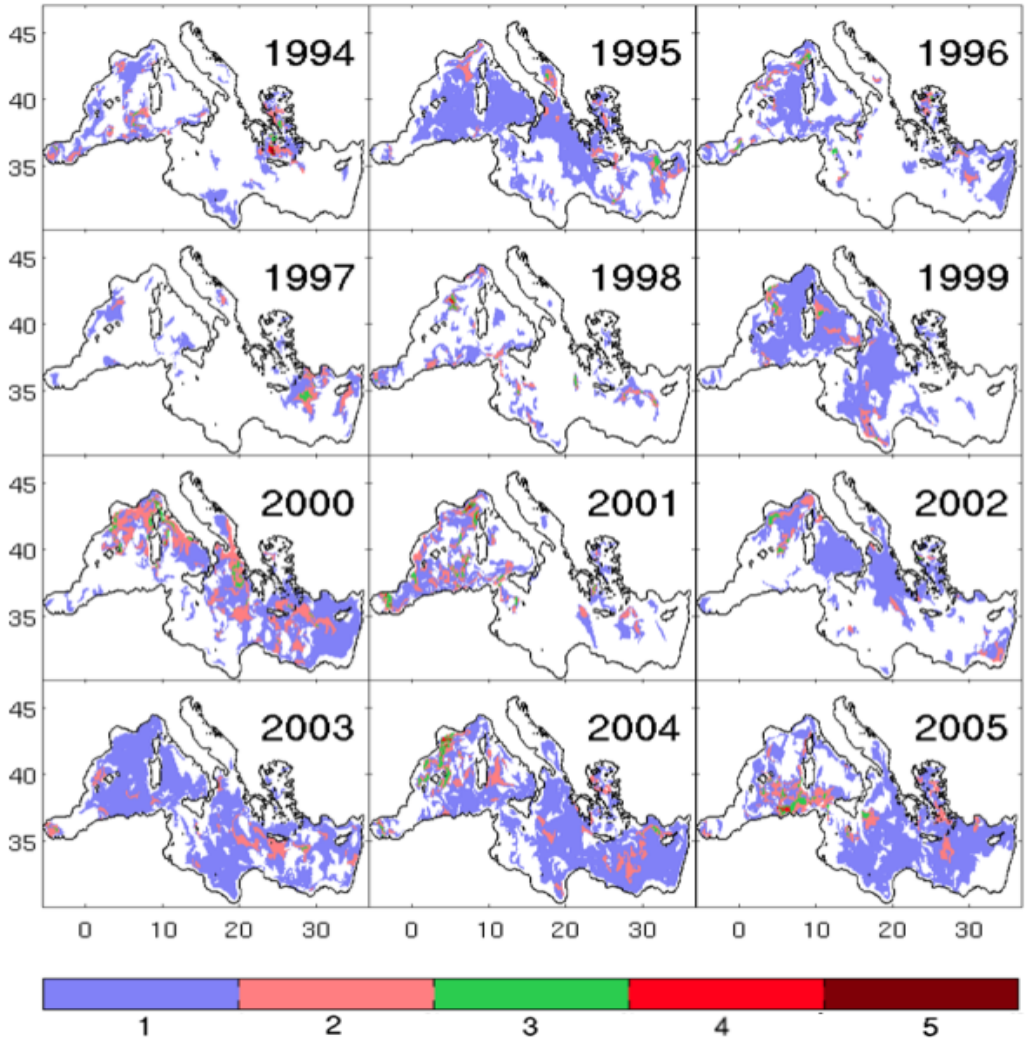

Figure 4.5. Annual maps of occurrence of the winter-spring macro-events (1994-2005). The coloured regions are referred to the areas covered by the macro-events, in a total number indicated by the colorbar.

taining the statistics of the **annual series** of the total number of macro-events and of the total coverage of the Mediterranean Sea associated to them, together with the medians of the mean severity and of the anomaly indexes.

The **number of macro-events** per year oscillates around a median value of 51 with an interannual variability (defined as the semi-range[4] of values divided by the median value) of 37%. The annual series does not exhibit an evident trend, with the highest numbers of macro-events occurring in 2000, 2009, 2010 and 2011 (not shown).

Further, we do not observe trend in the total percentage of the Mediterranean **coverage** ascribed to the macro-events, that oscillates around a median

[4]where the range of a data distribution is defined as the difference between the maximum and the minimum values

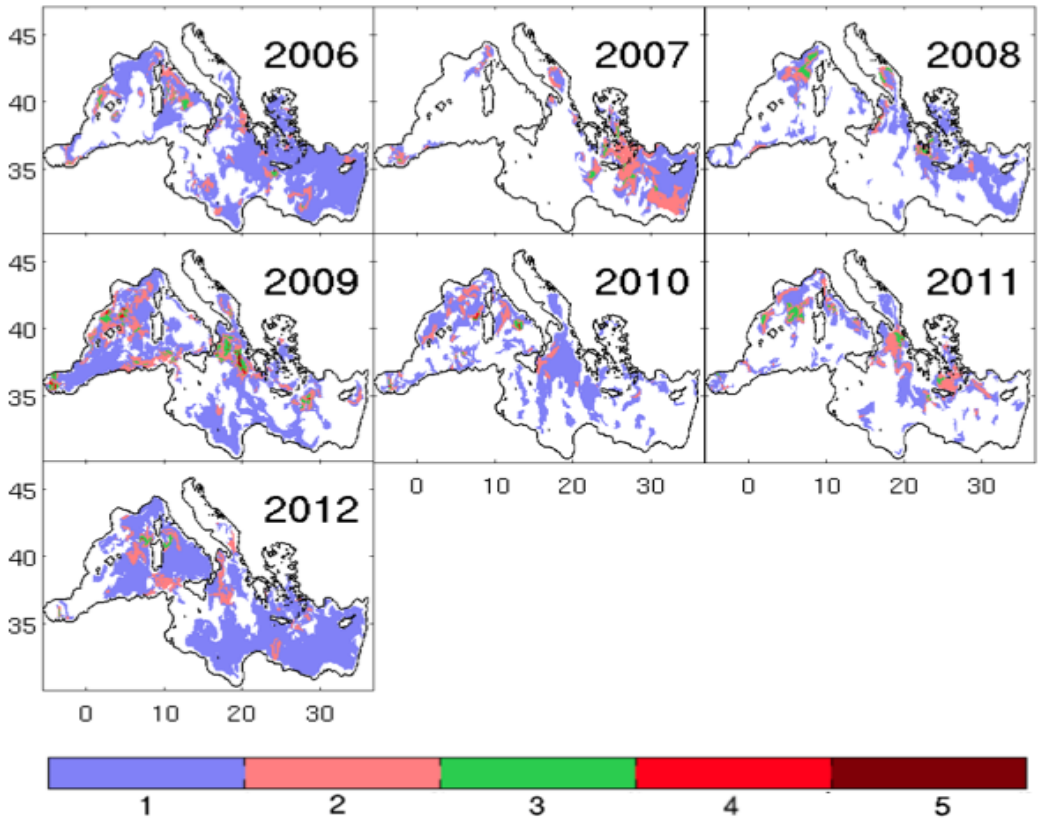

Figure 4.6. Annual maps of occurrence of the winter-spring macro-events (2006-2012). The coloured regions are referred to the areas covered by the macro-events, in a total number indicated by the colorbar.

	Min	**Max**	**P50**	**Var**
Nr. macro-events	30	68	51	37%
Mediterranean coverage	0.15	0.74	0.39	75%
$<\mathbf{S}>_{p50}$ $(kg/km^2/day)$	0.51	0.68	0.61	14%
$\mathbf{AN}_{p50}$	0.05	0.10	0.07	39%

Table 4.2. Statistics (minimum, maximum, median values and interannual variability as semi-range divided by the median) for the annual series, on the basin scale, of the total number of macro-events, the percentage of the Mediterranean domain covered by macro-events and the medians of their mean severity and anomaly.

value equal to 0.39 with an interannual variability of 75%.

There is not a clear correlation between total area and total number of macro-events. In fact, for the years showing the highest values of the total

area, the correspondent total number of macro-events for some years (1995 and 2012) is a relative minimum, but for others (2000 and 2009) is a relative maximum (not shown). However, the relative maxima in the annual series of the Mediterranean coverage are reached in all the years associated to the seven more extended single macro-events (with area larger than 500×10^3 km^2), as expected due to their extention, but also in 2009 (not shown).

As regards the annual series of the medians of **mean severity** and **anomaly**, the first one displays quite stable values in the 19 years around the total median value (variability of 14%), whereas the second one has a higher variability (39%, almost triple than the one of the mean severity). This means that, on average, there are years characterized by macro-events very anomalous even if their severity is not much higher than the median value. On the other hand, 2012 emerges as an year characterized by macro-events with very high values both of mean severity and anomaly with respect to the median values computed on the whole period (not shown).

4.1.2 The subdomain scale

The macro-events described in the previous section can be also analysed according to the sub-region they affect. In particular, the macro-events related to the North Western Mediterranean Sea (NWM), the Ionian Sea (ION), the Southern Adriatic Sea (ADS) and the Levantine Sea (LEV) subdomains are now discussed as distinct classes.

According to the metrics of the macro-events (sec. 3.3), each macro-event is attributed predominantly to the subdomain including its position coordinates (lon, lat). However, the macro-event can cover also neighbour subdomains. Therefore, within each of the 4 classes, a subclass of macro-events entirely contained (*internal*) in the subdomain can be identified. The total number of macro-events and the portion of internal macro-events in the 4 considered subdomains are indicated in tab. 4.3.

In principle, only the internal macro-events can be considered fully representative of the subdomain they belong. Nevertheless, the compliance of the

Nr. macro-events	**total**	**internal**
NWM	178	118
ION	163	143
ADS	36	28
LEV	172	127

Table 4.3. Number of macro-events occurred in the 4 Mediterranean subdomains, with subclasses indicated in the text.

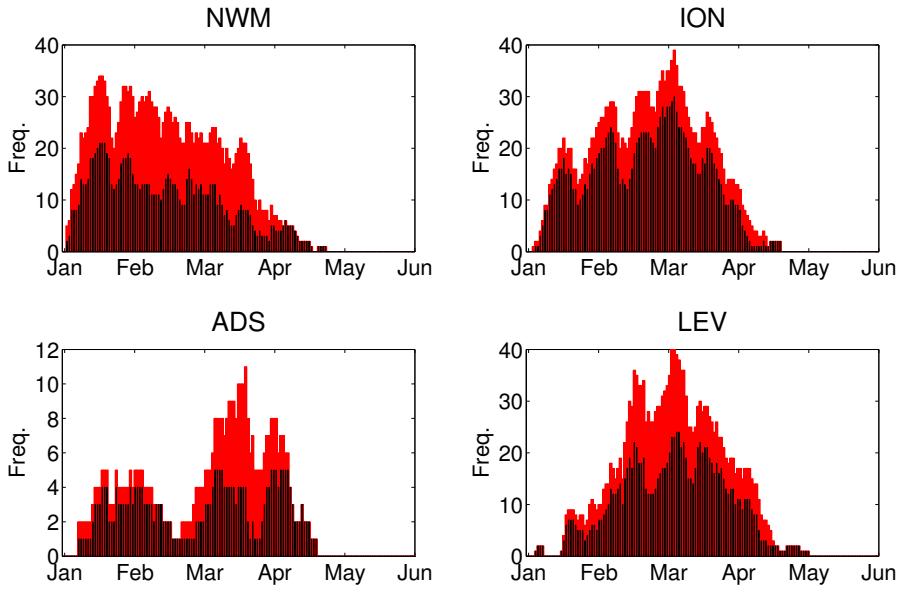

Figure 4.7. Frequency histogram of the developments day of the macro-events entirely contained (black series) and generally ascribed (red series) to the 4 subdomains NWM, ION, ADS and LEV (defined in fig. 3.4), in the Jan-May period.

features of the totality of the macro-events ascribed to the subdomain with respect to the features emerging from the internal ones are here evaluated, to decide whether to include all the macro-events of the 4 classes in the analysis.

In fig. 4.7 the frequency distribution of the **time development** of the macro-events in the January-May period is displayed for the internal macro-events and for all the macro-events ascribed to the subdomains.

The internal macro-events occurred in the North Western Mediterranean Sea are concentrated in the winter period, with a probability decreasing toward the spring months. In the Ionian and Levantine Sea they occur mainly in the late-winter early-spring period, whereas in the Southern Adriatic Sea their time distribution is trimodal, with macro-events developing in the first half of February, in middle March and in the first half of April.

In all cases, the shape of the distributions referred to the totality of the macro-events does not deviate significantly from the correspondent distributions of the internal macro-events. The main difference is observed in the Southern Adriatic subdomain, where the increase of the frequency of macro-events during March follows the same feature of the neighbour Ionian Sea subdomain. The trimodal trait of the distribution is however preserved.

The frequency distribution of the **mean severity** is shown in fig. 4.8 and exhibits a clear decreasing eastward gradient, as a feature of both internal and total macro-events in the subdomains. This characteristic clearly reflects the de-

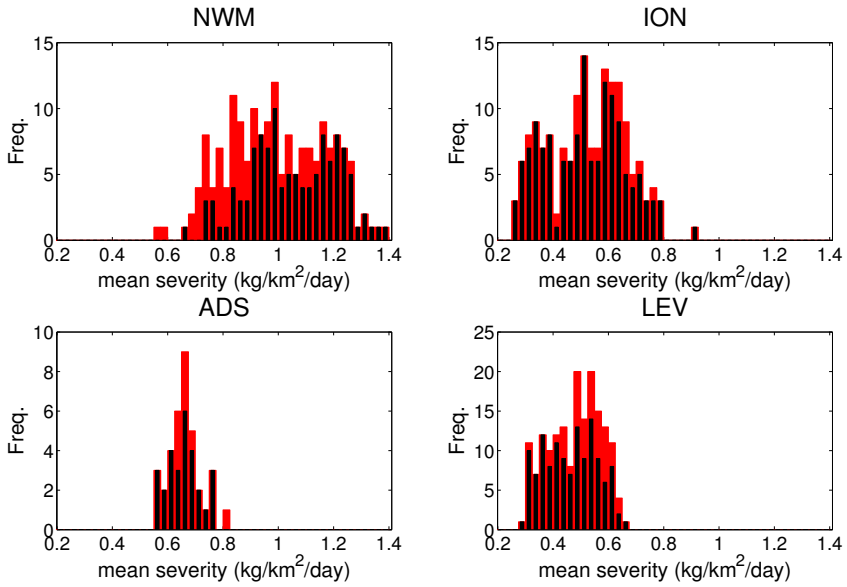

Figure 4.8. Frequency histogram of the mean severity of the macro-events entirely contained (black series) and generally ascribed (red series) to the 4 subdomains NWM, ION, ADS and LEV (defined in fig. 3.4), in the Jan-May period.

creasing eastward gradient of surface chlorophyll observed in the Mediterranean Sea and the patterns of 99th percentile thresholds already shown (fig. 3.3). In particular, the median values of the total distributions are equal to 0.99 (NWM), 0.65 (ADS), 0.53 (ION), 0.49 (LEV) $kg/km^2/day$. The highest range of the mean severity is observed in the North Western Mediterranean Sea, whose value is about 0.82 $kg/km^2/day$, whereas the lowest range is in the Southern Adriatic Sea, with a value of 0.27 $kg/km^2/day$. This means that the most severe macro-events occur in the North Western Mediterranean Sea, but in different possible extents. On the contrary, in the South Adriatic Sea the (fewer) macro-events are characterized by a more constant mean severity. This feature may be ascribed to the constraints of the topography and of the circulation structure (South Adriatic Gyre) on this subdomain, that lead to macro-events with quite regular mean severity.

Fig. 4.9 displays the frequency distribution of the **anomaly** index, without remarkable differences in the two distributions (internal and total). The Southern Adriatic Sea has the highest median value (0.12), followed by the one of the North Western Mediterranean Sea (0.09). The macro-events occurring in these two subdomains are therefore more anomalous with respect to the other two regions, where the median values are lower (about 0.06). Moreover, the Ionian Sea shows also a significant positive asymmetry index (0.25, not shown), i.e. there are few macro-events in this subdomains with (relatively) higher anomaly. These events are concentrated in the Western and Northern Ionian Sea.

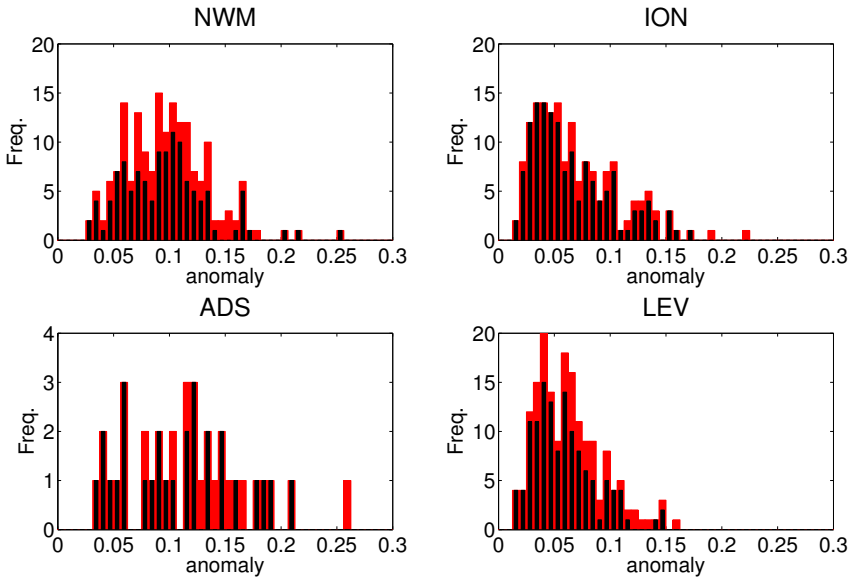

Figure 4.9. Frequency histogram of the anomaly of the macro-events entirely contained (black series) and generally ascribed (red series) to the 4 subdomains NWM, ION, ADS and LEV (defined in fig. 3.4), in the Jan-May period.

Finally, it is noticeable that the South Adriatic Sea displays a high range of anomaly (0.23), even if its range of mean severity is relatively low. As already mentioned, macro-events with high values of anomaly in a domain involve atypical sub-regions, i.e. sub-regions with (relatively to the domain scale) low 99th percentile thresholds of chlorophyll. In the ADS case, the topographic and circulation constraints could not only result in a regularity of the macro-events mean severity (low range in ADS, fig. 4.8), but also confine the interannual forcing conditions that can sustain macro-events also in atypical regions. As a consequence, the variability of the anomaly in the ADS is high (i.e. same order of magnitude of the ones of the other subdomains even if the variability of its mean severity is lower than the one of the others), showing that the ADS can be considered a region subjected to atypical behaviours in terms of highly impacting macro-events.

Finally, the frequency distribution of the **uniformity** index is represented in fig. 4.10. Here the main difference between the distribution referred to all the macro-events and to the internal ones is observed in the North Western Mediterranean Sea and in the Southern Adriatic subdomains. In these cases the macro-events not entirely contained in it correspond to uniformity values lower than the minimum reached by the internal macro-events (that is equal to 0.16 and 0.19, respectively). Nevertheless, the shift of the medians referred to the distributions of the internal and of the total macro-events is lower than 4% and therefore also in this case the differences in the two distributions were considered negligible. Overall, the median value in the Southern Adriatic Sea

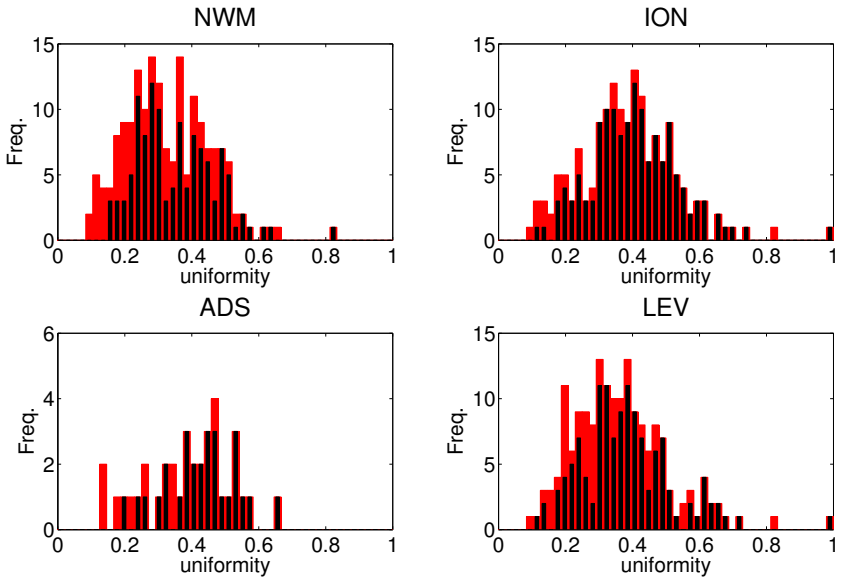

Figure 4.10. Frequency histogram of the uniformity index of the macro-events entirely contained (black series) and generally ascribed (red series) to the 4 subdomains NWM, ION, ADS and LEV (defined in fig. 3.4), in the Jan-May period.

is the highest (0.41), followed by the values 0.39 in ION, 0.35 in LEV and 0.31 in NWM. This means that the most uniform macro-events in the 4 considered subdomains are in the South Adriatic Sea. Also for this index, as for the mean severity and the anomaly, the results referred to the ADS can be interpreted in light of the spatial constraints, that promote persistent macro-events in the subdomain area. The ION and LEV subdomains contain also the two macro-events with uniformity $U = 1$, of only 1 day duration, already mentioned in sec. 4.1.1.

Since the overall differences between the two kinds of frequency distribution referred to total and internal macro-events were considered negligible for the main indexes, hereafter the totality of the macro-events ascribed to the 4 subdomains is used as the representative sample for the subdomains.

Tab. 4.4 summarizes the main statistics of the **annual series** of the total number of macro-events and of their median values of mean severity and anomaly in the 4 subdomains.

First of all, in all subdomains there is at least one macro-event in the simulated period. In particular, the Adriatic Sea shows for the most of the years only one macro-event, and the maximum number is equal to 4 in 2007-2009 and 2012. The medians for the other sub-domains are 10 (NWM), 8 (ION), 9 (LEV), without evident trends (not shown).

		Min	Max	P50	Var
Nr. macro-events	**NWM**	3	18	10	75%
	ION	1	18	8	106%
	ADS	1	4	1	150%
	LEV	2	18	9	89%
<S>$_{p50}$ $(kg/km^2/day)$	**NWM**	0.81	1.13	1.00	16%
	ION	0.39	0.65	0.55	24%
	ADS	0.56	0.75	0.65	15%
	LEV	0.41	0.60	0.49	19%
AN$_{p50}$	**NWM**	0.05	0.13	0.10	42%
	ION	0.04	0.10	0.06	55%
	ADS	0.03	0.19	0.12	64%
	LEV	0.04	0.10	0.06	45%

Table 4.4. Annual statistics (minimum, maximum, median and interannual variability defined as the semi-range divided by the median) of the number of macro-events and of the medians of their mean severity and anomaly in the 4 subdomains.

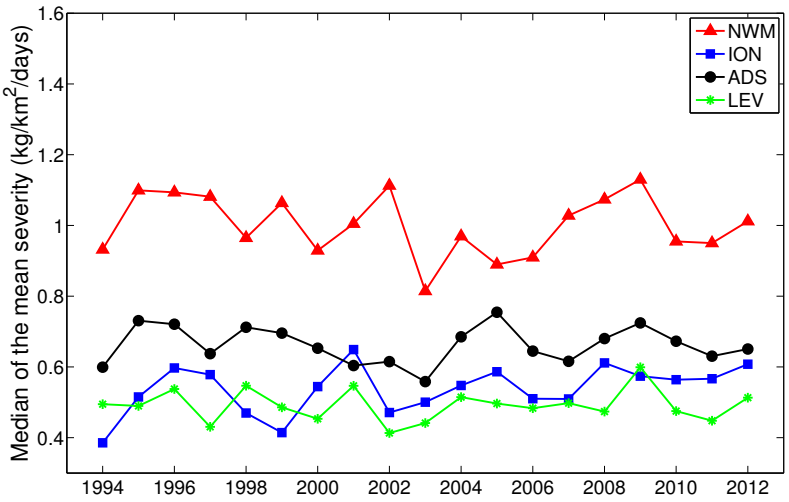

Figure 4.11. Median of the values of mean severity of the macro-events occurred predominantly in the 4 subdomains at each year.

As regards the mean severity, the annual series of its median values are displayed in fig. 4.11, where the eastward decreasing gradient across the 4 subdomains (a well-known feature, already noticed in the frequency distributions) is mantained in the median values of almost every year, except 4 cases in which the LEV medians are higher than the ION ones and one year in which on average the ION values are higher than the ADS ones.

In fact, the ION is the subdomain with the highest interannual variability (24%) and, moreover, it is also the only one displaying a positive trend.

Overall, the annual series of the median values of mean severity are more stable with respect to the ones referred to the anomaly, as in the basin scale case. In fact, the time variability associated to the medians of anomaly are at least double and in the ADS case quadruple with respect to the correspondent mean severity.

4.2 Classification

In order to classify the macro-events according to their potential impact on the ecosystem, the medians of the mean severity and of the anomaly distributions on the whole domain (tab. 4.1) were chosen as **basin-scale references**. Therefore, macro-events with values of mean severity (anomaly) higher than the median value of the same index on the whole basin are defined as macro-events with high (H) mean severity (anomaly). Conversely, values of the mean severity (anomaly) lower than the median on the basin scale are defined as macro-events with low (L) mean severity (anomaly).

Representing each macro-event occurring in the Mediterranean Sea as a dot in the **anomaly** *vs* **mean severity plane** (fig. 4.12), the two basin-scale medians, represented by the vertical and horizontal dashed lines, divide the plane in 4 quarters, allowing to classify the macro-events in the 4 groups determined by the combinations of the two indexes. Starting from the first quarter (top right with respect to the intersection of the two medians) and proceeding counter-clockwise, the quarters identify macro-events with high-high (HH), low-high (LH), low-low (LL), high-low (HL) values of the mean severity and anomaly, respectively. Clearly, the macro-events with the highest impact on the ecosystem are identified by the HH quarter.

With this basin-scale reference, the macro-events belonging to the 4 subdomains were represented in the same plane in the figs. 4.13-4.14. The number of macro-events turning up in each quarter is indicated in tab. 4.5 for the 4 considered subdomains.

Overall, the macro-events in the North Western Mediterranean Sea (fig. 4.13(a)) and in the Southern Adriatic Sea (fig. 4.14(a)) are definitely (78% and 71% of the total, respectively) characterized by high mean severity and high anomaly. The Ionian Sea and the Levantine Sea are instead subdomains of occurrence of macro-events mainly with low mean severity and low anomaly (51% and 63% of the total cases, respectively). Moreover, in the Levantine Sea almost

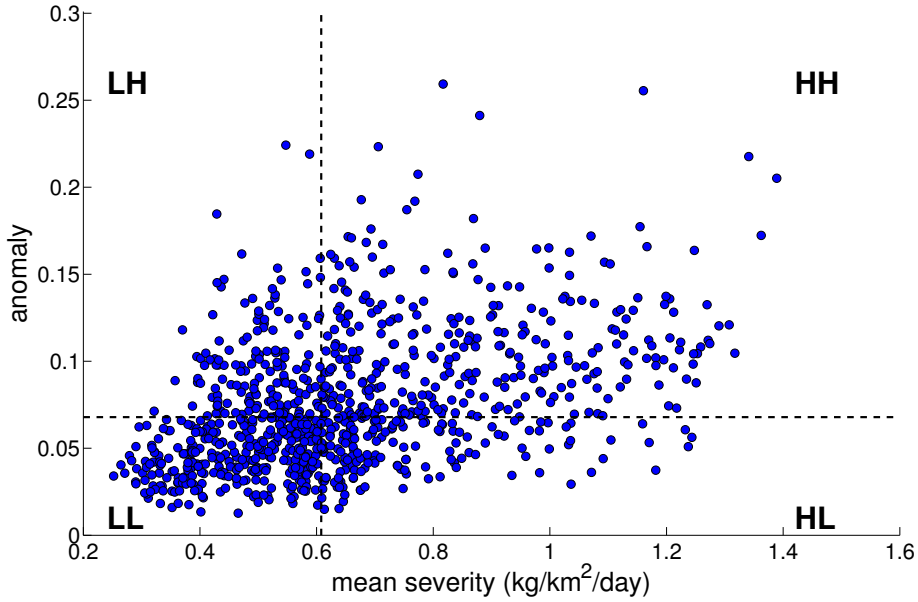

Figure 4.12. Distribution of mean severity and anomaly for all the winter-spring macro-events occurred in the Mediterranean Sea in the 1994-2012 simulated period. The median values of the indexes on the basin scale are indicated by the dashed lines and divide the plane in 4 quarters, defined in the text. Acronyms: HH= high mean severity and high anomaly, HL= high mean severity and low anomaly, LH= low mean severity and high anomaly, LL= low mean severity and low anomaly.

Nr. of macro-events	HH	LH	LL	HL
NWM	138	0	2	38
ION	38	28	84	13
ADS	25	3	4	4
LEV	12	50	109	1

Table 4.5. Number of macro-events occurred in the 4 Mediterranean subdomains, classified by their combination of mean severity and anomaly indexes, as defined in the text.

all of the macro-events (92%) have low values of the mean severity index. Nevertheless, both in this subdomain and in the Ionian Sea there are also macro-events heavily impacting on the ecosystems (23% and 7% of the total number, respectively). On the whole, the Ionian Sea is the region with higher variance with respect to the medians on the basin scale.

The coordinates of the macro-events with higher mean severity and anomaly in the Ionian Sea (fig. 4.15(a)) and in the Levantine Sea (fig. 4.15(b)) show that they are concentrated in the central and western part of the North Ionian

Sea and in the southern coast of Sicily (ION) and in the Rhodes Gyre and Western Cretan Gyre regions (LEV). Despite the two subdomains are generally characterized by macro-events with low mean severity and low anomaly, these regions can be therefore considered basin scale hot-spots for sporadic macro-events with heavy impacts on the ecosystem on a basin scale reference.

In particular, in the LEV subdomain, the HH macro-events cover areas between 3 and 20 $\times$ 10^3 km^2 for a number of days between 3 and 21 and with a median of the uniformity index equal to 0.46 (higher than the overall LEV median, equal to 0.35). In the ION subdomain, instead, the same indexes are referred to larger ranges of the same indexes. In fact, these macro-events cover areas between 1.6 and 230 $\times$ 10^3 km^2, for a number of days between 5 and 58 and a median of the uniformity index of the same order of the overall ION distribution. We assume that such a wide range of the shape parameters can be attributed to the different possible processes supporting the macro-events in the ION subdomain (e.g. cyclonic dynamics, coastal upwelling). Nevertheless, further analyses should be conducted to point out these relationships.

Finally, since the 78% of the macro-events of the North Western Mediterranean Sea are located in the HH quarter, in order to visualize the areas of this subdomain with the highest values of the two indexes, the 90th percentile threshold computed on the whole basin was selected as the reference for the very high (VH) values of both mean severity and anomaly in this subdomain. As can be seen in fig. 4.16, the most severe and anomalous macro-events in this area are concentrated mainly in the Gulf of Lion, but we can observe few of them also in the Catalan Sea and in the Ligurian Sea.

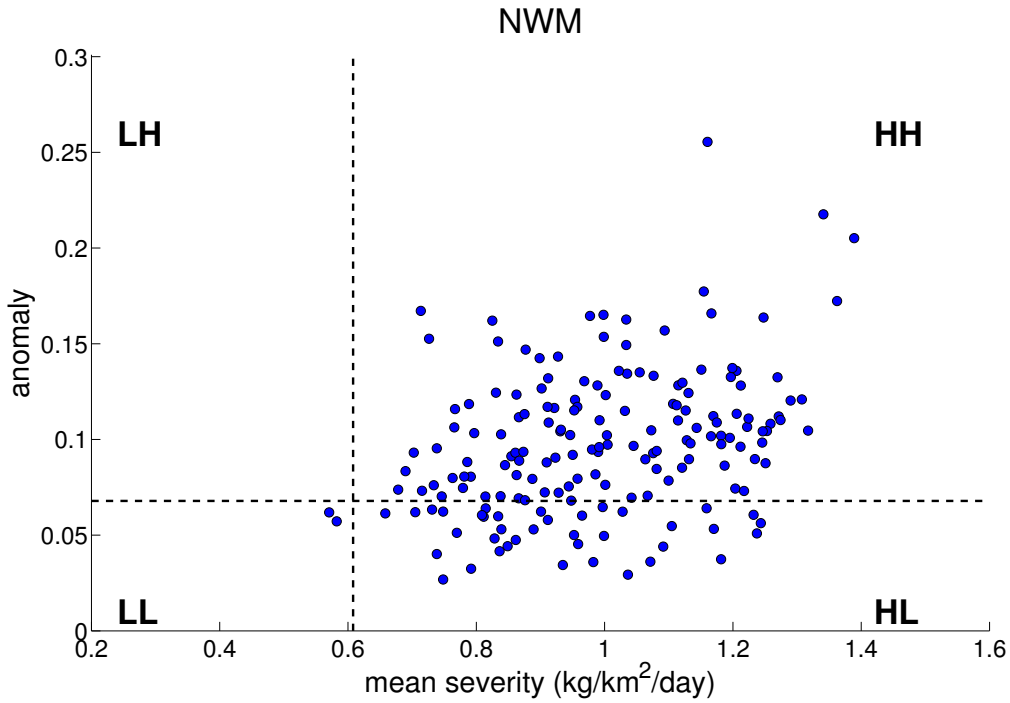

(a)

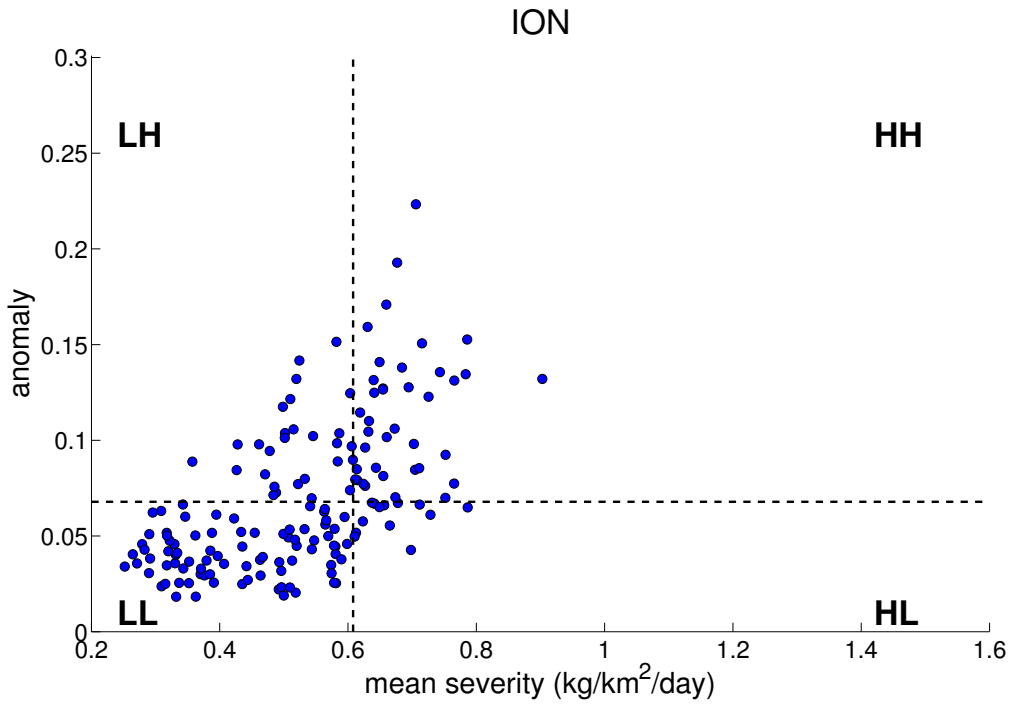

(b)

Figure 4.13. Mean severity and anomaly for the macro-events occurred in the North Western Mediterranean Sea (a) and in the Ionian Sea (b) in the 1994-2012 simulated period. Dashed lines and acronyms like in fig. 4.12.

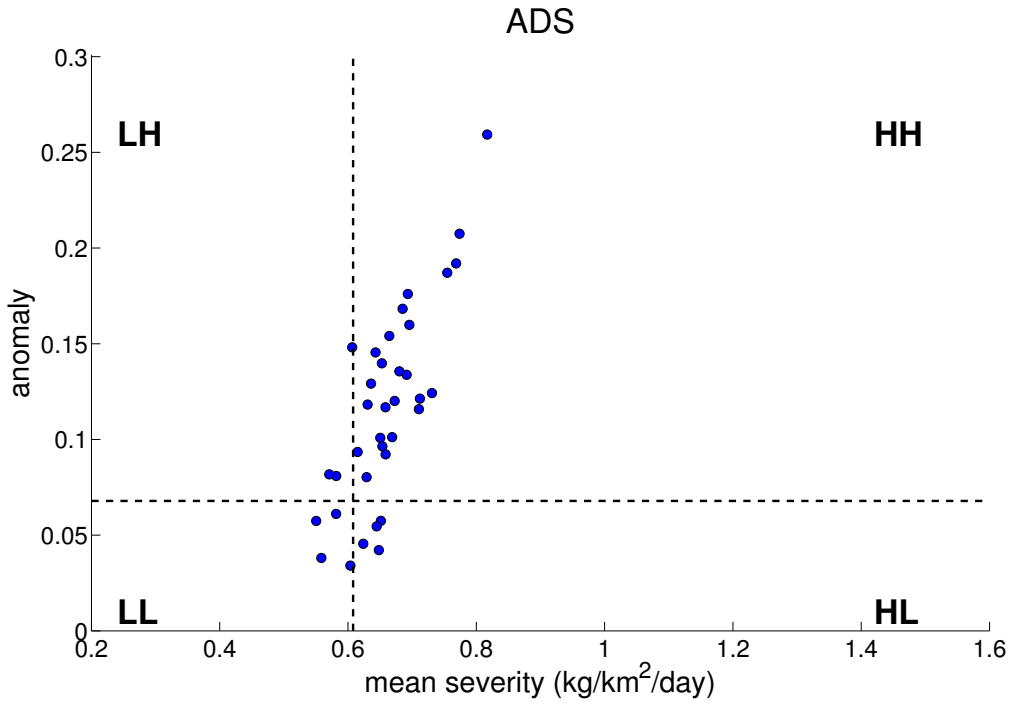

(a)

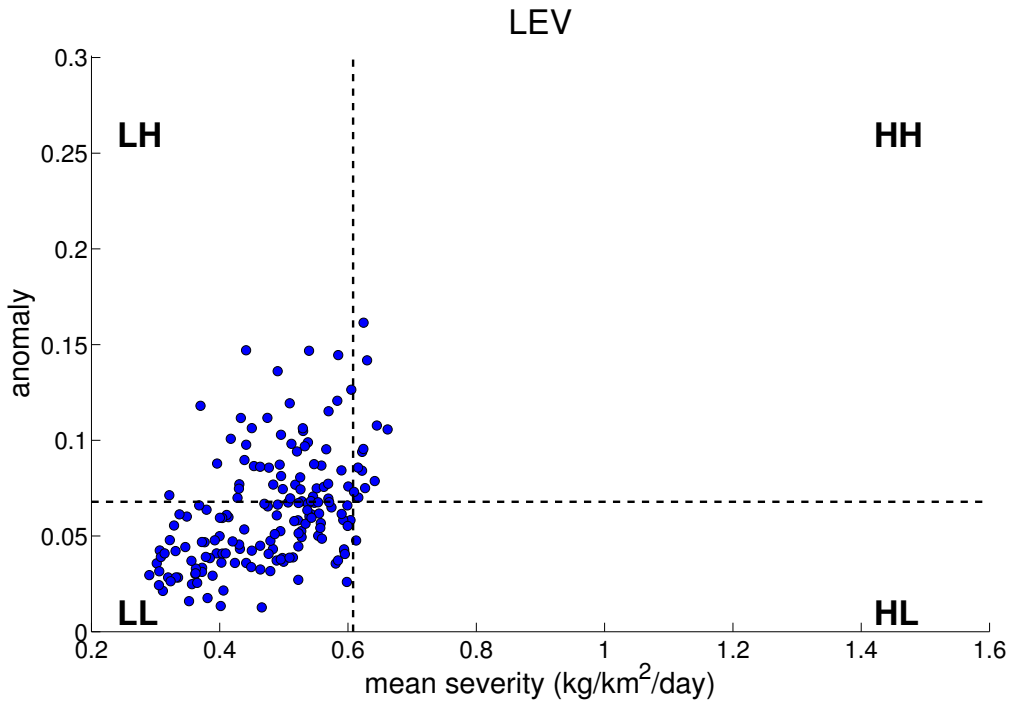

(b)

Figure 4.14. Mean severity and anomaly for the macro-events occurred in the South Adriatic Sea (a) and in the Levantine Sea (b) in the 1994-2012 simulated period. Dashed lines and acronyms like in fig. 4.12.

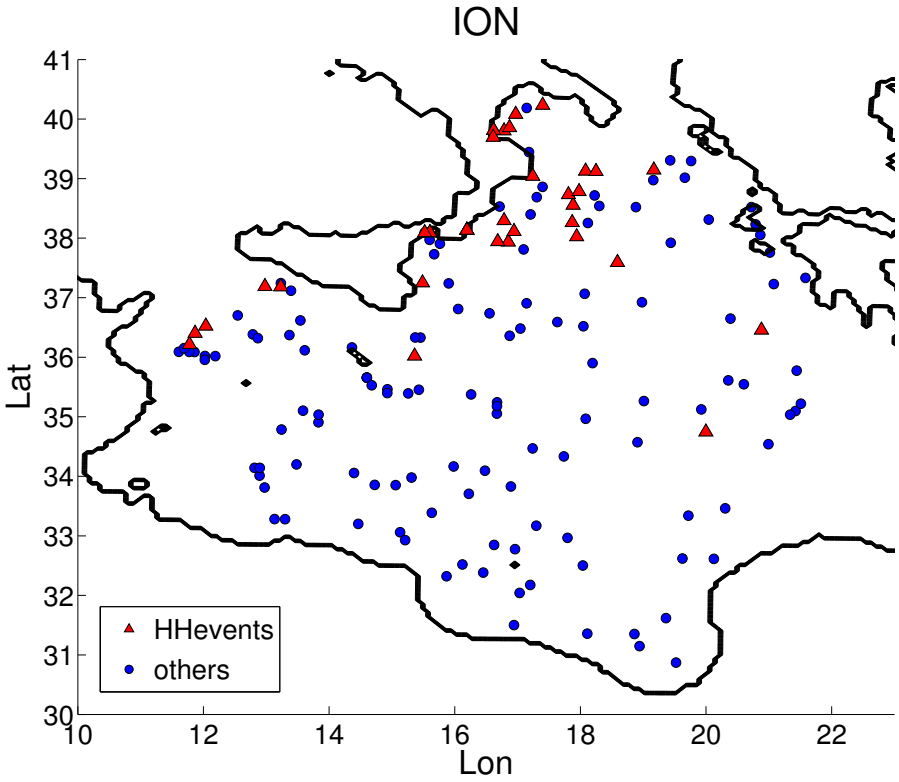

(a)

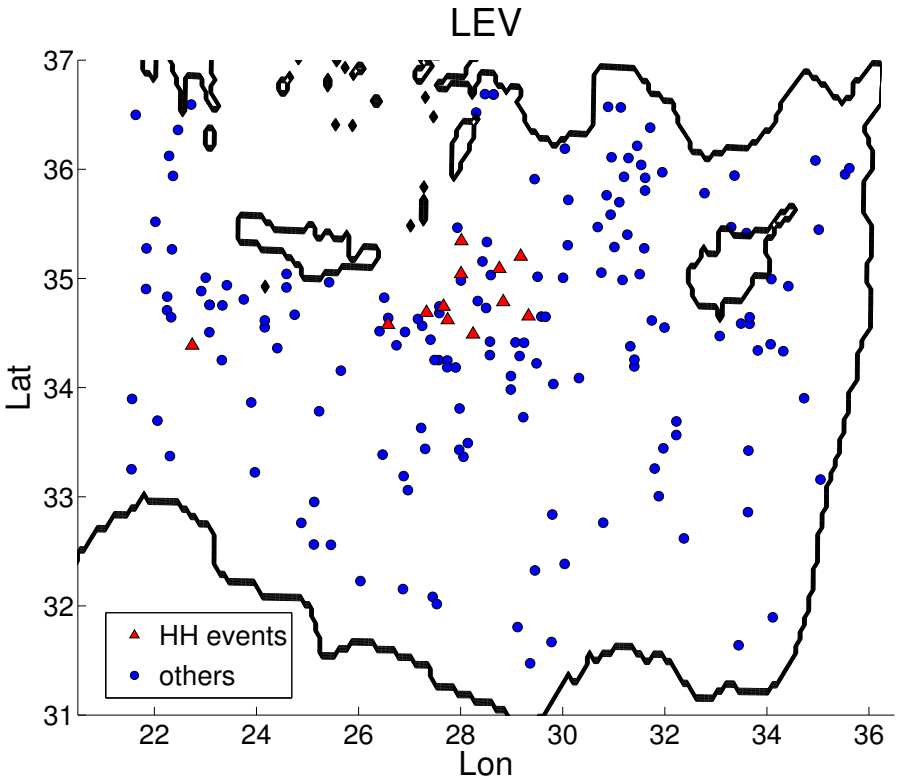

(b)

Figure 4.15. Spatial distribution of the macro-events characterized by high severity and high anomaly (HH, red triangles) and by lower values of the two indexes (blue circles), in the Ionian Sea (a) and in the Levantine Sea (b). The position of each macro-event is referred to the local maximum of chlorophyll within the macro-event.

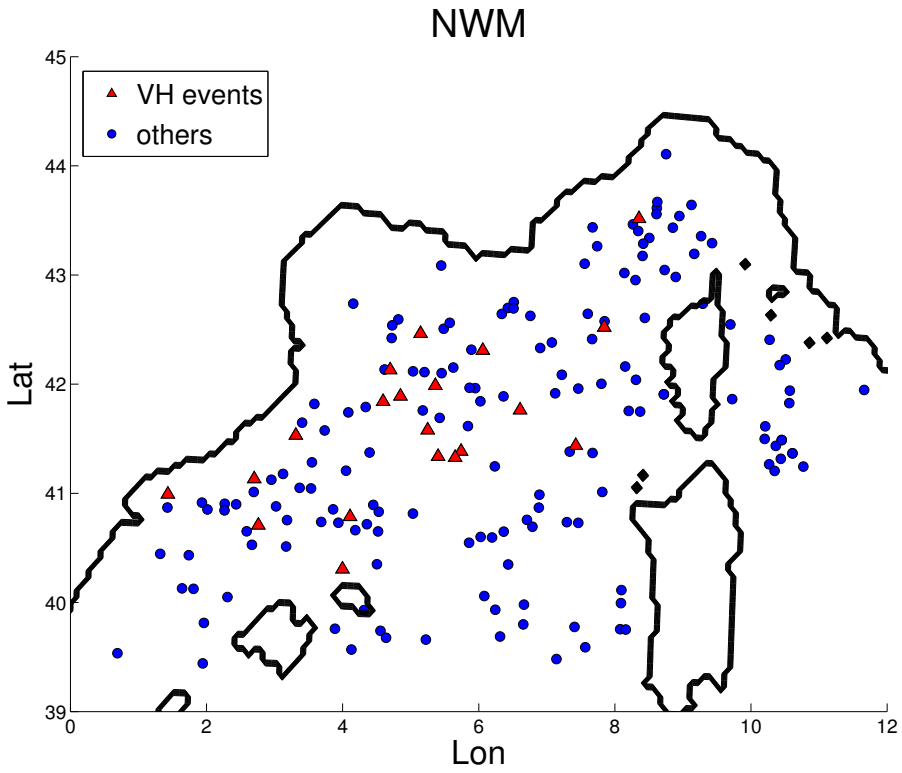

Figure 4.16. Spatial distribution of the macro-events occurred in the North Western Mediterranean Sea, characterized by severity and anomaly above the 90th percentile threshold computed on the basin scale (indicated as very high, VH, red triangles) and by lower values of the two indexes (blue circles).

Chapter 5

Representative macro-events of chlorophyll

This section describes details of some surface chlorophyll macro-events that significatively affected the Mediterranean open sea ecosystem, as reproduced by the multi-decadal simulation (1994-2012).

The selected macro-events belong to the HH quarter of the anomaly vs mean severity plane (fig. 4.12) and supplied a quantity of chlorophyll to the involved areas that was very high and anomalous on the basin scale reference. This means that they had the heaviest impacts on the ecosystem, as illustrated in sec. 3.3. These macro-events occurred in the North Western Mediterranean Sea, South Adriatic Sea and Levantine Sea subdomains, whose spatial limits and nomenclature were defined in sec. 3.2.1 and whose statistics referred to the macro-events indexes was presented in sec. 4.1.2. In the NWM and LEV cases, the ESA-CCI satellite data (`http://marine.copernicus.eu/` and [Volpe et al., 2017]) are also displayed, in order to draw a qualitative comparison between the model-derived macro-events and the available observations. In the discussed examples, the spatio-temporal dynamics of the phytoplankton chlorophyll is also investigated in the four phytoplankton components (introduced in sec. 2.2).

5.1 North Western Mediterranean Sea (2005)

The selected macro-event occurred in an area of about 33 $\times 10^3$ km^2 of the Gulf of Lion region (fig. 5.1), from the 15th to the 31st March 2005 (early-spring period).

This is the macro-event that had the most significant impact in the Mediterranean open sea ecosystem in the whole simulation. In fact, due to its mean severity equal to 1.389 $kg/km^2/day$, it is the **most severe macro-event** in the totality of the 933 macro-events detected in the investigated period. Moreover, it is also the 9th macro-event more **anomalous**, with an anomaly index equal to 21%. This means that the huge amount of chlorophyll that

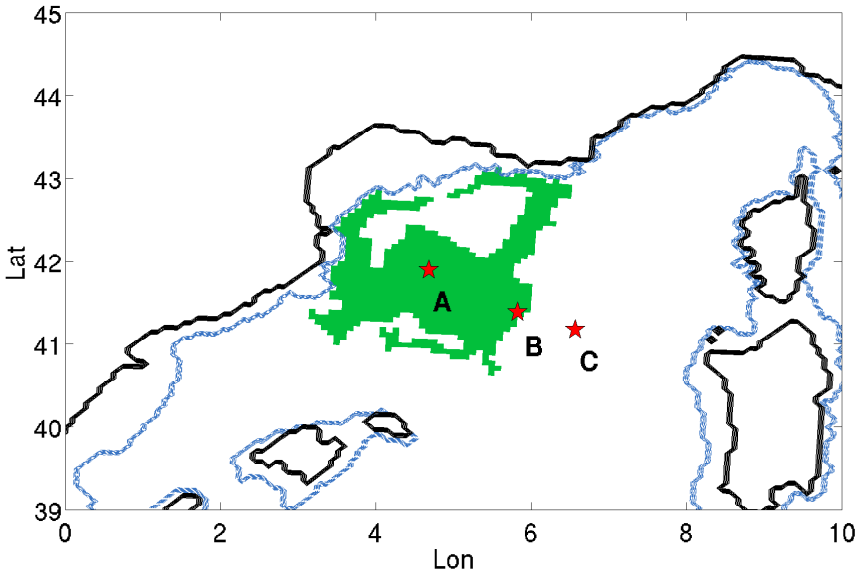

Figure 5.1. Area of the macro-event of chlorophyll occurred in the Gulf of Lion from the 15th to the 31st March 2005 (green patch). The red stars indicate grid points in central (A), peripheral (B) and external (C) positions with respect to the macro-event. The blue contours limit the open sea (i.e. depths higher than 200 m).

it supplied was also considerably higher than the carrying capacity of the impacted ecosystem.

Fig. 5.2(a) shows the map of the chlorophyll mass M_{chl} supplied by all the local extremes involved in the macro-event (sec. 3.2.1). This figure highligths the points of higher supply of chlorophyll to the local ecosystem (central part of the macro-event).

Fig. 5.2(b) displays the map of the local anomaly of chlorophyll, defined as the ratio between M_{chl} and the chlorophyll intensity above the 99th percentile threshold I_{chl}. It allows to identify the points in which the chlorophyll values were anomalously high with respect to the local capacity of the ecosystem. This pattern largely coincides with fig. 5.2(a), but extends to a wider central region. It provides evidence that there exist areas in which the chlorophyll values are anomalously higher than the local thresholds, even if their absolute values are relatively low.

Fig. 5.3 shows the maps of the surface chlorophyll (left column) and of the surface nitrate (right column), in selected days during the period of development of the macro-event. The middle panels show the red patterns that represent the evolution of the macro-event superimposed to the surface velocity field, following the same scheme of fig. 3.6.

The general interpretation of this macro-event is similar to the case already

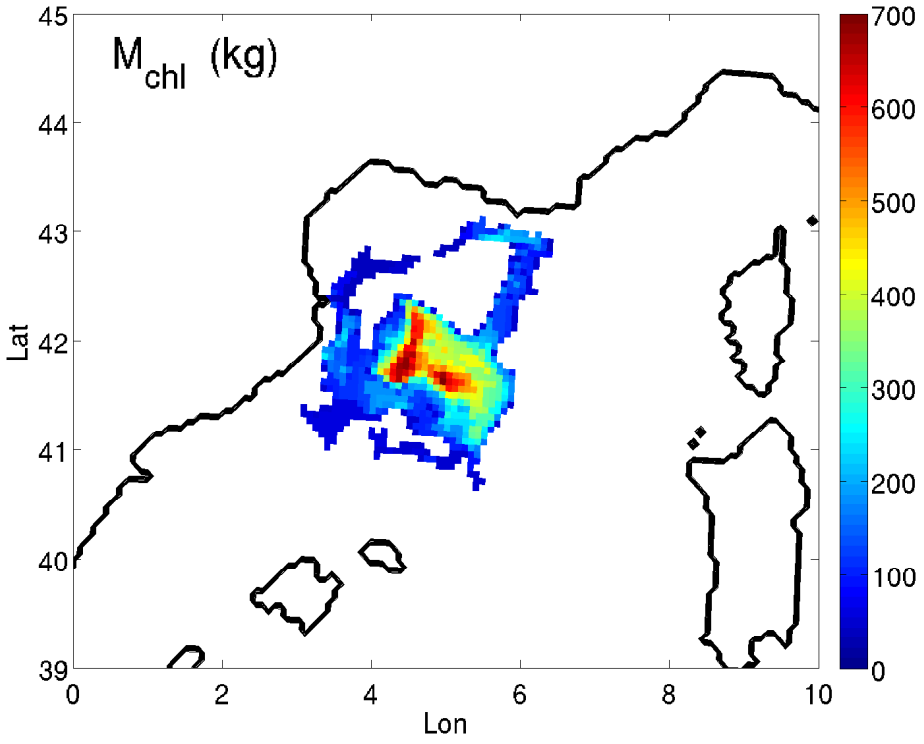

(a)

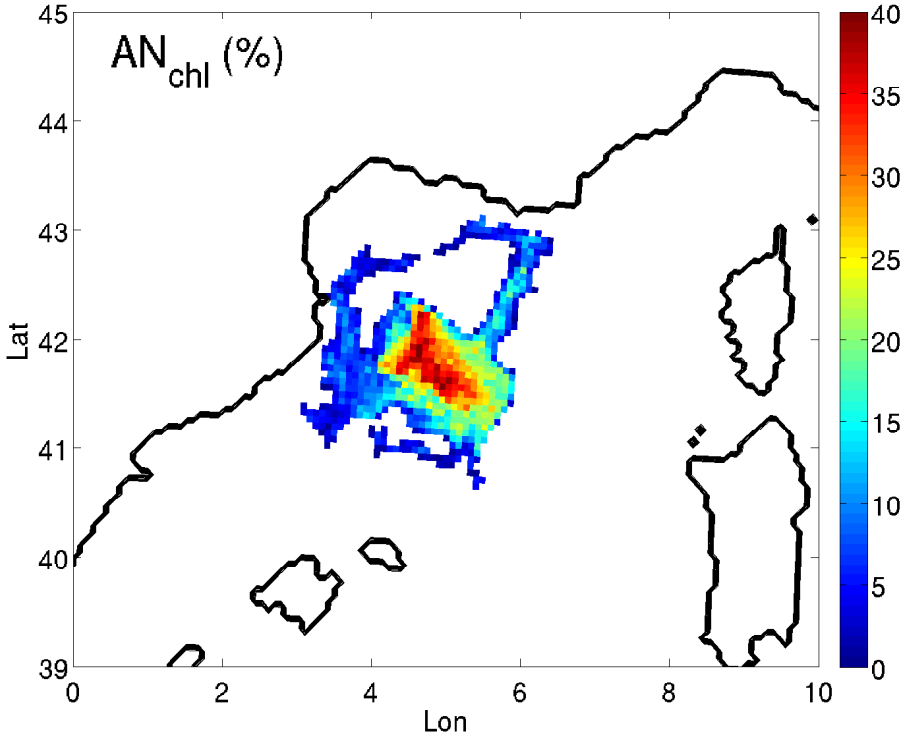

(b)

Figure 5.2. Maps of the chlorophyll mass supplied to the first meter of depth by all the local extremes involved in the NWM macro-event (a) and of the local anomaly (b).

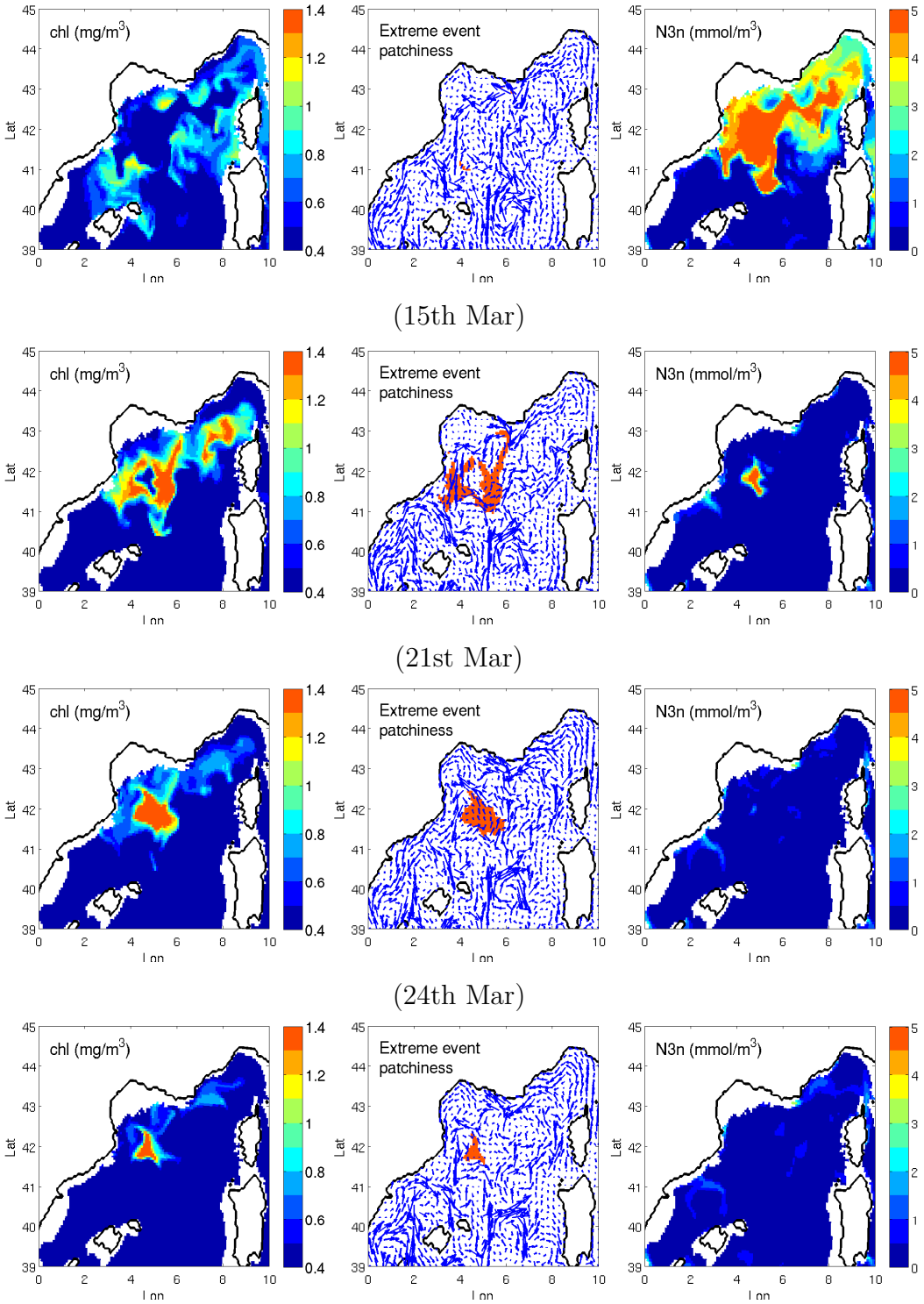

Figure 5.3. Maps of the surface chlorophyll (first column), daily portion of the macro-event area superimposed to the surface velocity field, (second one) and surface nitrate (third one), for some single days of development of the macro-event, occurred in the Gulf of Lion from the 15th to the 31st March 2005. The surface chlorophyll and nitrate are averaged in the first 10 m of depth. The horizontal velocity field (scaled by a factor 1.5) is referred to the depth of 5 m.

analysed in sec. 3.2.2, with the macro-event patches that appear to follow the convection weakening (by comparison of consecutive middle panels) and the patches of high nutrient concentrations (by comparison of each middle panel with the right panel referred to the day before).

Nevertheless, in this case the macro-event occurred almost a month later than the one in sec. 3.2.2 and it lasted for a shorter period (17 days rather than 25). Moreover, the convection area interested for the longer duration (identified by the *blue hole* pattern in the second left panel) is shifted with respect to the other previously analysed.

The model-derived chlorophyll patterns are in good agreement with the **remote sensing** (ESA-CCI) data in the same temporal interval of the macro-event (fig. 5.4). In the satellite maps, a strong increase of chlorophyll in the Gulf of Lion and in the Ligurian Sea is recognizable starting from 20th Mar, after a period of very low chlorophyll concentration (also lower than 0.05 mg/m^3, not

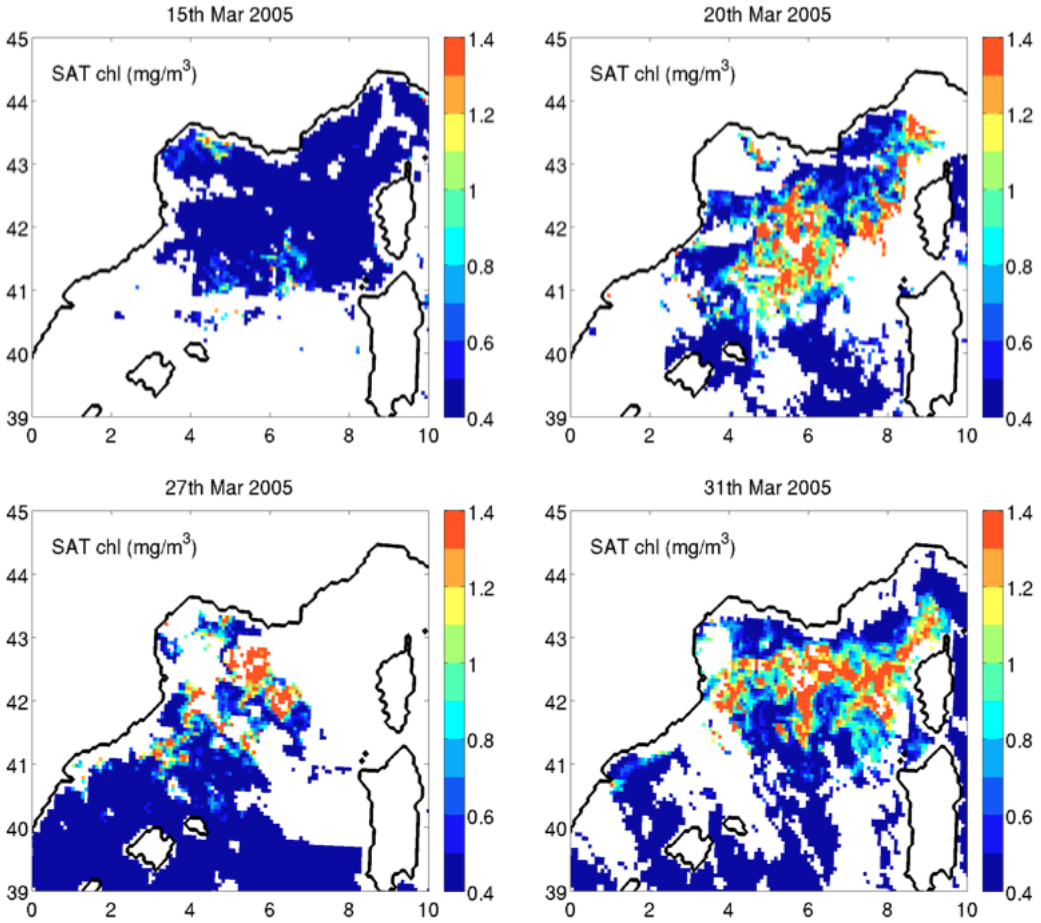

Figure 5.4. Maps of the satellite-derived surface chlorophyll for some single days of development of the model-derived macro-event in the NWM subdomain. Original data were interpolated on the MITgcm grid.

shown). The highest values of chlorophyll observed within the macro-event duration are equal to about 2.7 mg/m^3 (whereas the model-derived results reach 2.2 mg/m^3). Nevertheless, according to the satellite data, high values of chlorophyll (larger or equal to 1 mg/m^3) appear to be maintained until the end of April (not shown), whereas the model-provided chlorophyll does not exceed 0.8 mg/m^3 after the 1st April. We also observe that the cloud coverage affecting the remote sensing measurements is a limiting factor for the reconstruction of the spatio-temporal dynamics of the extremes of chlorophyll.

In order to highlight the **physical and biological processes** related to the macro-event, the spatial and temporal dynamics of the main variables provided by the model were reconstructed in some different **points** of the NWM subdomain, indicated in fig. 5.1. In particular, the first point (A) is located where the convection lasted for the longer time, in a central part of the macro-event area, the second one (B) is a peripheral point belonging to the macro-event and the third one (C) is external to the macro-event area and not involved in other macro-events detected in the same year.

Figs. 5.5, 5.6 and 5.7 display physical and biogeochemical variables (heat flux, mixed layer depth, potential temperature, nitrate and chlorophyll) in the points A, B and C, respectively, from January to April 2005. In each panel of the figures, the data referred to 2005 are compared with the correspondent climatological mean, computed on the 1994-2012 period. The net heat flux (top of each figure) is a forcing field for the simulation (sec. 2.1), here daily averaged to be compared with the daily output variables of the coupled model.

In point A, during the 30-40 days preceding the macro-event onset, strong heat losses up to 1000 W/m^2 (top panel of fig. 5.5) due to the wind fields (not shown) led to a **strong deep convection** that mixed all the water column, down to the sea bottom (second panel). Surface and subsurface nitrate, whose concentration at the beginning of the year was already above the climatological values, was further enhanced during the mixing (fourth panel). As soon as the stratification was quickly established (second panel) and the surface temperature rose (third panel), an abrupt rise of surface chlorophyll occurred (bottom panel). The surface chlorophyll, that in January, February and the first half of March had exhibited values much lower than the climatological ones due to the strong convective phase, in the third week of March increased by a factor of almost 800% in 4 days. A full consumption of surface nitrate can be observed in the same days (fourth panel). A following weaker mixing phase (in the half of April) replenished the surface layers with a relatively low amount of nitrate (yet above their climatological values), triggering two weak increases of chlorophyll. On the whole, the features here described are in agreement with the well known characterization of the chlorophyll blooms in the NWM area ([Barale et al., 2008], [Mayot et al., 2016]).

The interpretation of the results referred to the point B belonging to the macro-event (fig. 5.6) is similar to the point A, but in presence of a less intense vertical mixing. The heat losses reached values of 800 W/m^2 and

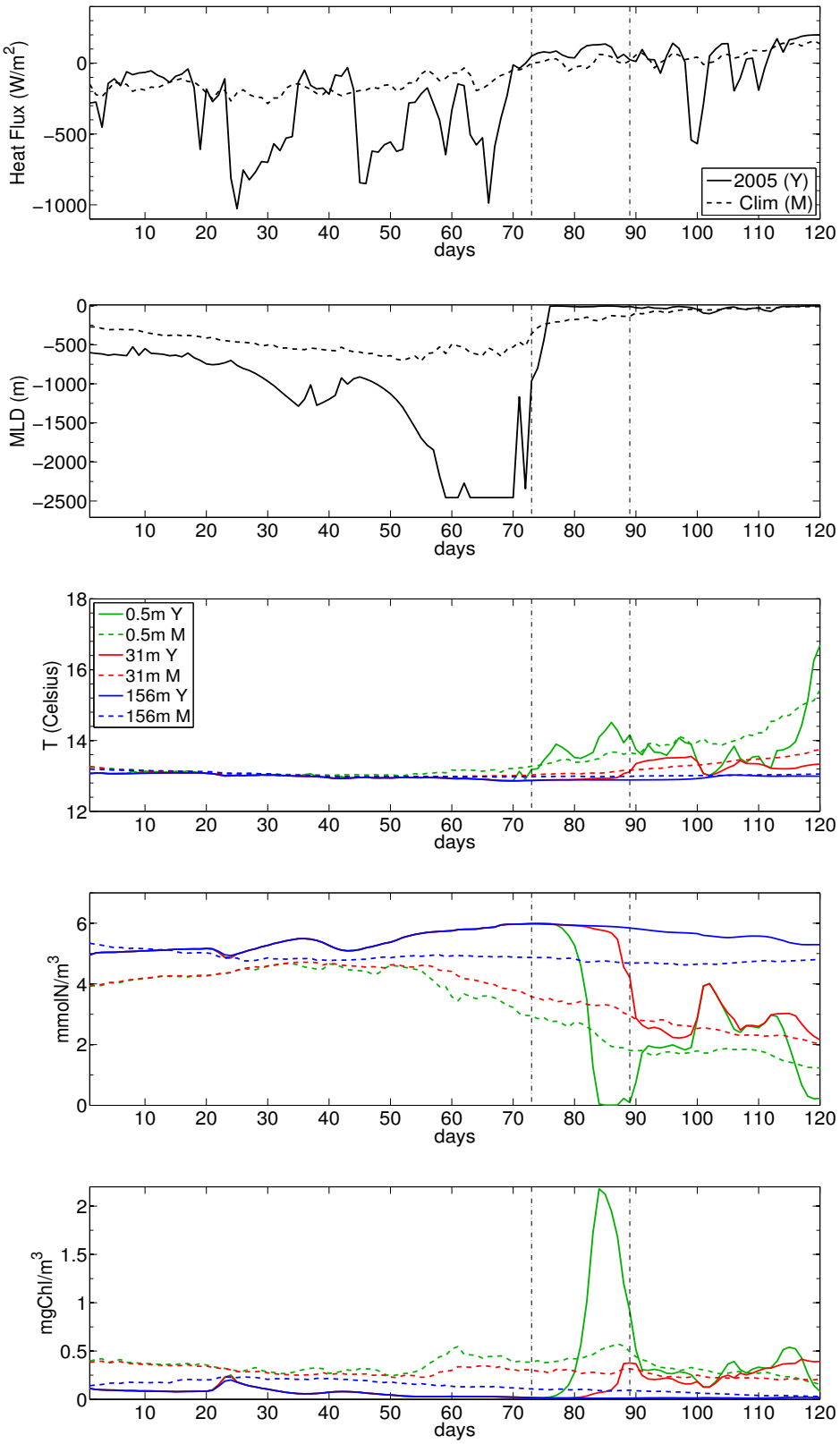

Figure 5.5. Net surface heat flux, with negative sign for ocean cooling, mixed layer depth and potential temperature, nitrate and chlorophyll at different depths (see legend in central panel), computed at the central A point of the NWM macro-event (fig. 5.1). Acronyms: Y = Year (2005), M = (climatological) Mean. Days are computed from the 1st Jan 2005. The vertical dashed lines delimit the duration of the macro-event.

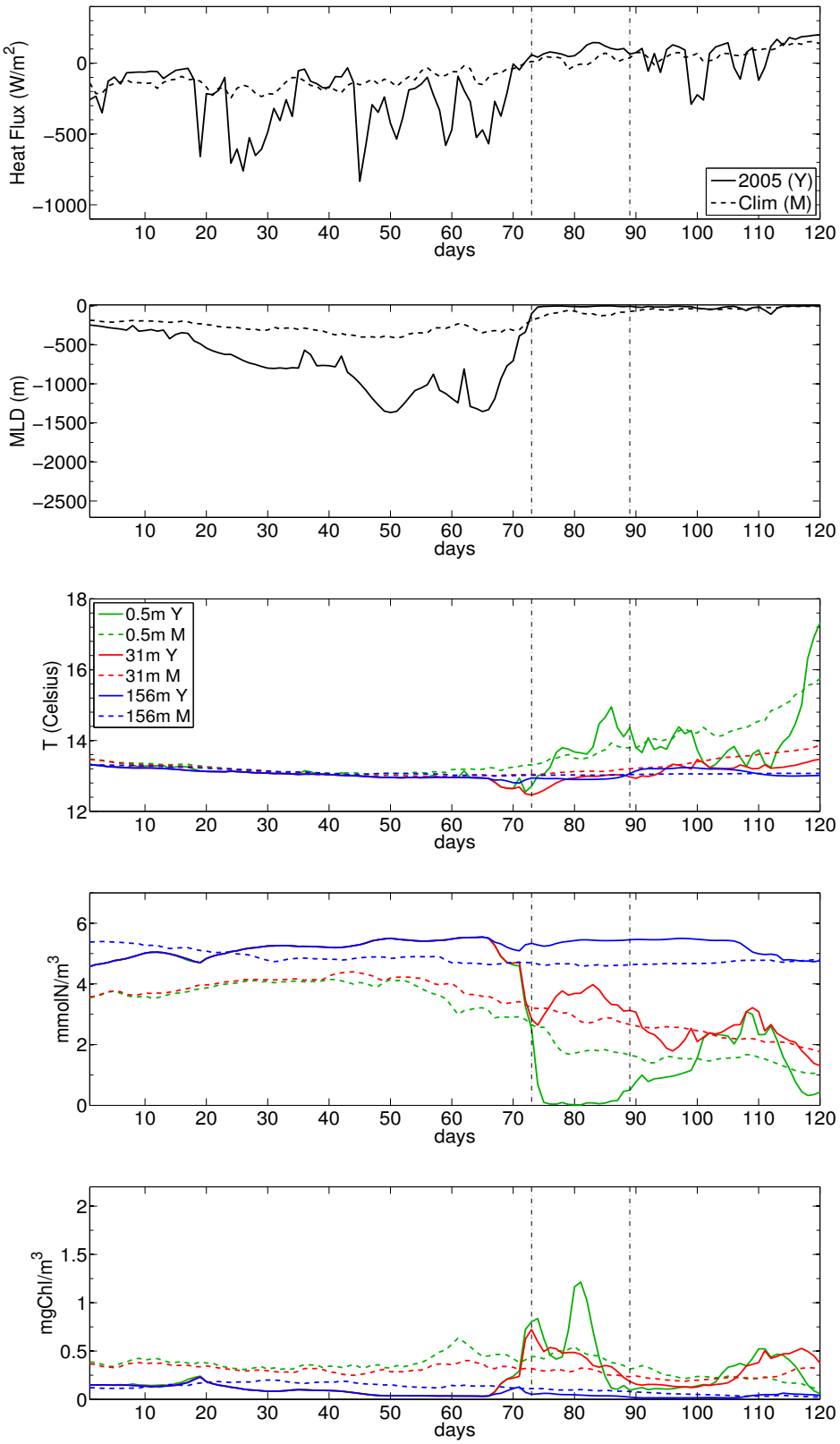

Figure 5.6. Net surface heat flux, with negative sign for ocean cooling, mixed layer depth and potential temperature, nitrate and chlorophyll at different depths, computed at the peripheral B point of the NWM macro-event (fig. 5.1). Acronyms: Y = Year (2005), M = (climatological) Mean. Days are computed from the 1st Jan 2005. The vertical dashed lines delimit the duration of the macro-event.

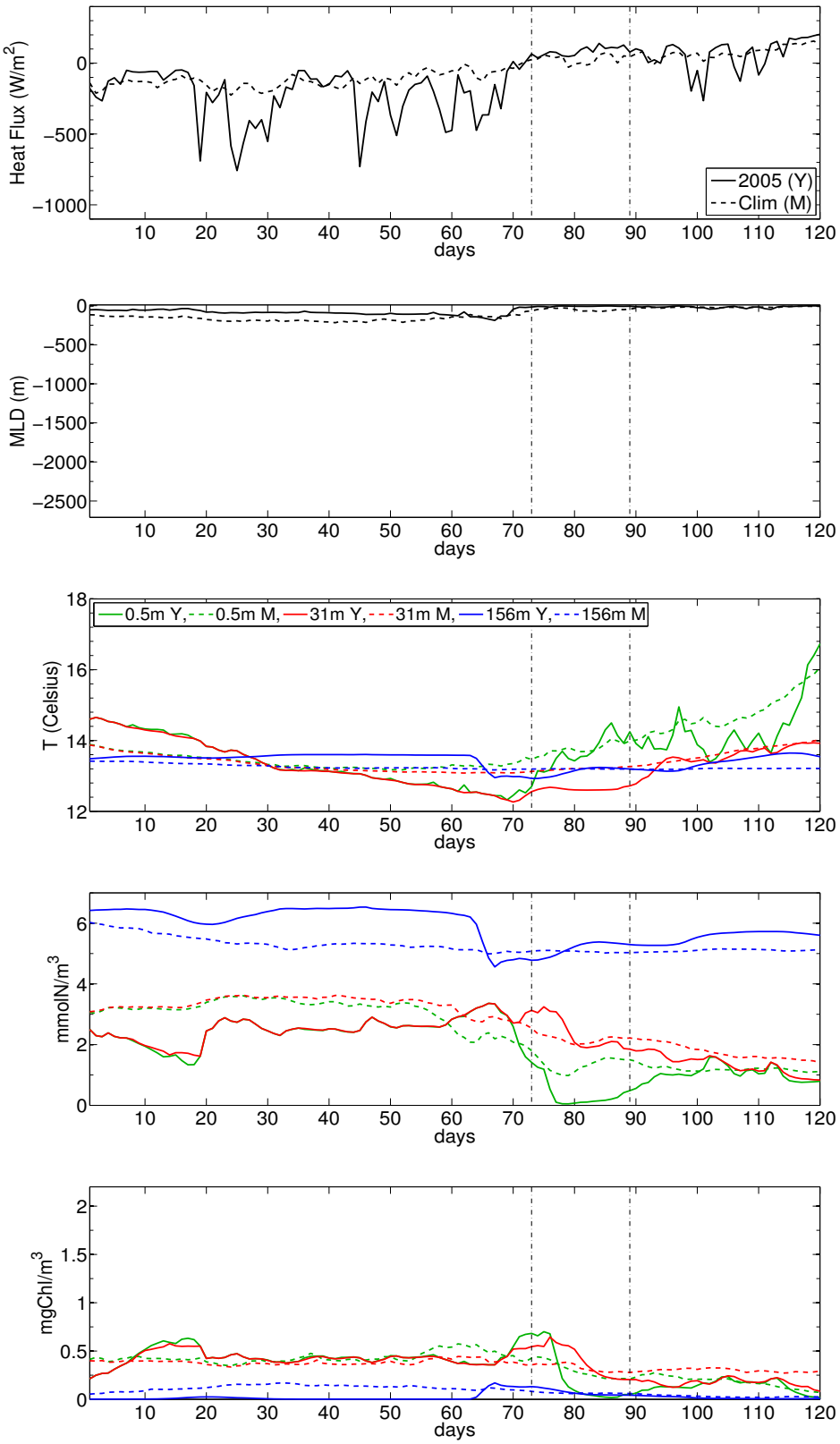

Figure 5.7. Net surface heat flux, with negative sign for ocean cooling, mixed layer depth and potential temperature, nitrate and chlorophyll at different depths, computed at the C point external to the NWM macro-event (fig. 5.1). Acronyms: Y = Year (2005), M = (climatological) Mean. Days are computed from the 1st Jan 2005. The vertical dashed lines delimit the duration of the macro-event.

the maximum mixed layer depth was of the order of the threshold of deep convection typical of the NWM area (1200 m, [Leaman, 1994]). The amount of nitrate available at the surface and subsurface layers was higher than the climatological values, but slightly lower than the point A.

Accordingly, the increase of surface chlorophyll was less pronounced and more similar to the one referred to the subsurface layers. Nevertheless, the surface chlorophyll values exceeded the local 99th percentile threshold (not shown), fixed as the starting point to identify the (connected) macro-events.

On the other hand, in the point C, external to the macro-event area (fig. 5.5), an evident stratification of the water column below the 30 m of depth was mantained for all the winter months (JFM), despite the cooling of the surface layers. The nitrate content in the surface and subsurface layers was much lower with respect to the deeper ones and only a small increase of the surface chlorophyll developed within the duration period of the macro-event.

However, the strong deep convection (i.e. interannual variability of the local vertical mixing) appears to be the key factor for the exceptionality of this macro-event, from the point of view of both (mean) severity and anomaly.

Finally, fig. 5.8 displays the **four components of the phytoplankton**

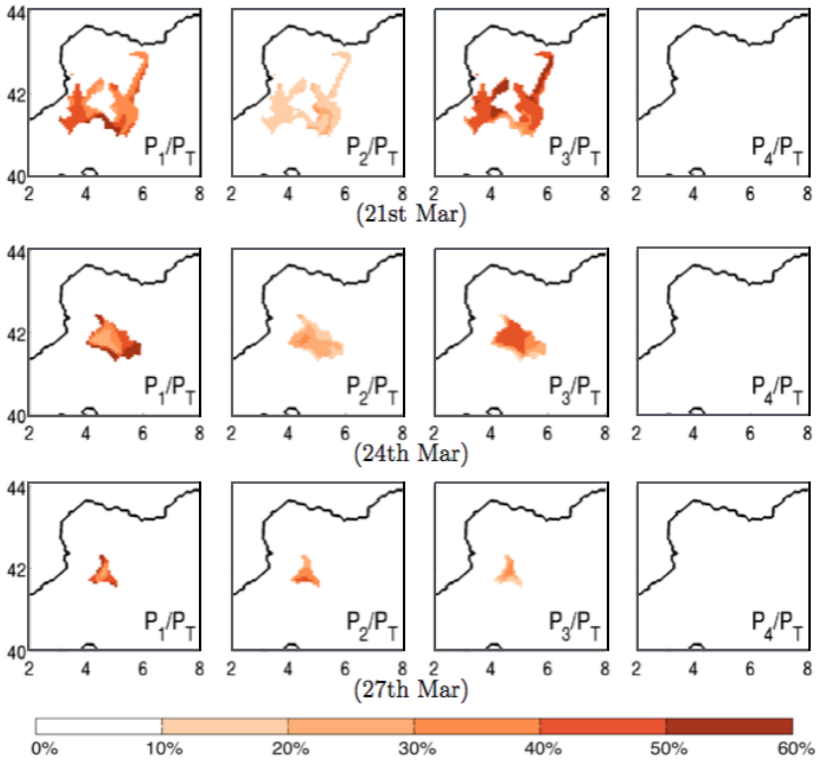

Figure 5.8. Maps of the percentage of the total chlorophyll in the 4 phytoplankton subgroups: P1 (first column), P2 (second one), P3 (third one), P4 (fourth one) in the spatio-temporal domain of the NWM macro-event shown in fig. 5.3.

chlorophyll provided by the coupled model (sec. 2.2), as the percentage of the total chlorophyll concentration shown in fig. 5.3, in some days of the NWM macro-event. The P4 component (i.e. the model parametrization of the large phytoplankton), exhibits values of chlorophyll lower than 10% for the whole duration of the macro-event. On the other hand, the P1 subgroup (i.e. diatoms) prevails in the outer points of the macro-event, whereas the P3 subgroup (i.e. picophytoplankton) predominates in the central area, mainly in the first days of the macro-event. The weight of the P2 component (i.e. flagellates) is lower (about 20%) and remains quite constant for the duration of the macro-event.

5.2 South Adriatic Sea (1995)

The macro-event occurred in the South Adriatic Sea from the 25th February to the 22nd March 1995 (fig. 5.9) is **the most anomalous** of the whole simulation, with the anomaly index equal to 26%. Its position in the classification of the most severe events on the whole Mediterranean Sea is only the 206th, but it is the 1st in the ADS subdomain (mean severity equal to 0.817 $kg/km^2/day$). Despite the macro-event is mainly ascribed to the ADS subdomain, it covers also a small portion of the ION area, for a total coverage of 25 $\times 10^3$ km^2.

The maps of local chlorophyll mass and anomaly (fig. 5.10) show that the larger impact of the macro-event on the local ecosystem is concentrated in the eastern side. As in the NWM case, the high local anomaly pattern follows to a large extent the chlorophyll mass. In addition, since the local 99th percentile

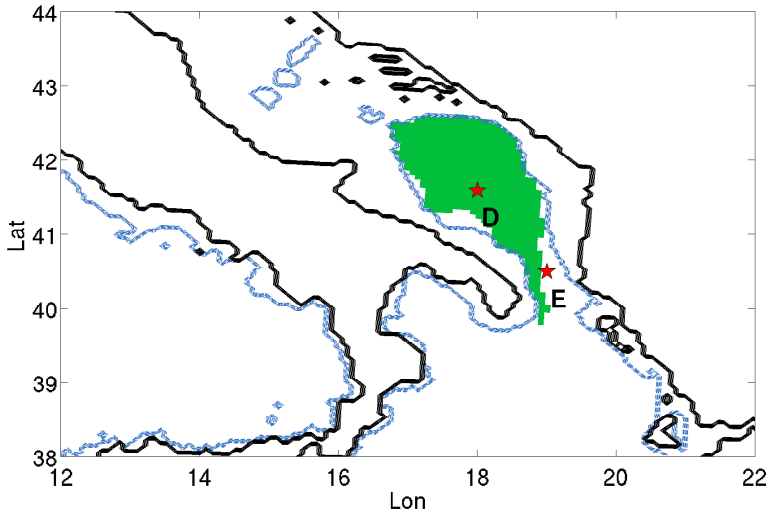

Figure 5.9. Area of the macro-event of chlorophyll occurred in the South Adriatic Sea from 25th February to 22nd March 1995 (green patch). The red stars indicate grid points internal (D) and external (E) with respect to the macro-event. The blue contours limit the open sea (i.e. depths higher than 200 m).

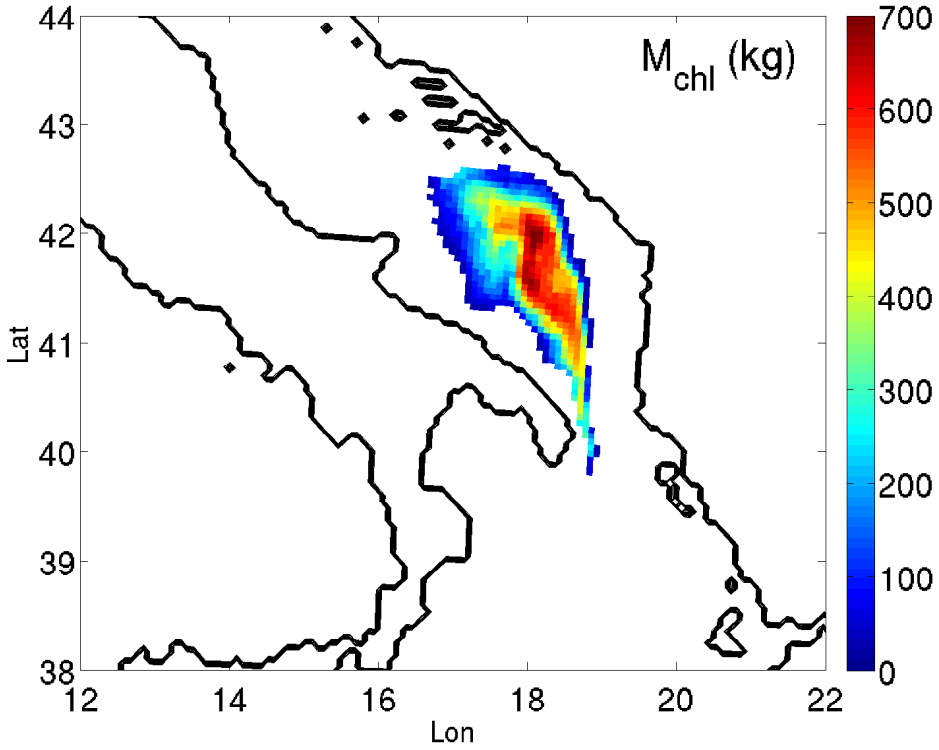

(a)

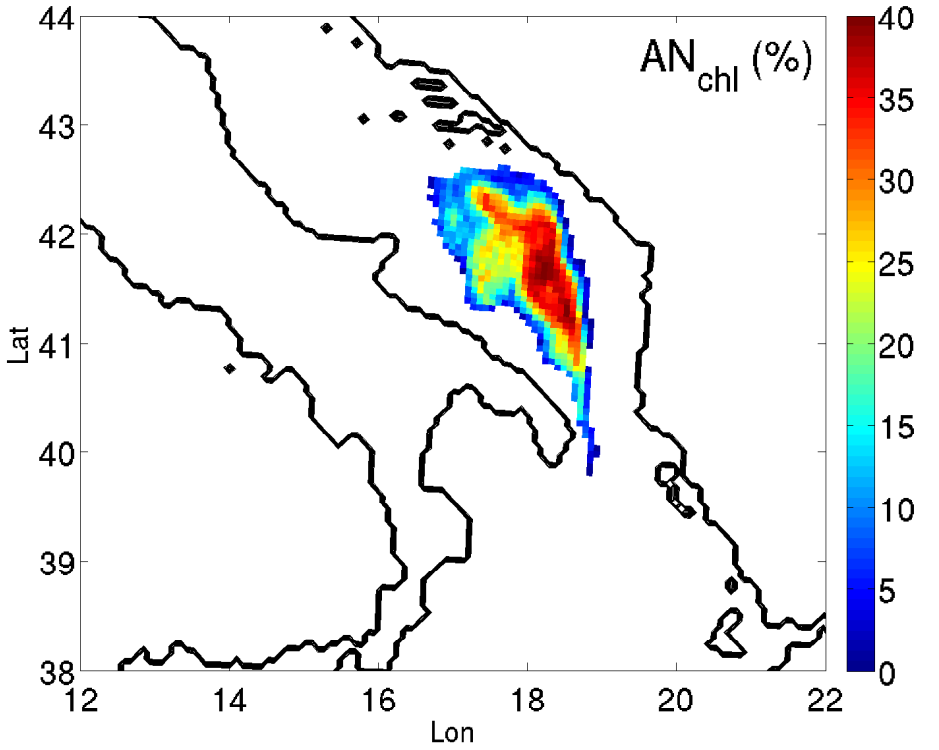

(b)

Figure 5.10. Maps of the chlorophyll mass supplied to the first meter of depth by all the local extremes involved in the ADS macro-event (a) and of the local anomaly (b).

thresholds of the surface chlorophyll are higher in the western side, (see fig. 3.3 as reference), the presence of high values in the eastern side qualify this latter as an atypical region for the very high supply of biomass.

The spatio-temporal evolution of this macro-event is displayed in fig. 5.11, in which the patches of chlorophyll and nitrate appear to be **confined** by the topography and the velocity field **within the cyclonic structure**. The highest values of chlorophyll (about 1.1 mg/m^3) are correlated with the nitrate consumption (by comparison of consecutive right panels) and localised mainly in the northeastern area, as expected from the maps of local indexes of chlorophyll mass and anomaly (fig. 5.10).

No comparison between model and satellite data is here shown since ESA-CCI dataset is available from 1997.

The analysis on the main variables carried out in the previous example was here applied to the two points D and E, as internal and external to the macro-event area (fig. 5.9).

In the internal point D (5.12), the topographic constraint and the cyclonic circulation generally sustained a marked mixing phase in January and February, characterized by an early pre-conditioning related to heat flux in the first 20 days of January and followed by a progressive re-stratification in March (second panel). On the other hand, the intra-annual variability of the water column depth in the year considered led to values of the mixed layer depth exceeding 1000 m in February, followed by the alternation of mixing and re-stratification phases, that lasted until the third week of April. The **early re-stratification phase** (from the end of February to the third week of March) resulted in the gradual development of a peak of chlorophyll (associated with the nitrate consumption), limited by the instability of the water column on the time scale of few days. A further and less pronounced peak was then triggered by a later stratification phase in April.

In the point E external to the macro-event and to the South Adriatic Gyre (5.13), the mixing phase is instead much weaker, the surface layer is poor of nitrate content and the chlorophyll does not display significant increases.

Overall, the anomaly of this macro-event of chlorophyll appears to be related to the spatially confined (interannual and intra-annual) variability of the physical forcing, superimposed to the mean circulation structure.

Fig. 5.15 shows the **four components of the phytoplankton chlorophyll**, as the percentage of the total chlorophyll concentration, in some days of the ADS macro-event. As in the NWM example (sec. 5.1), the P4 component is negligible and P3 and P1 are predominant (here with a percentage equal to about 45%) in the first and in the last days of the macro-event, respectively. The alternation of the two subgroups is evident (comparing 8th and 13th March) in particular in the eastern side of the macro-event, where the total chlorophyll mass is higher (fig. 5.10(a)). The weight of the P2 component is lower (on average about 25%), but it increases during the macro-event evolution.

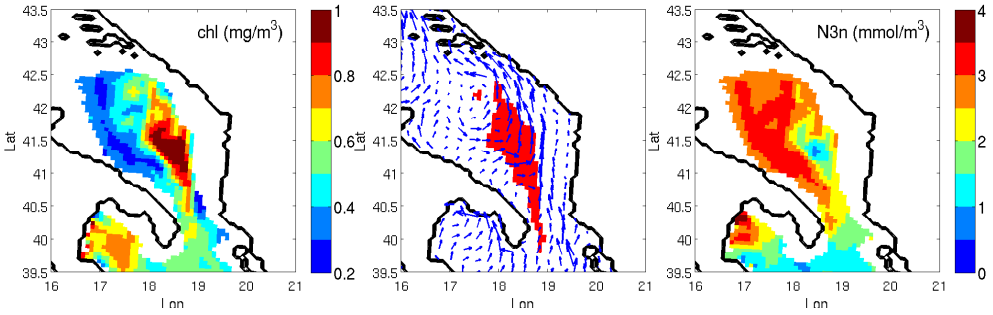

(3rd Mar)

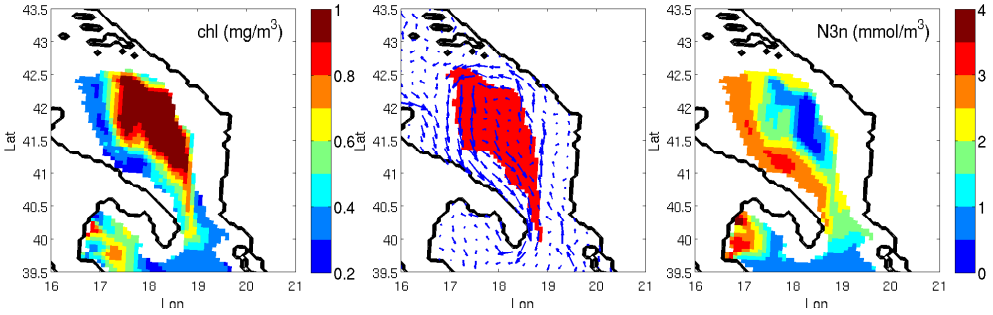

(8th Mar)

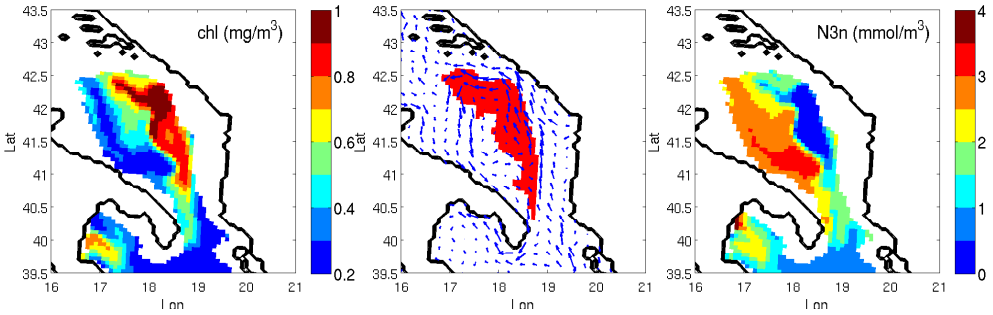

(13th Mar)

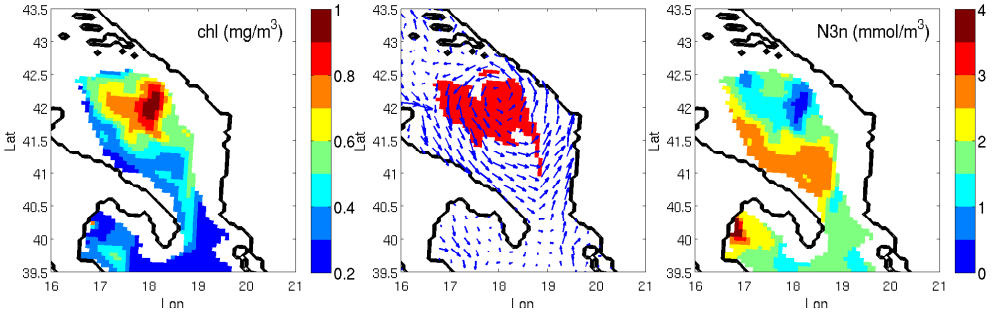

(21st Mar)

Figure 5.11. Maps of the surface chlorophyll (first column), daily portion of the macro-event area superimposed to the surface velocity field, (second one) and surface nitrate (third one), for some single days of development of the macro-event, occurred in the ADS from the 25th February to the 22nd March 1995. The surface chlorophyll and nitrate are averaged in the first 10 m of depth. The horizontal velocity field (scaled by a factor 1.5) is referred to the depth of 5 m.

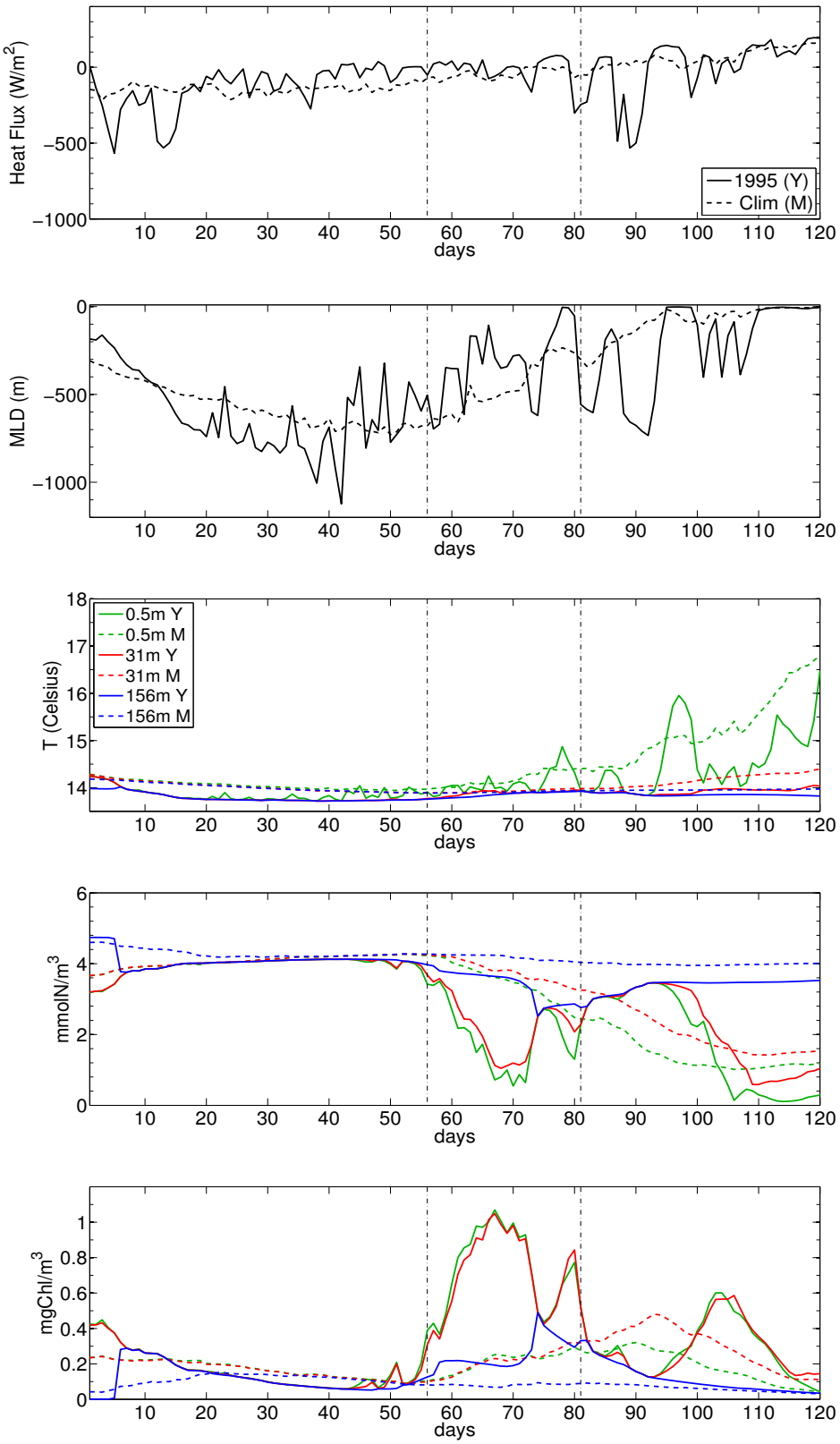

Figure 5.12. Net surface heat flux, with negative sign for ocean cooling, mixed layer depth and potential temperature, nitrate and chlorophyll at different depths, computed at the internal D point of the ADS macro-event (fig. 5.9). Acronyms: Y = Year (1995), M = (climatological) Mean. Days are computed from the 1st Jan 1995. The vertical dashed lines delimit the duration of the macro-event.

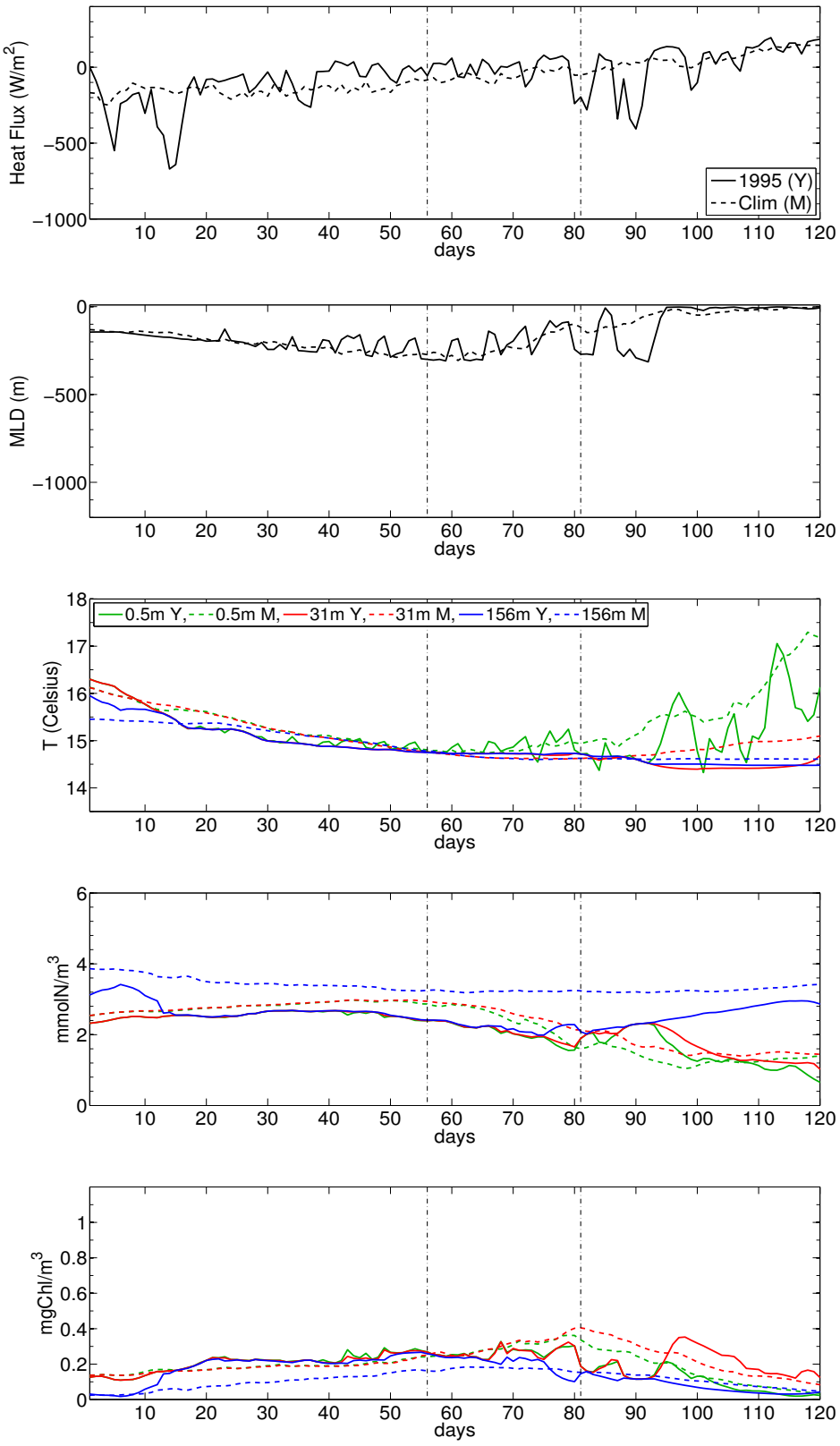

Figure 5.13. Net surface heat flux, with negative sign for ocean cooling, mixed layer depth and potential temperature, nitrate and chlorophyll at different depths, computed at the point E external to the ADS macro-event (fig. 5.9). Acronyms: Y = Year (1995), M = (climatological) Mean. Days are computed from the 1st Jan 1995. The vertical dashed lines delimit the duration of the macro-event.

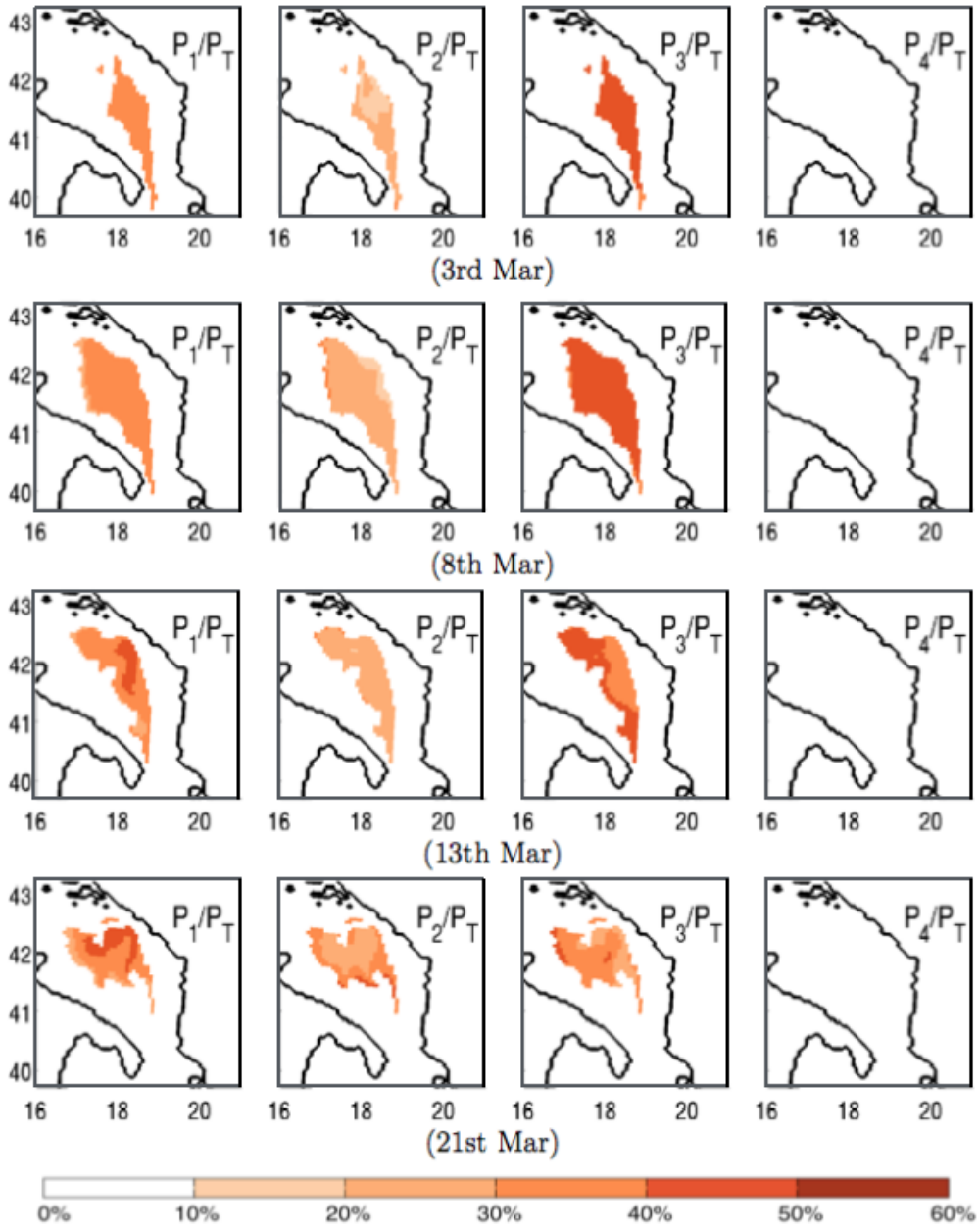

Figure 5.14. Maps of the percentage of the total chlorophyll in the 4 phytoplankton subgroups: P1 (first column), P2 (second one), P3 (third one), P4 (fourth one) in the spatio-temporal domain of the ADS macro-event.

5.3 Levantine Sea (2001)

As shown in sec. 4.2, the few HH macro-events occurred in the Levantine Sea are concentrated in the Rhodes Gyre region. Actually, this region is characterized by a **surface chlorophyll dynamics** that is typically **instable and intermittent** (intermittently blooming regimes in this area were recognized in D'Ortenzio and Ribera D'Alcalà [2009], fig. 1.3).

As an example, the small (6×10^3 km^2 covered area) **macro-event** of 0.642 $kg/km^2/day$ as mean severity and 8% as anomaly index, occurred about 100 km east of Crete from the 12th to the 15th February 2001 (fig. 5.16(a)), is here analysed at the two internal (F) and external (G) points. F point also belongs to a subsequent and more extended macro-event, occurred from the 28th February to the 15th March (fig.5.16(b)), but the mean severity and anomaly indexes associated to this **second macro-event** are lower than the previous ones and they do not classify it as HH macro-event.

Focusing on the first macro-event, the maps of local chlorophyll mass and local anomaly are in fig. 5.17. Despite the biomass appears to be concentrated in the eastern side of the macro-event area, also in this case the pattern related to the high values of supplied chlorophyll is similar to the one high anomaly values (central part of the macro-event).

The spatio-temporal evolution of the two macro-events is shown in fig. 5.18 and fig. 5.19, respectively. In both cases, multiple patches of chlorophyll are recognizable in the area and correlated with the nutrient consumption (by comparison of consecutive right panels). The second macro-event develops after an enrichment of surface nitrate in the central region (comparing the last right panel in fig. 5.18 with the first one in fig. 5.19), as a possible consequence of a mixing process. The instability of the area will be evident from the dynamics of the heat flux and of the mixed layer that will be shown in figs. 5.21-5.22.

As in the NWM case, the model-derived dynamics of the extremes of chlorophyll is qualitatively compared with the ESA-CCI **satellite available data** (fig. 5.20) in the subdomain. As a general remark, the spatial gradients and the timing of the increase of chlorophyll in the examined period are in good agreement with the satellite patterns. Nevertheless, model data overestimate the mean state of chlorophyll in the area, exhibiting values about double with respect the observations.

In particular, there are very few satellite observations in the area covered by the first event (fig. 5.16(a)), from 12th to 15th February 2001. The highest values of chlorophyll are about 0.25 mg/m^3 (15th Feb), in some grid points that display also the highest values provided by the model (see F point in fig. 5.16). On the other hand, in some days (3rd - 9th Mar) belonging to the second event (fig. 5.16(b)) higher values of chlorophyll are actually detected (e.g. about 0.5 mg/m^3 in 3rd Mar) in proximity of the same points. However, the values of chlorophyll appear to be lower than 0.2 mg/m^3 in the LEV area already after the 13th Mar (not shown).

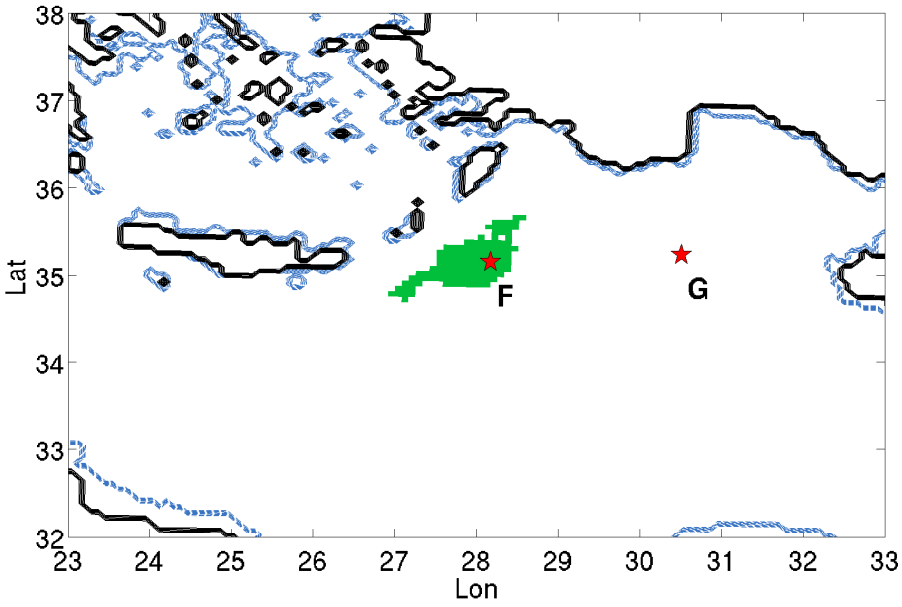

(a)

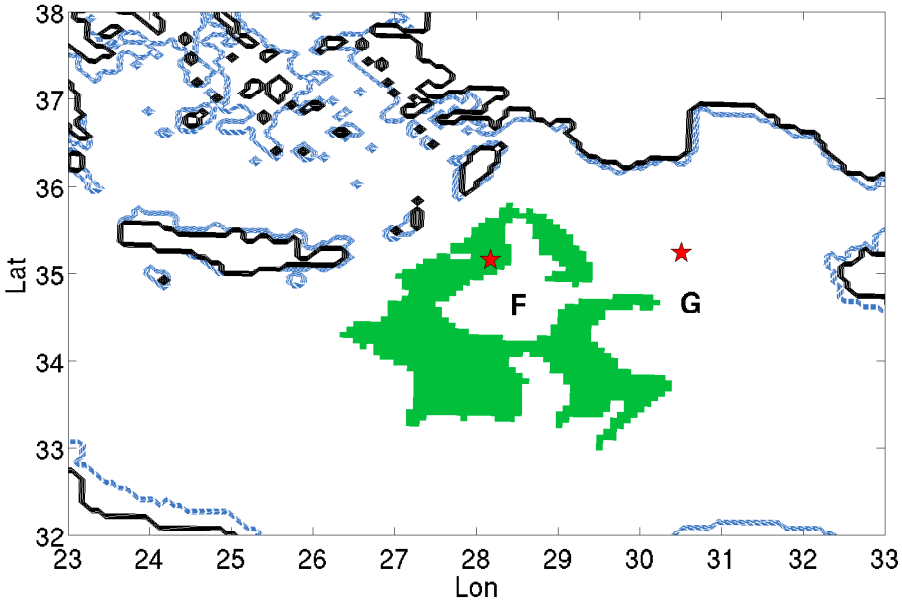

(b)

Figure 5.15. Area of the HH macro-event of chlorophyll occurred in the Levantine Sea from the 12th to the 15th February 2001 (a) and of the less intense macro-event occurred in the same subdomain from the 28th February to the 15th March 2001 (b). The red stars indicate grid points at internal (F) and external (G) positions with respect to the macro-events. The blue contours limit the open sea (i.e. depths higher than 200 m).

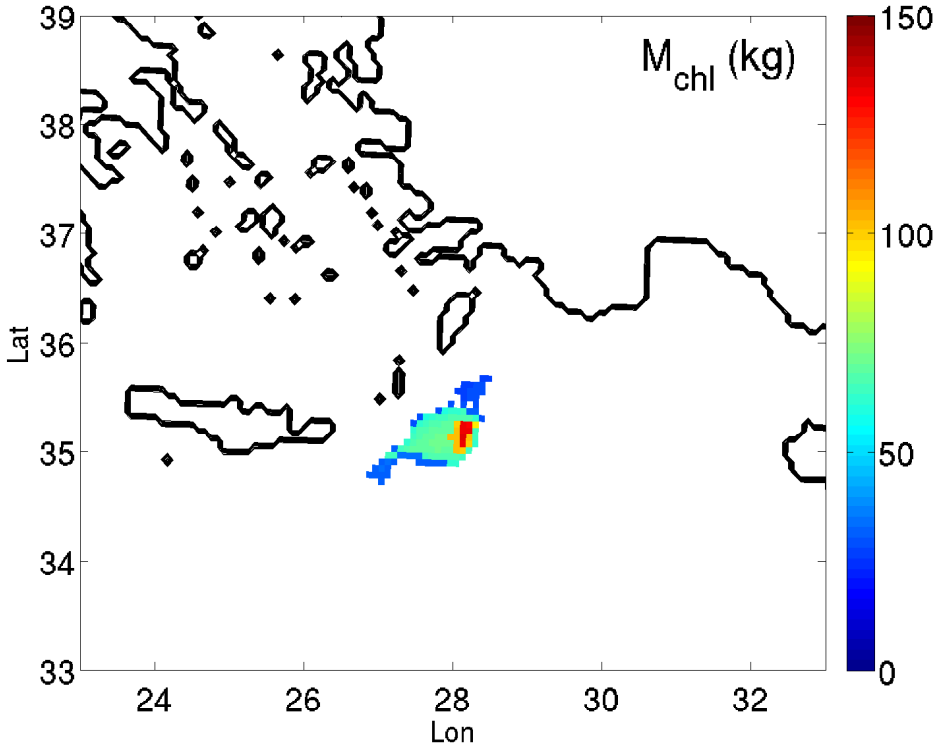

(a)

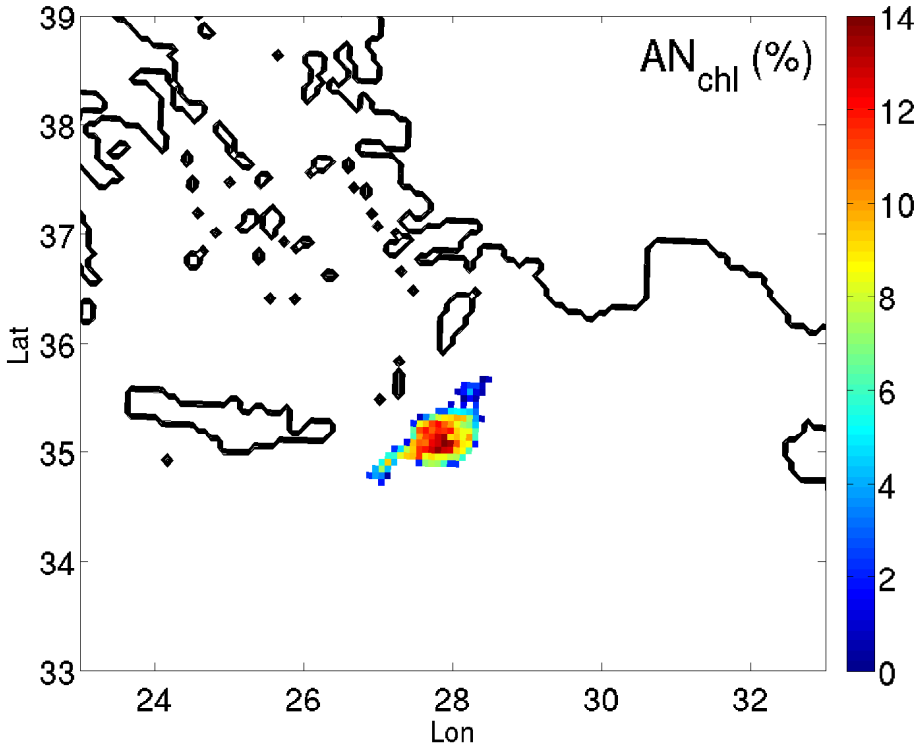

(b)

Figure 5.16. Maps of the chlorophyll mass supplied to the first meter of depth by all the local extremes involved in the first (HH) LEV macro-event (a) and of the local anomaly (b).

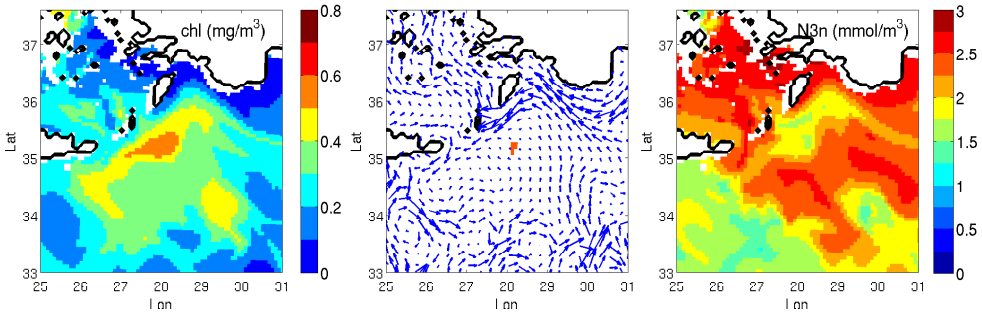

(12th Feb)

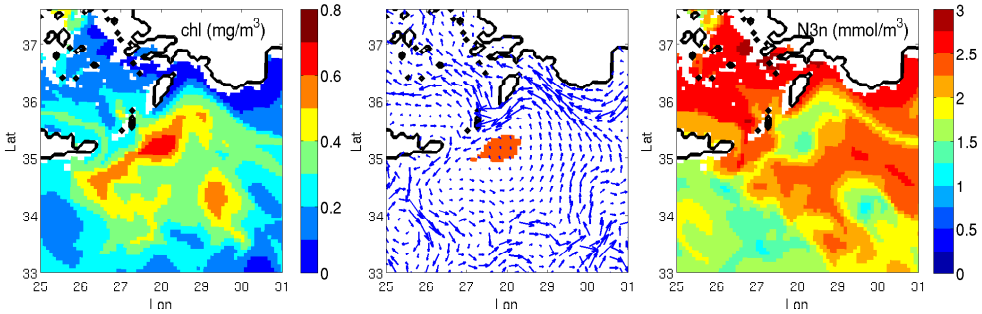

(13th Feb)

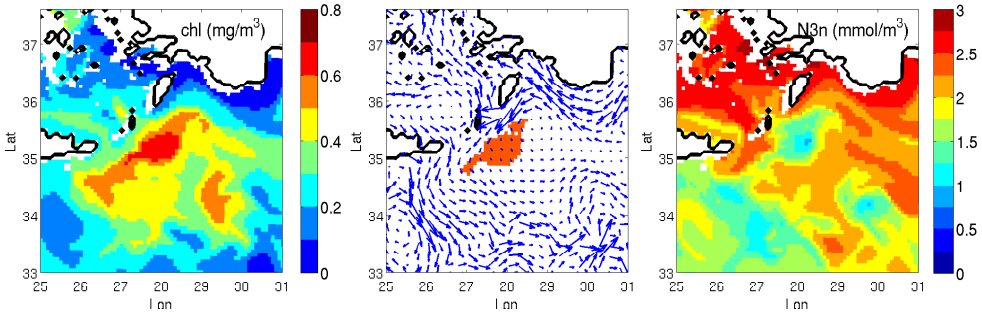

(14th Feb)

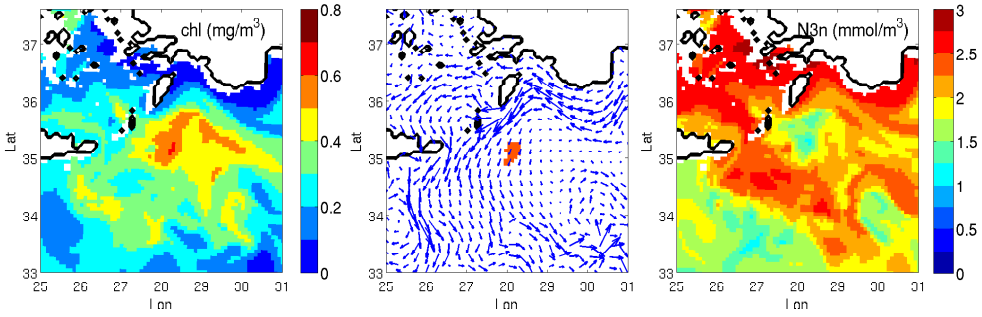

(15th Feb)

Figure 5.17. Maps of the surface chlorophyll (first column), daily portion of the macro-event area superimposed to the surface velocity field, (second one) and surface nitrate (third one), for some single days of development of the first macro-event, occurred in the LEV from the 12th to the 15th February 2001. The surface chlorophyll and nitrate are averaged in the first 10 m of depth. The horizontal velocity field (scaled by a factor 1.5) is referred to the depth of 5 m.

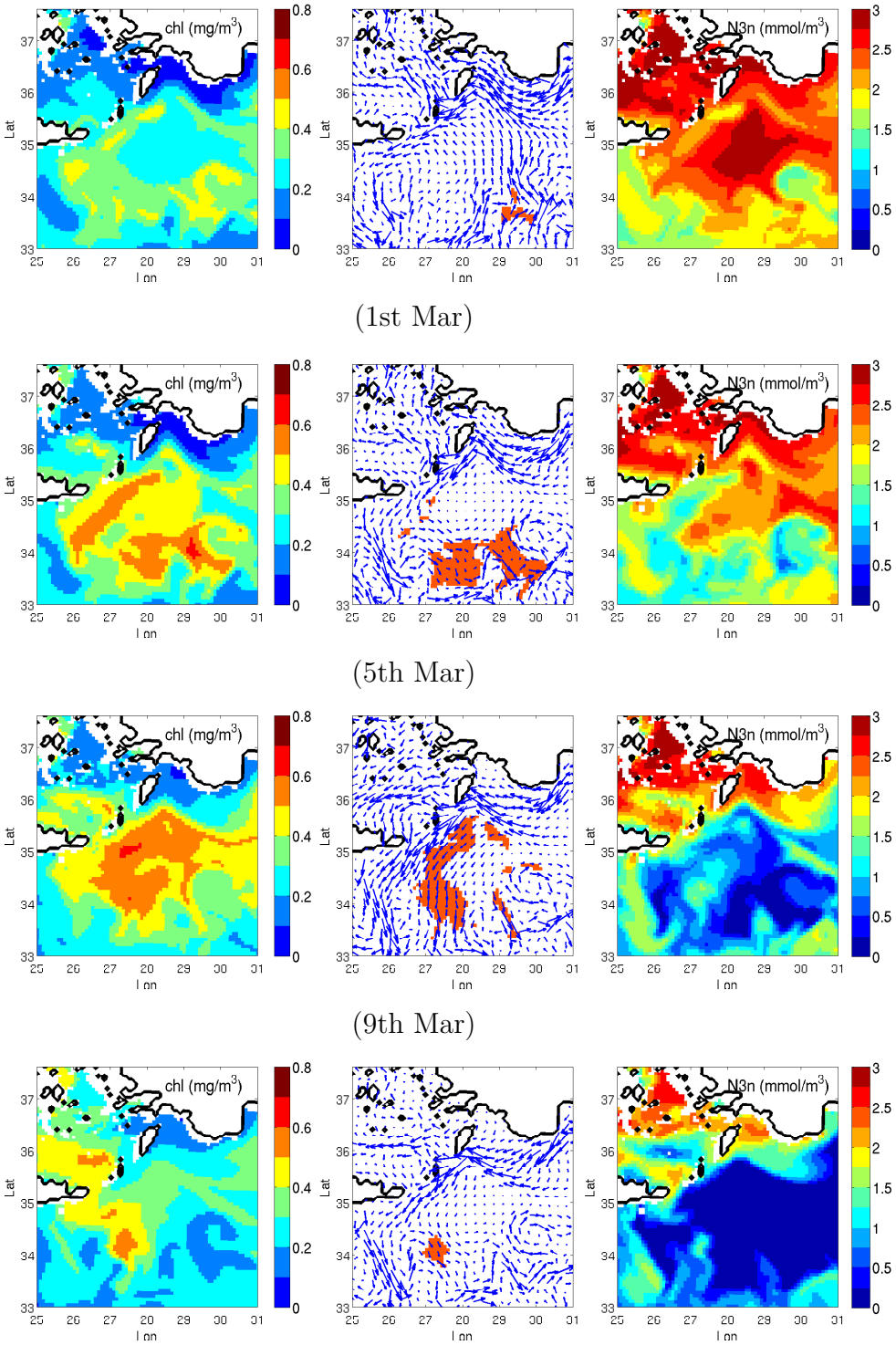

Figure 5.18. Maps of the surface chlorophyll (first column), daily portion of the macro-event area superimposed to the surface velocity field, (second one) and surface nitrate (third one), for some single days of development of the second macro-event, occurred in the LEV from the 28th February to the 15th March 2001. The surface chlorophyll and nitrate are averaged in the first 10 m of depth. The horizontal velocity field (scaled by a factor 1.5) is referred to the depth of 5 m.

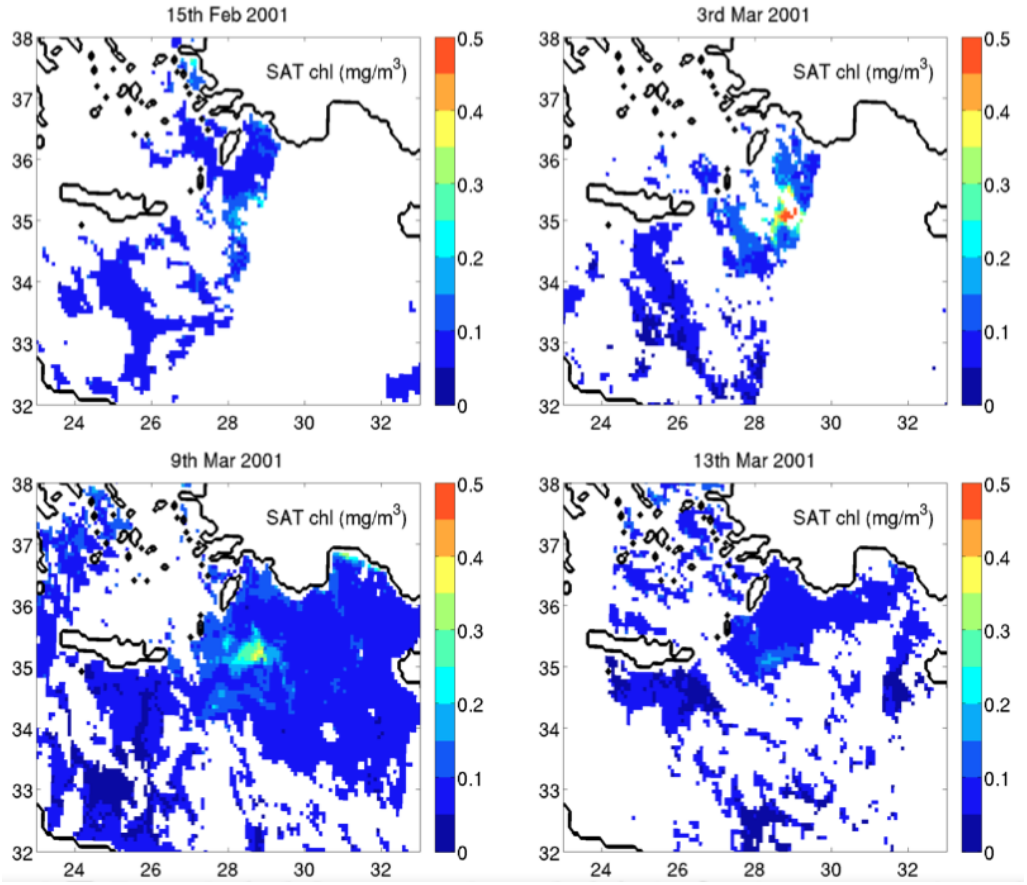

Figure 5.19. Maps of the satellite-derived surface chlorophyll for some single days of development of the two model-derived macro-events (fig. 5.16) in the LEV subdomain. Original data were interpolated on the MITgcm grid.

The trigger of the development of the first macro-event (fig. 5.21) appears to be the **early stratification** occurred in the days immediately before its start, as well as its extinguishing can be ascribed to the (stronger) new mixing phase, driven by a marked upward heat flux (about 800 W/m^2). In fact, the January mixing phase is less intense than the climatological mean and an increase of nitrate content as a consequence of the mixing is not observed. The abrupt increase of chlorophyll could be instead due to the limited transport and/or diffusion associated to the temporary stabilization of the water column, or to a high PAR level (not shown). After the sudden establishment of the **seasonal stratification** (first days of March), the peak of chlorophyll related to the second macro-event was detected, together with the full consumption of surface layer nitrate.

On the other hand, the G point (fig. 5.22), external to both the first and the second macro-event, displays a more stratified water column and peaks of chlorophyll that are less pronounced, but also in this case controlled by the mixing/stratification phases.

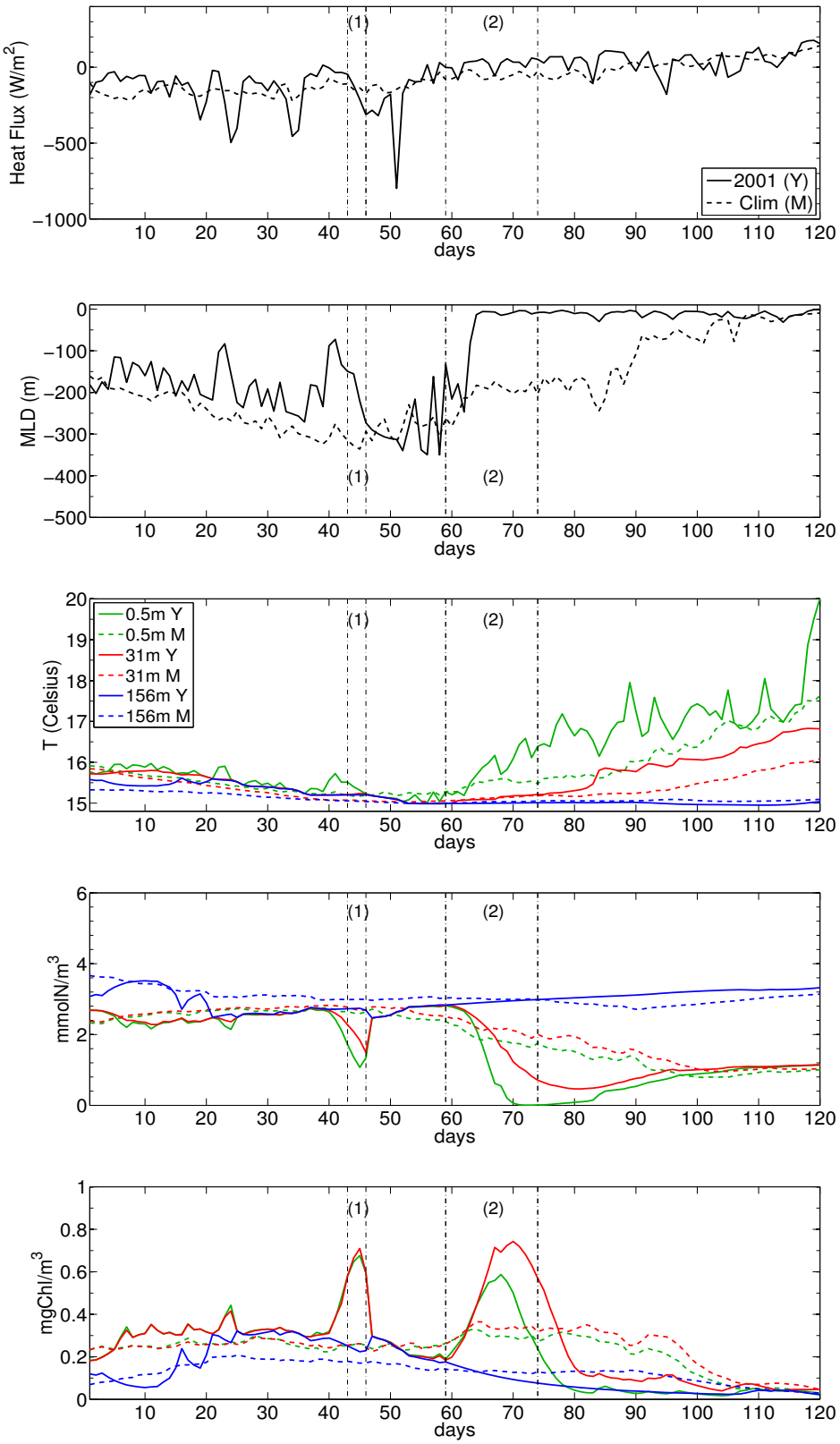

Figure 5.20. Net surface heat flux, with negative sign for ocean cooling, mixed layer depth and potential temperature, nitrate and chlorophyll at different depths, computed at the internal F point, referred to the macro-event under consideration, fig. 5.16(a) (1), and to the subsequent macro-event in fig. 5.16(b) (2). Acronyms: Y = Year (2001), M = (climatological) Mean. Days are computed from the 1st Jan 2001. The vertical dashed lines delimit the duration of the macro-event.

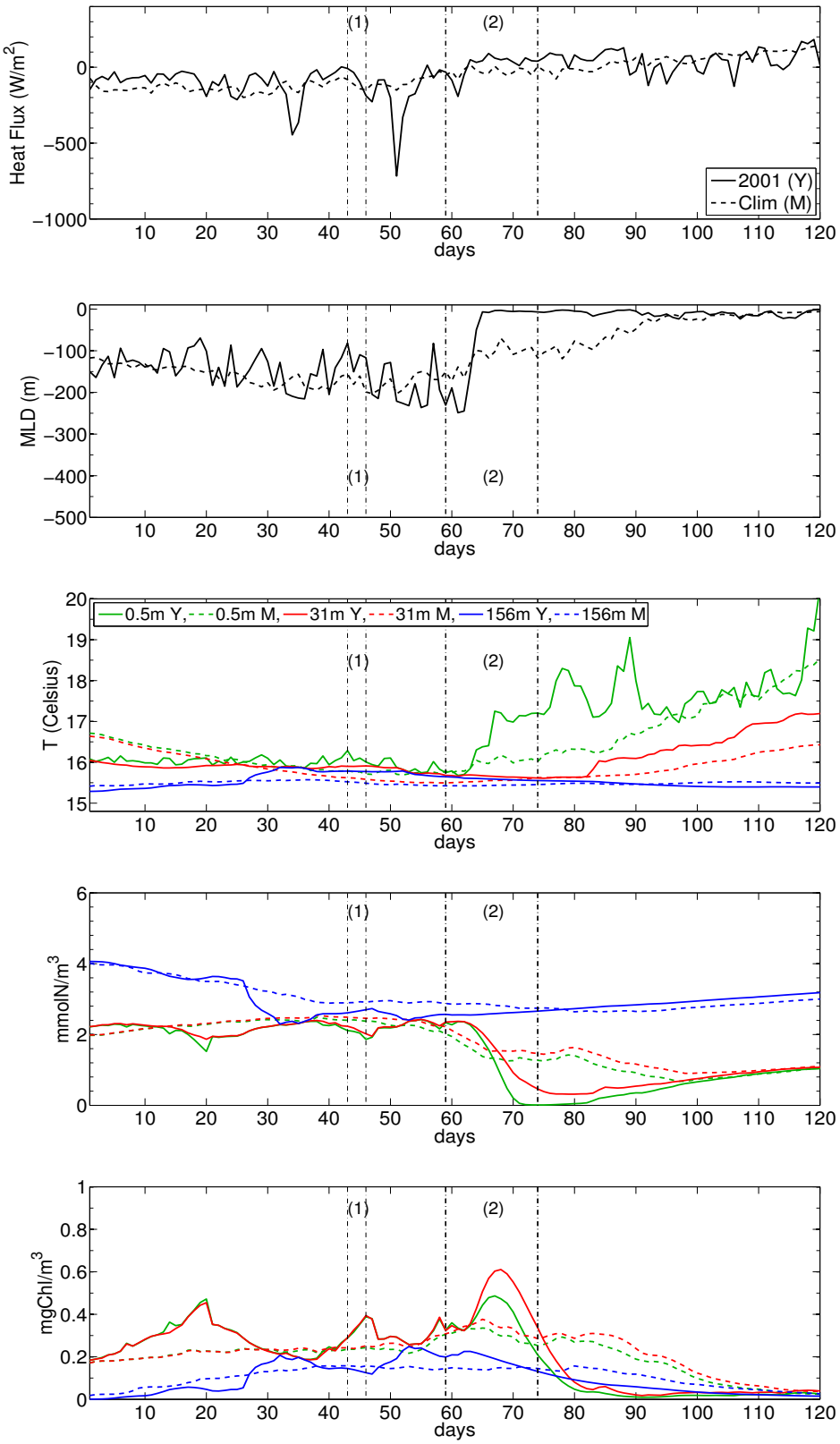

Figure 5.21. Net surface heat flux, with negative sign for ocean cooling, mixed layer depth and potential temperature, nitrate and chlorophyll at different depths, computed at the external G point, referred to the macro-event under consideration, fig. 5.16(a) (1), and to the subsequent macro-event in fig. 5.16(b) (2). Acronyms: Y = Year (2001), M = (climatological) Mean. Days are computed from the 1st Jan 2001. The vertical dashed lines delimit the duration of the macro-event.

Also other macro-events of high severe and anomalous supply of surface chlorophyll to the local ecosystem in this region are subjected to multiple increases of chlorophyll of similar intensity within the winter-spring period (not shown). Their intermittency is ascribed, as in this case, to the strong physical (interannual and intra-annual) variabilities of the mixing/stratification phases in the open sea.

Finally, the two LEV macro-events present different percentage of the **phytoplankton subgroups**. In fact, the first macro-event (fig. 5.23) is ascribed mainly (about 40%) to the P3 subgroup, with a considerable contribution (about 30%) also of the P2 subgroup. Since the overall duration of this macro-event is 4 days, it is not possible to evaluate and compare the temporal dynamics of the subgroups. In the second macro-event (fig. 5.24) the highest percentage (higher than 50%) is instead shown by the P2 subgroup, followed by the P1 percentage (about 30%). This partition is maintained for all the macro-event duration. However, in both the macro-events, the P4 percentage is negligible.

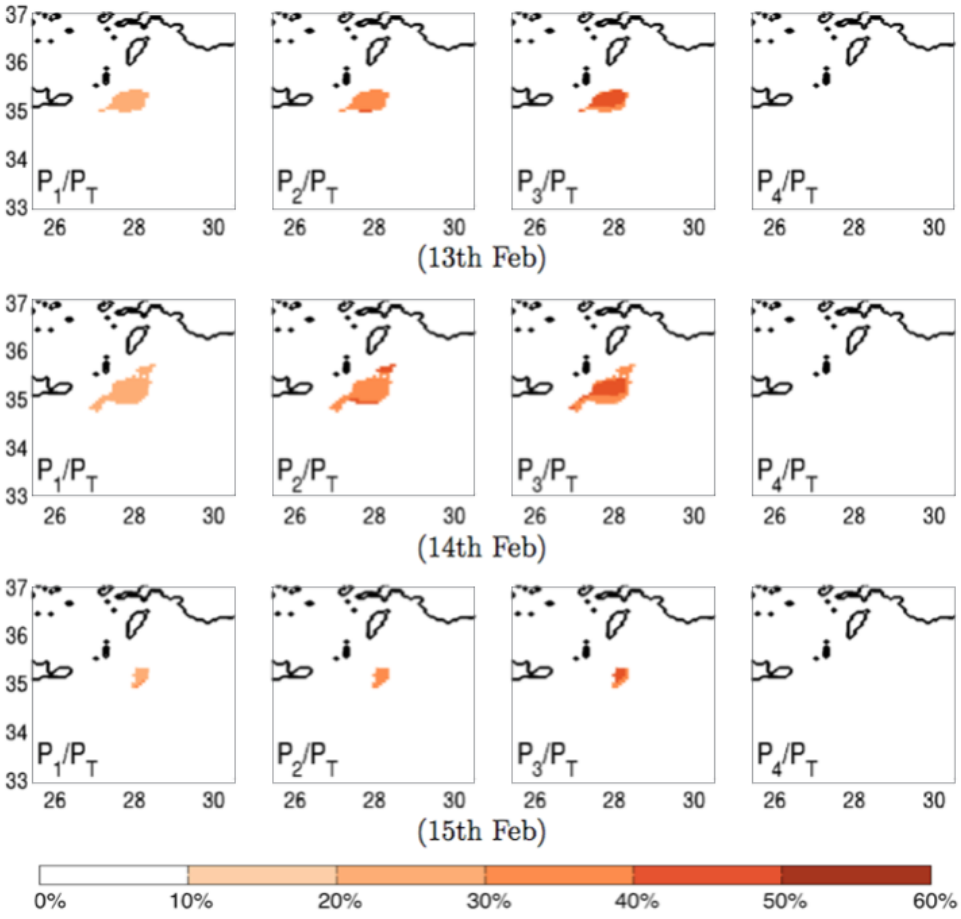

Figure 5.22. Maps of the percentage of the total chlorophyll in the 4 phytoplankton subgroups: P1 (first column), P2 (second one), P3 (third one), P4 (fourth one) in the spatio-temporal domain of the first LEV macro-event under consideration (fig. 5.16(a)).

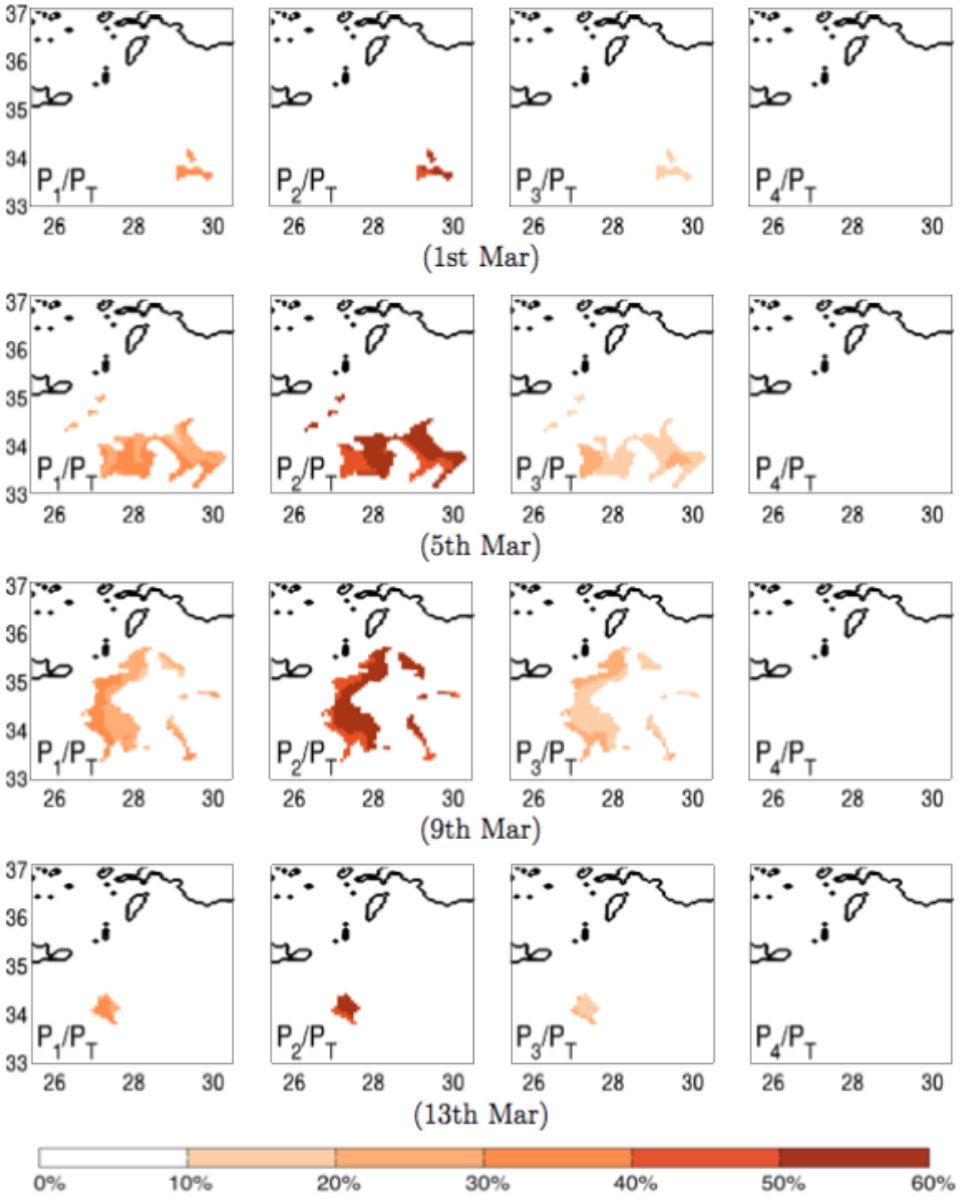

Figure 5.23. Maps of the percentage of the total chlorophyll in the 4 phytoplankton subgroups: P1 (first column), P2 (second one), P3 (third one), P4 (fourth one) in the spatio-temporal domain of the second LEV macro-event under consideration (fig. 5.16(b)).

Discussion and conclusions

Biogeochemical extreme events, defined as sets of peaks over the 99th percentile threshold that are connected in space and time, are investigated in this PhD thesis in the case of the surface chlorophyll of the Mediterranean open sea.

An online coupled **physical-biogeochemical model** (MITgcm-BFM) was implemented in order to deal with a continuous dataset of chlorophyll on such a wide area, overcoming the limitations of the remote sensing (missing data due to the cloud coverage) and of the in-situ measurements (data recorded at fixed stations). The spatial resolution of the model is 1/12°, with 75 vertical levels. A multidecadal simulation with daily output (1979-2012) was run to collect the statistics needed to carry out the study. Since the chlorophyll time series are typically characterized by sharp peaks developing in very few days, the online coupling between the physical and the biogeochemical part of the model allowed to retain the high frequencies of the physics also in the chlorophyll time evolution. The coupled model was corroborated with available observations and other validated models on a climatological basis, showing that it can reproduce the main features of the physical and biogeochemical dynamics of the Mediterranean Sea.

The chosen approach considers statistical chlorophyll extremes and is based on the **99th percentile threshold**. To account for the heterogeneity of the chlorophyll features and dynamics across the Mediterranean area, the definition of **extremes of chlorophyll** as peaks over the threshold (POTs) was initially applied at each grid point. In a later stage, this definition was refined to include in the same extreme event all the grid points near in space with extremes at the same time. The **macro-events**, identified by spatio-temporal volumes including connected POTs, were then characterized by a set of **indexes**, referred to their spatio-temporal localisation, shape and impact on the local marine ecosystem due to their supply of high and/or anomalous biomass production. Each macro-event was described in its shape characteristics by area, duration and uniformity (this latter used to evaluate its local persistency) and in its chlorophyll content by mean severity (total amount of chlorophyll in each spatio-temporal unit) and anomaly (percentage of the chlorophyll above the threshold with respect to the total amount in the macro-event).

The macro-events occurred in the Mediterranean area in the **winter-spring** months (January-May) of the 1994-2012 period were then described and classified using the introduced set of indexes.

For some **representative macro-events** further analyses were carried out, to reconstruct the physical and biological dynamics and to compare the model-derived results with available observations.

Overall, the macro-events occurred in all years, especially in the northern part of the Mediterranean Sea, during the **winter months**. They have a wide range of possible shapes, mainly corresponding to **durations shorter than 20 days** and **areas smaller than 100 $\times$ 10^3 km^2** (corresponding to a radius scale of about 180 km, that is within the range of the larger mesoscale of the Mediterranean Sea, [Lionello, 2012]) .

The **most persistent macro-events** (i.e. with uniformity index higher than about 60%) are relatively **small and short** with respect to the total range, with an inverse proportionality between area and duration.

The **most severe macro-events** (i.e. with mean severity higher than 1.1 $kg/km^2/day$ in the first meter of depth) have **intermediate area and duration** with respect to the total range; generally they are **not very persistent**, but sometimes they are very anomalous (anomaly higher than 15%). They are located mainly in the Mediterranean regions with the highest values of the thresholds of chlorophyll and they can be associated to a variety of processes of development and manteinance of the macro-events (e.g. the cyclonic dynamics).

On the other hand, **the most anomalous macro-events** have typically **medium or long duration** (up to 84 days) and they can be **also very large** (up to the whole sub-basin scale), but **not very persistent**. They involve areas with relatively low chlorophyll capacity (i.e. that can be considered atypical from the point of view of the occurrence of chlorophyll macro-events of a certain severity) and they can be associated to the relatively long persistance of the internal ecosystem processes and/or of the forcing conditions that promote them (e.g. the horizontal transport).

No significant trends throughout the investigated period are observed in the total number, coverage, mean severity and anomaly indexes of all the macro-events on the basin scale.

Some subdomains were analysed more in detail: the North Western Mediterranean Sea (NWM), the Ionian Sea (ION), the South Adriatic Sea (ADS) and the Levantine Sea (LEV), with a total number of macro-events in ADS equal to about one fifth of the number of macro-events of the other subdomains.

The **decreasing eastward** gradient of the **mean severity** across the four subdomains reflects the well known gradients of the mean surface chlorophyll and the pattern of 99th percentile local thresholds computed for the simulation period.

The **most severe** macro-events among the four subdomains are in **NWM**. They mainly occur in winter months and are associated to a wide range of anomaly. In **ADS** we observed macro-events with a wide range of anomaly even if their mean severity range is narrow. ADS is the subdomain with the **most persistent** macro-events, occurring in March and in the first halves of

February and April. These features are ascribed to the spatial constraints of the topography and of the circulation structure (South Adriatic Gyre) of the subdomain.

ION is the subdomain with the most variable **mean severity** in the years and also the only one exhibiting a **(positive) trend**. The macro-events ascribed to this subdomain happen mainly in the late-winter early-spring period, as the ones associated to **LEV**, that is characterized on average by **low** values of all the impact indexes.

The absence of significant trends in the chlorophyll extremes ascribed to both the subdomains and the whole basin is in general agreement with Colella et al. [2016].

An **overall classification** of all the identified macro-events, based on basin-scale mean severity and anomaly, was made using the medians of the distribution of the two indexes on the whole Mediterranean domain. Macro-events were then classified by the 4 combinations of high/low values of the indexes, with the same scheme adopted for the 4 subdomains, in order to quantify their main character with respect to the overall Mediterranean perspective. This general classification confirms the identification of **NWM and ADS** as subdomains of macro-events with **high severity and high anomaly**, quantifying this feature with a percentage higher than 70% of the total macro-events occurring in those subdomains. On the contrary, in ION and LEV >50% of macro-events show low values of both indexes, even if **hot spots** of macro-events heavily impacting the ecosystem can be observed in the **North Ionian Sea**, in the **southern coast of Sicily** and in the **Rhodes Gyre** regions.

Considering the examined examples of macro-events in NWM, ADS and LEV subdomains, **the model is able to reproduce** the main features of timing and location of the phytoplankton **patterns observed by remote sensing** in NWM and LEV areas. The intensity associated to the highest values of the model-derived surface chlorophyll is in good agreement with the observations in the NWM case, whereas it is overestimated in LEV macro-events. Satellite data in the year of occurrence of the ADS macro-event are not available.

In all investigated cases, the **physical forcing anomalies** with respect to climatology appears to play the major role as **trigger** of the chlorophyll macro-events and, therefore, of the most pronounced biological processes occurring in the marine ecosystem. However, this aspect requires further investigation.

Finally, we explored how the investigated macro-events are characterized in terms of the different **phytoplankton subgroups** (BFM parametrization of picophytoplankton, flagellates, diatoms, large phytoplankton). The picophytoplankton and the diatoms are predominant in the analysed macro-events in NWM and ADS. Flagellates are abundant only in LEV macro-events and the large phytoplankton is negligible in all cases[1]. Further macro-events should be

[1]The contribution of the large phytoplankton is significant only in the Alboran Sea (not shown).

analysed in order to characterize the relative abundance and dynamics of the phytoplankton subgroups in the Mediterranean subdomains.

As general remarks, the proposed **method** provides a **new perspective** for the chlorophyll dynamics, shaped on the spatio-temporal evolution of its local extreme values, which are associated to a strong increase of the ecosystem primary production (i.e. to eutrophication, outstanding food availability for secondary production and high production of particulate organic carbon, with resulting enhanced carbon sequestration). In fact, the spatio-temporal volume containing the local extremes of chlorophyll is considered an event itself (the macro-event), characterized by global scalar properties (the indexes of coordinates, shape and strenght) and analysed separately. In this way, the indexes of the macro-events, resulting from the summary of a lot of local information, can be used to characterize and to evaluate trends in the chlorophyll extremes. Moreover, since the present study was carried out from a multidecadal dataset, it can be used as a **reference statistics** for the future investigations of the chlorophyll extremes on the Mediterranean Sea.

On the other hand, the spatio-temporal volume provides a mask to identify the domain of development of the macro-event starting from its first occurrence and, therefore, to investigate its **internal dynamics and feedbacks**, in connection also with other biogeochemical and physical variables. This potentiality of the method was shown in the study of the single macro-events, but should be exploited more in order to draw general conclusions about the processes responsible for the onset and of the depletion of the chlorophyll extremes in the Mediterranean regions.

Overall, the **3D state-of-the-art coupled model** implemented to conduct this study allows to describe the Mediterranean biogeochemistry at mesoscale on the intra-week frequency. The climatological physical and biogeochemical features of the Mediterranean Sea reproduced by the coupled model are in good agreement with available observations and validated models. Moreover, focusing on the marine biogeochemical extremes, the model-derived evolution of the chlorophyll extremes appears to generally catch the spatio-temporal patterns shown by the satellite maps.

On the other hand, some **limitations** of the model are evident in the parametrizations of the river discharge and of the light extinction factor.

In the first case, the use of a monthly climatology can actually represent a coarse approximation of the riverine input of biogeochemical quantities (e.g. the nutrients) that affects the coastal dynamics. Nevertheless, the investigation of the extreme events in this study is referred only to the open sea domain, that is not directly influenced by the river discharge.

The light extinction is parametrized using climatological satellite data as the background component, plus self-shading of phytoplankton. In fact, formulations based only on the water absorption coefficient and plankton self-shading do not reproduce the observed light attenuation along the water column and the DCM gradients across the Mediterranean Sea. However, self-

shading component for the phytoplankton reflects the internal dynamics of the model and acts as a correction on the background factor.

Although the coupled model configuration used in this study was considered adequate to describe the Mediterranean biogeochemical extremes, this clearly does not preclude further improvements or modifications for **future developments of this work**.

Among them, the investigation of the triggers of the surface chlorophyll macro-events, shown in some representative cases, could be extended in the whole dataset of macro-events. This can be done also for the study of the dynamics of the four phytoplankton subgroups.

In addition, other kind of studies can be carried out using the same approach. For example, the proposed method can be applied to the integrated chlorophyll (computed from the model-derived 3D chlorophyll field). A comparison between the macro-events of integrated and surface chlorophyll, in the case of concomitant and asinchronous macro-events, could allow to evaluate the importance of the vertical dynamics in the extremes occurrence.

Another valuable application of the method is running the coupled model for future scenario, in order to assess possible trends in the future projections of the extremes of chlorophyll on the Mediterranean Sea.

Finally, the method for the identification and characterization of the extremes could be used on other biogeochemical variables (e.g. the nutrients), also for the evaluation of their extremely low values, in dependence of the lowest percentile thresholds (e.g. in a study related to the oxygen minima), rather than the highest ones. Furthermore, the method can be even applied to other Earth Science disciplines (e.g. precipitations in Atmospheric Science).

Appendix A

The model corroboration

A.1 Climatological means of temperature, salinity and nutrients over Mediterranean sub-regions

Following the procedure introduced by Manca et al. [2004], the Mediterranean Sea can be divided in sub-regions (fig. A.1) which exhibit typical features in the upper layer circulation and that can be then used as reference domains for the corroboration of physical and biogeochemical models.

The climatological means of the model-derived temperature, salinity and nitrate and phosphate concentrations were computed on three different sub-regions representative of the western, central and eastern part of the basin: Gulf of Lion, Ionian South and Levantine North (from the reference terminology,

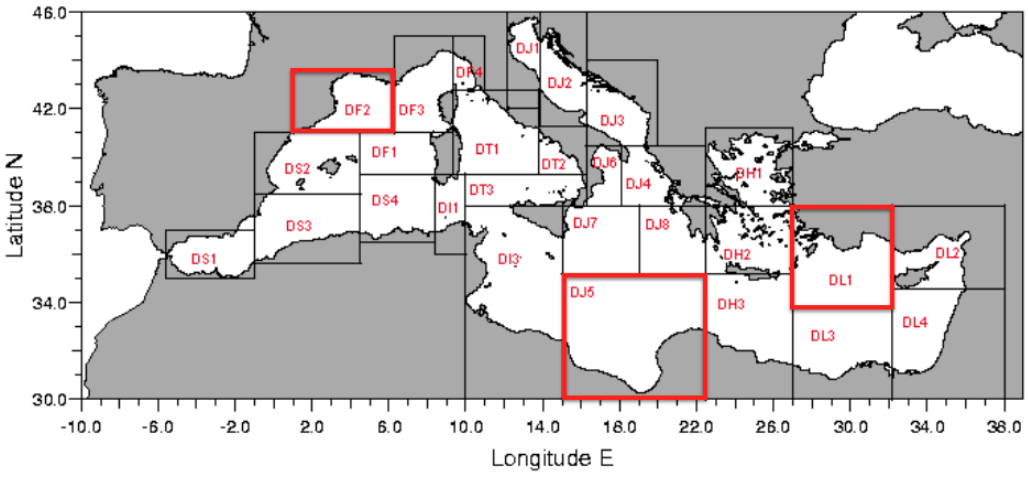

Figure A.1. Map of the Mediterranean Sea showing the spatial limits and the nomenclature of the regions established by Manca et al. [2004]. The bold red boxes indicate the regions used as domains of corroboration in the present study (original figure taken from the reference article).

Water mass	SURF (m)	LIW (m)	DW (m)
DF2	0-5	400	> 1500
DJ5	0-5	250	> 1500
DL1	0-5	125	> 1500

Table A.1. Depths for the three vertical layers of the Mediterranean sub-domains considered in the analysis.

corresponding to the DF2, DJ5 and DL1 sub-regions, respectively, in fig. A.1). In each sub-region three different means were computed for the surface water, the LIW and the DW, at depths indicated in tab. A.1.

Overall, the model-derived quantities (red crosses) appear in good agreement with the literature data (black circles) for all the analysed sub-regions (fig. A.2-A.3), considering that the time range of computation for the model and the one for the reference are not exactly the same and accounting for the intrinsic limitation of the sampling in time and space for the in-situ measurements. However, considering the overestimation of the nitrate concentration in the upper Levantine North (fig. A.3(b)) we expect a possible corresponding overestimation of the surface chlorophyll and/or primary productivity in that area, actually found as reported in the secs. A.3 and A.4, respectively.

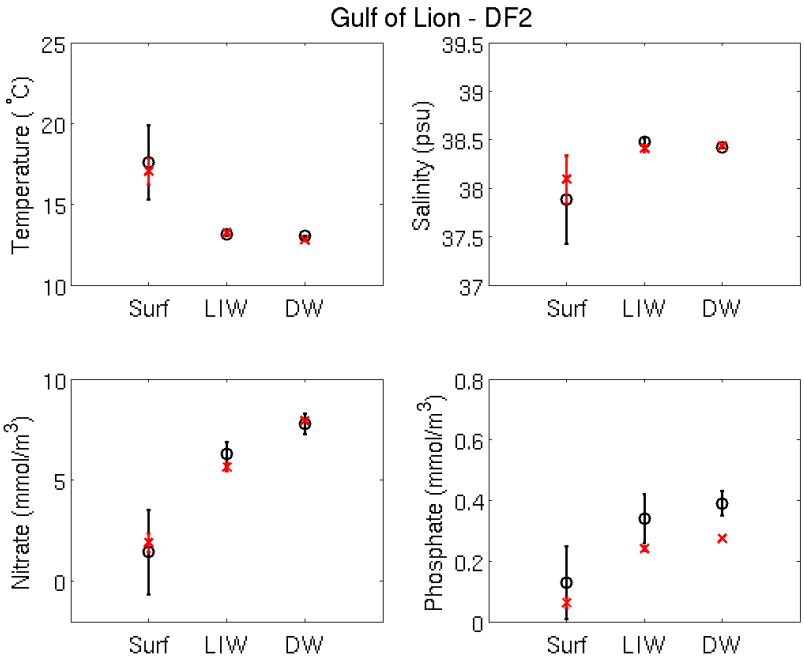

Figure A.2. Model-derived climatological means for temperature, salinity, nitrate and phosphate in the DF2-Gulf of Lion (red crosses), compared with literaure data (Manca et al. [2004], black circles).

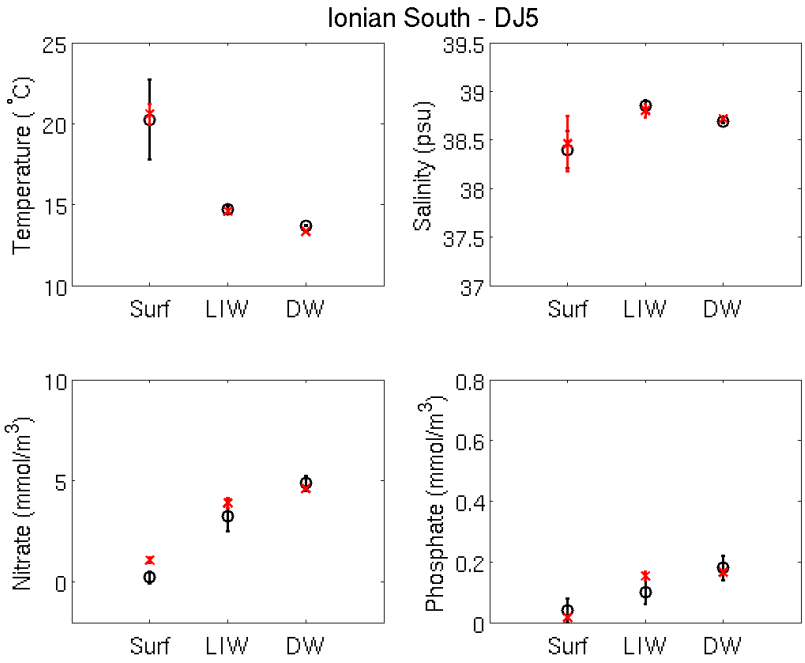

(a)

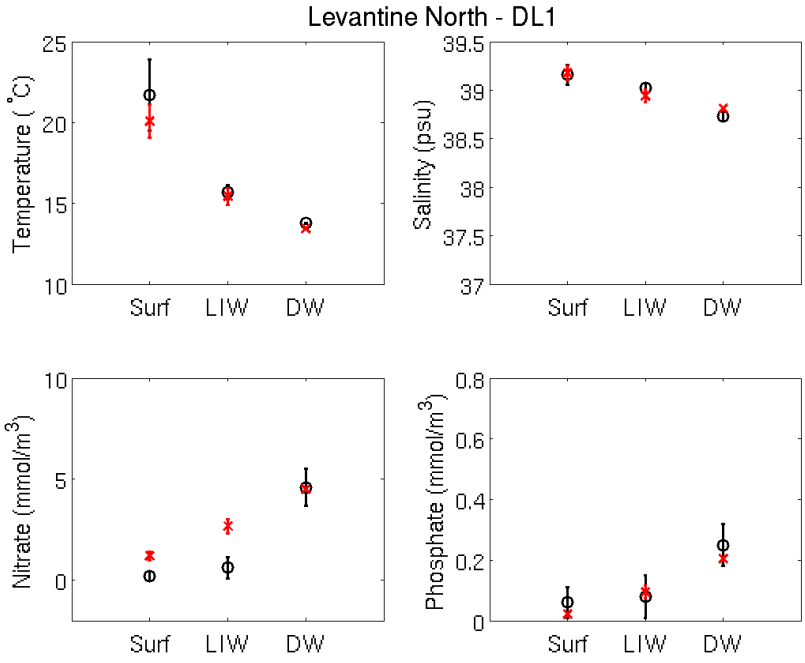

(b)

Figure A.3. Model-derived climatological means for temperature, salinity, nitrate and phosphate (red crosses), compared with literature data (Manca et al. [2004], black circles), in the DJ5-Ionian South (a) and in the DL1-Levantine North (b) sub-regions.

A.2 The Mixed Layer Depth

The Mixed Layer Depth (MLD) is the key variable connecting the physics and the biology, since it provides an indication about the preconditioning factor of the nutrient supply to the euphotic layer and of the subsequent establishment of the stratification. The MLD is a daily output variable of the MITgcm model, computed according the (selected) density-based criterion as the depth at which the water temperature is $\Delta T = 0.2$°C colder than the surface water. The model-derived monthly-averaged MLD for the period 1994-2012 is depicted in fig. A.4(a), where the grid points showing a mixing depth higher than 400 m (full scale) do not exceed the depth of 680 m, reached in the South Adriatic Sea.

These model results can be compared with the D'Ortenzio et al. [2005] reference climatology, where the MLD was computed on data available from 1940 to 2004, following temperature-based and density-based criteria referred to the same range of temperature $\Delta T = 0.2$°C (fig. A.4(b)).

On the whole, we can assert that the most important feature related to the MLD, that is its annual dynamics of alternation of mixing/stratification in the areas referred to higher biomass and production, provided by the MITgcm model is consistent with the reference.

In fact, the MITgcm model reproduces distinctly the signature of the annual cycle of mixing and stratification, with the MLD that deepens in autumn and reaches the higher values in the late-winter months (Jan-Feb-Mar). Moreover, the well known areas of higher convection (the Gulf of Lion and the South Adriatic Sea) and the Northern Ionian Sea depict the highest values of the monthly climatology, despite a small overestimate of the corresponding "hot spots" in the reference data. Also the spring and summer model-derived depths of stratification are in good agreement with D'Ortenzio et al. [2005].

The winter values of 200-300 m of depth in the Eastern Ionian Sea, in the Cretan Sea and in the Rhodes Gyre instead deviate more from the reference, showing almost double values, whereas in the western sub-basin the major overestimation with respect to the literature data are found in the southern part in December. However, there is also an underestimation of the MLD computed by the model in other areas, e.g. the Southern and Eastern Levantine Sea, for the most part of the year.

A.3 The chlorophyll

The comparison between the model-derived **surface chlorophyll** concentration (averaged in the first 10m) and the ESA-CCI satellite data (`http://marine.copernicus.eu/` and [Volpe et al., 2017]) in the open sea. i.e. for grid points referred to depths higher than 200 m, is depicted in fig. A.5.

The west-east gradient across the Mediterranean Sea, the pattern in the Alboran Sea and the values of chlorophyll (about 0.25 mg/m^3) in the Gulf

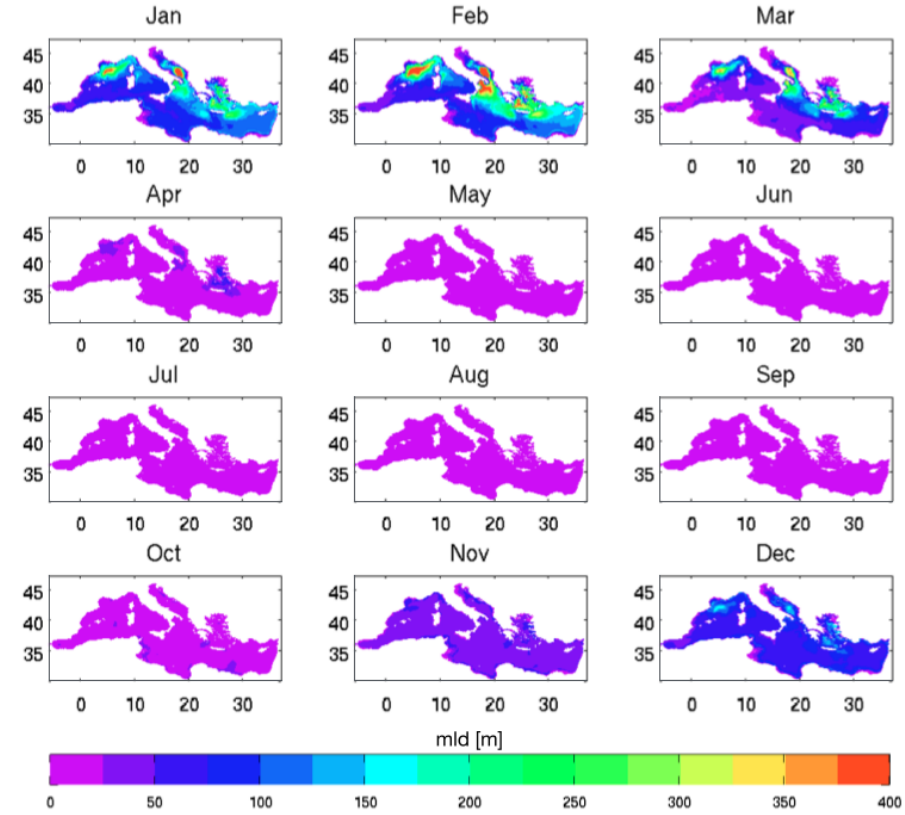

(a)

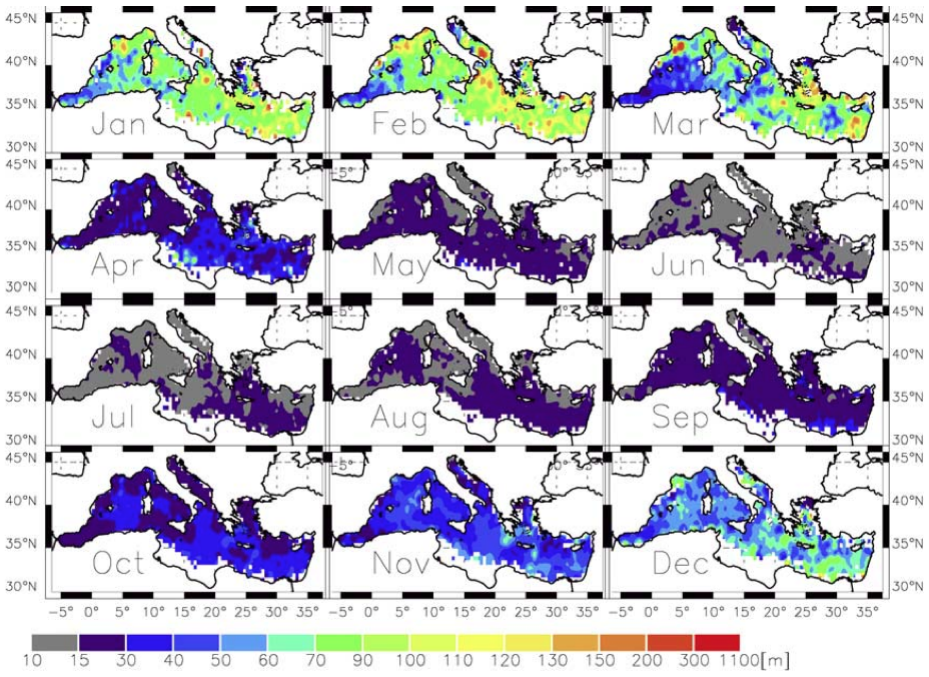

(b)

Figure A.4. Model-derived MLD climatology in the Mediterranean Sea, monthly averaged in the period 1994-2012, (a), compared with literature data, as reported in D'Ortenzio et al. [2005], (b).

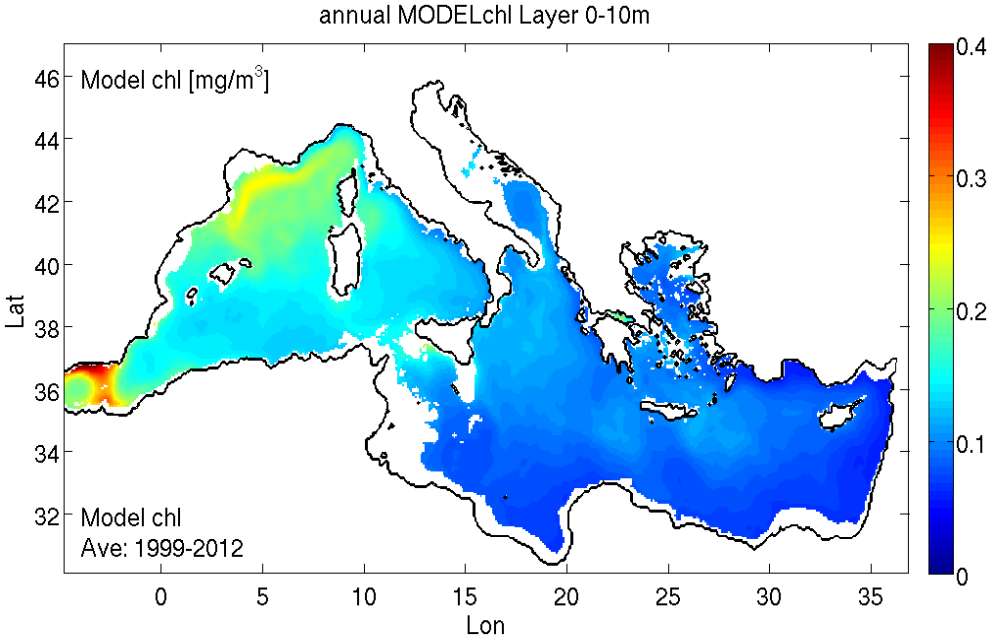

(a)

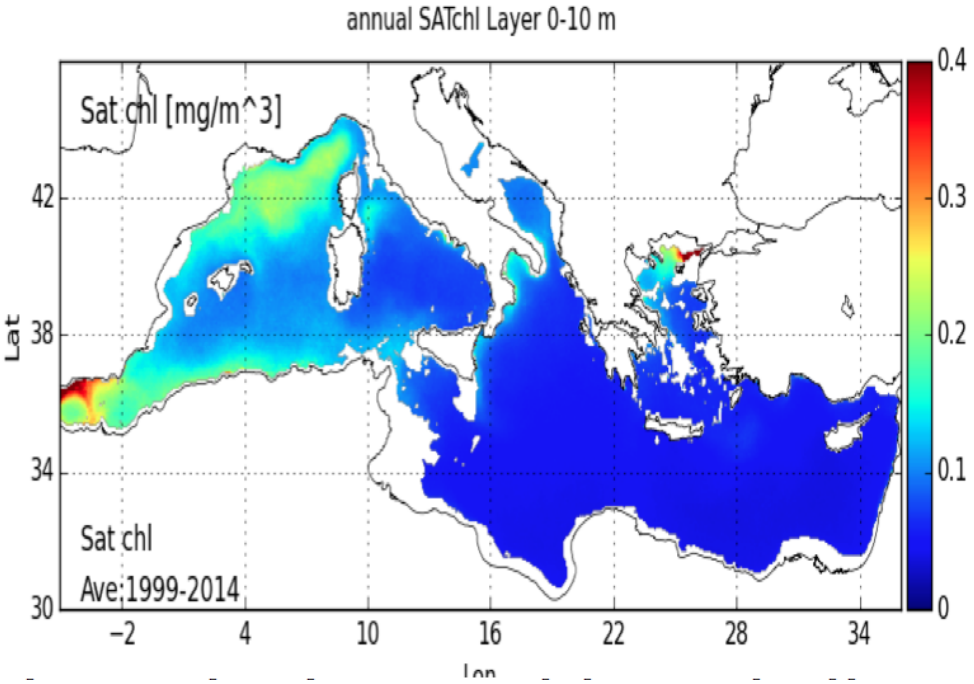

(b)

Figure A.5. The model-derived 1999-2012 time-mean (a) and the satellite-derived 1999-2014 time-mean (b) of the surface chlorophyll computed as the mean concentration on the first 10 m, for grid points with depth higher than 200 m. The figure of the satellite chlorophyll is taken from Cossarini et al. [2017b].

of Lion in the model output (A.5(a)) are consistent with the satellite map (A.5(b)). We attributed the overestimation of the chlorophyll values in the South Western Mediterranean Sea and in the Ionian and Western Levantine Seas to the overestimations of the vertical mixing already recognized in the sec. A.2, and the relatively higher values in the Tyrrenian Sea to the following advection/diffusion of nutrients and chlorophyll from the western areas. However, these overestimations appears not to compromise the capture of the main patterns in the western sub-basin.

In order to characterize also the vertical distribution of the chlorophyll in the Mediterranean Sea, the **vertical sections** of the chlorophyll concentration were computed from the 3D climatological means, averaging in space along the four transects indicated in the fig. A.6 as T1, T2, T3 and T4. These transects cross the Mediterranean Sea divided in the sub-domains as in Lazzari et al. [2012], that is the reference for this analysis. The same article, in which a coupled model with the BFM model as the biogeochemical part was validated against observations, is taken as reference also for the computation of the integrated net primary production, in the sec. A.4.

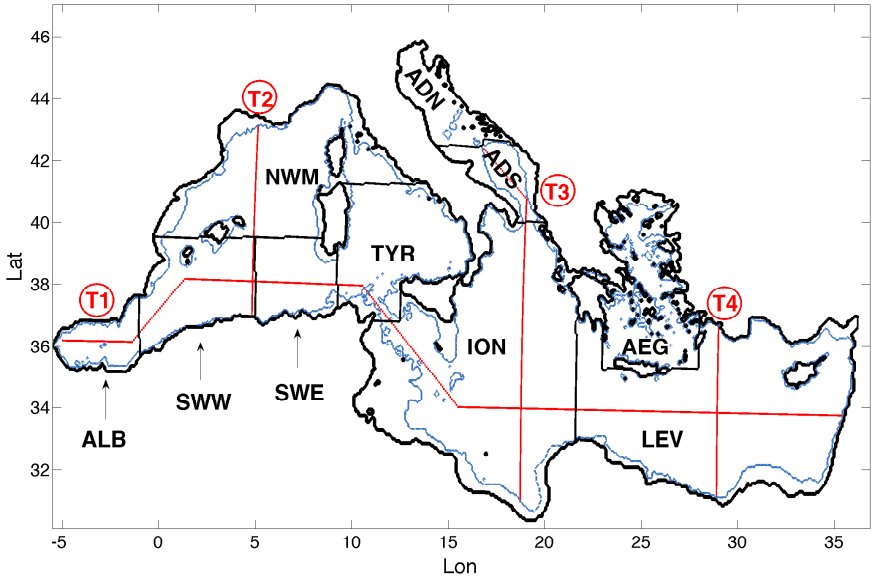

Figure A.6. Map of the Mediterranean Sea, with the gray contours limiting the areas with depth higher than 200 m (i.e. open sea) the red lines defining the T1, T2, T3, T4 transects and the black contours limiting the sub-domains defined as in Lazzari et al. [2012]: ALB = Alboran Sea, SWW = western side of the South Western Mediterranean Sea, SWE = eastern side of the South Western Mediterranean Sea, NWM = North Western Mediterranean Sea, TYR = Tyrrenian Sea , ION = Ionian Sea, LEV = Levantine Sea, plus ADS = Southern Adriatic Sea and AEG = Aegean Sea (this latter considered only in the next chapter).

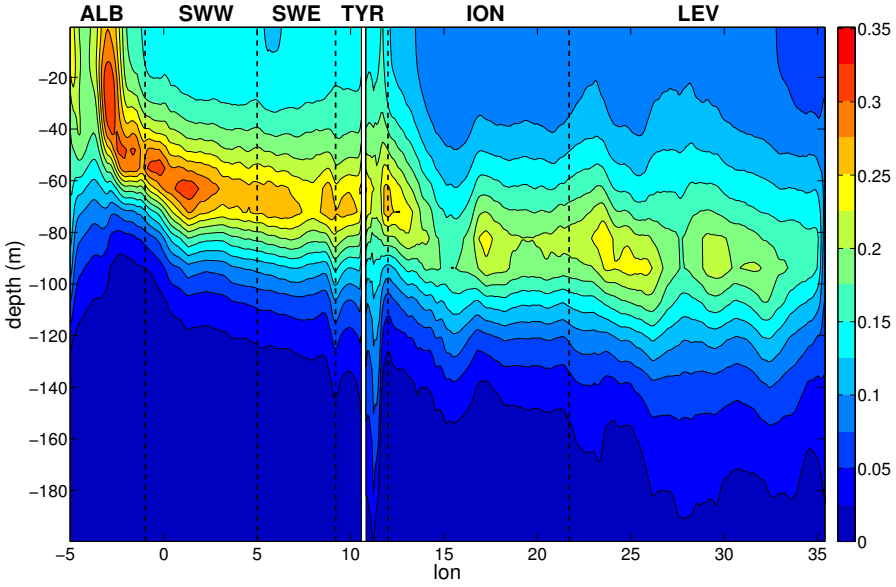

(a)

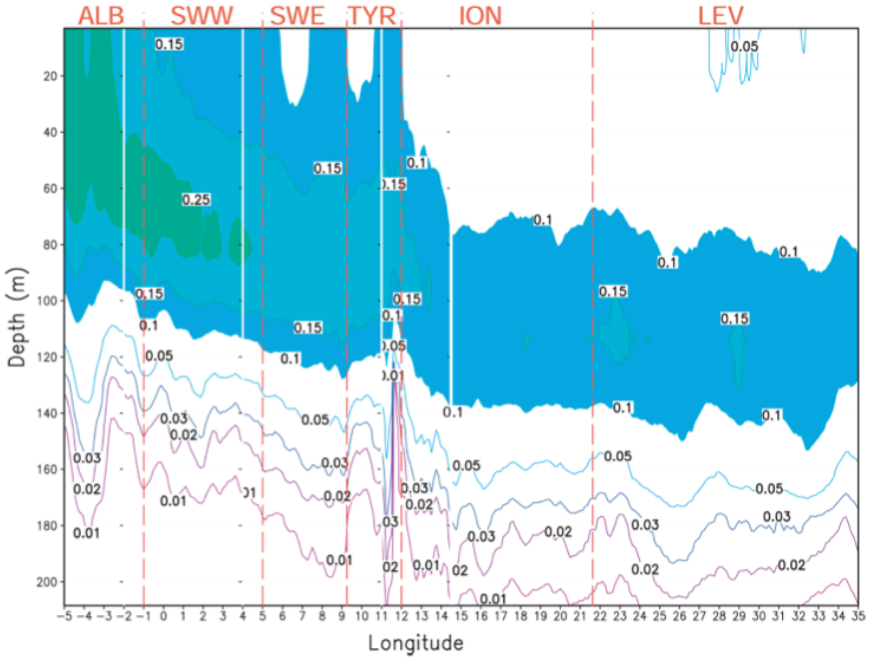

(b)

Figure A.7. Vertical sections along the T1 transect of the average chlorophyll (mg/m^3) according to the 1994-2012 MITgcm-BFM simulation (a) and Lazzari et al. [2012] reference (b).

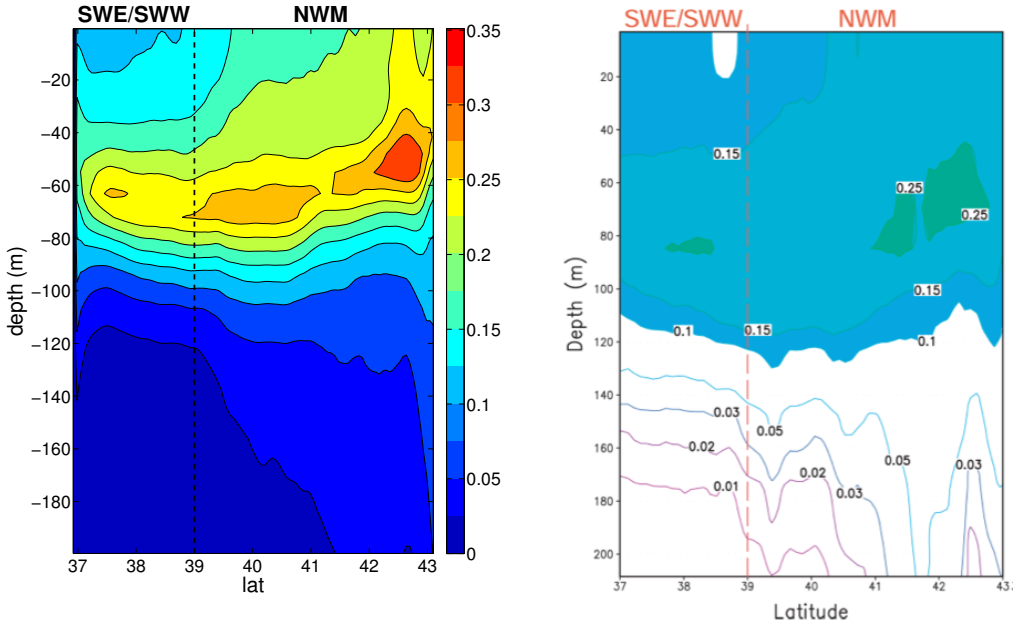

(a) (b)

Figure A.8. Vertical sections along the T2 transect of the average chlorophyll (mg/m^3) according to the 1994-2012 MITgcm-BFM simulation (a) and Lazzari et al. [2012] reference (b).

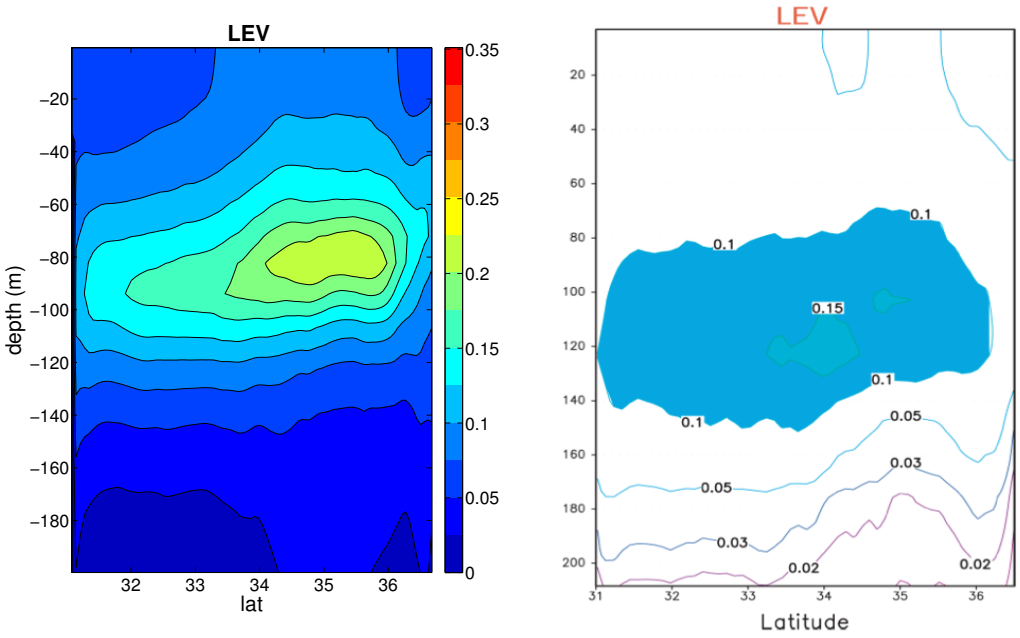

(a) (b)

Figure A.9. Vertical sections along the T4 transect of the average chlorophyll (mg/m^3) according to the 1994-2012 MITgcm-BFM simulation (a) and Lazzari et al. [2012] reference (b).

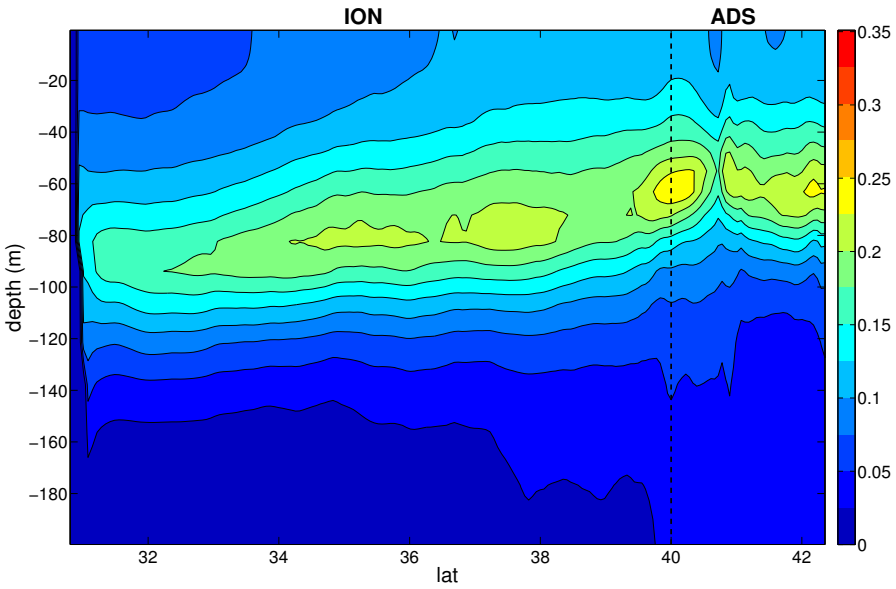

(a)

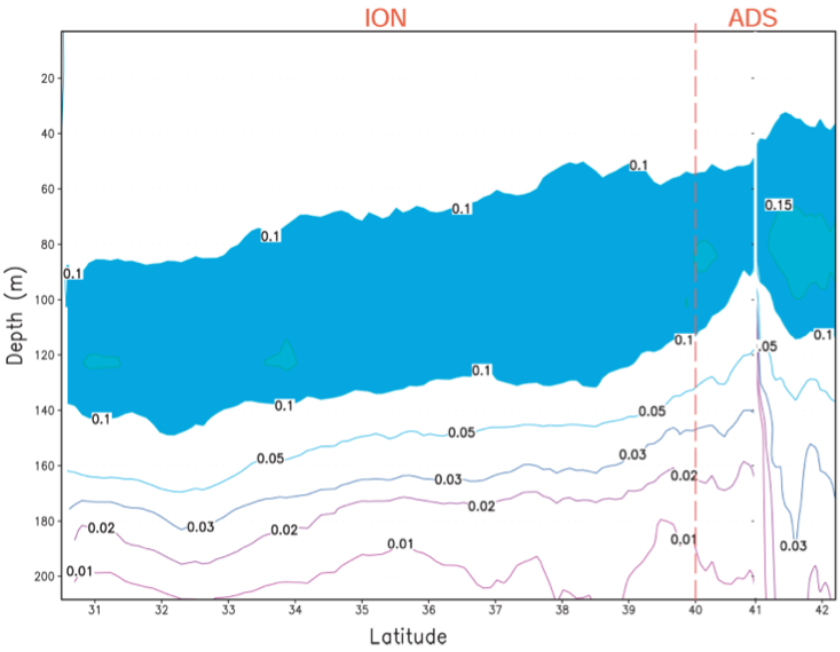

(b)

Figure A.10. Vertical sections along the T3 transect of the average chlorophyll (mg/m^3) according to the 1994-2012 MITgcm-BFM simulation (a) and Lazzari et al. [2012] reference (b).

All the MITgcm-BFM model-derived patterns in fig. A.7(a)-A.10(a), show values of chlorophyll higher in the western sub-domains (ALB, SWW, SWE and NWM) with respect to the eastern ones (ION, ADS, LEV), reproducing also at higher depths the zonal gradient already recognized in the surface map. Moreover, zonal and meridional gradients of the DCM with higher depth in the eastern and in the southern Mediterranean regions are detected.

More in detail, maximum values of chlorophyll approximately equal to 0.3 mg/m^3 are found in the Alboran Sea between 20 and 50 m of depth and in the western side of the South Western Mediterranean Sea between 50 and 65 m (fig. A.7(a)).

Moving eastward along the T1 transect, the highest concentrations decrease to 0.275 mg/m^3 between 60 and 75 m in the eastern side of the South Western Mediterranean Sea and in the Tyrrenian Sea, to 0.225-0.25 mg/m^3 in the Ionian Sea between 60 m and 80 m (displayed also in fig. A.10(a)) and in the Levantine Sea between 80 and 95 m (also in fig. A.9(a)) in the areas recognizable as the Western Cretan Cyclonic Gyre ([Pinardi et al., 2015]) and the Rhodes Gyre. In the North Western Mediterranean Sea (fig. A.8(a)) the DCM stands at about 50 m of depth and shows values approximately equal to 0.325 mg/m^3 in the Gulf of Lion area, whereas in the Adriatic Sea (fig. A.10(a)) it reaches about 70 m of depth, with concentrations of about 0.25 mg/m^3, both in the northern part of the sub-domain and at the Otranto Strait.

Negligible values of chlorophyll (with concentrations lower than 0.05 mg/m^3) are found below 200 m of depth along the four transects. In this study this range of depth is used as a proxy for the euphotic layer.

In comparison with the reference results (fig. A.7(b)-A.9(b)), bottom of the figures, the MITgcm-BFM model provides generally higher values of chlorophyll and a shallower DCM, but the main features of the Mediterranean Sea are in agreement with the reference.

A.4 The integrated net primary production

The net primary production integrated on the first 200 m (euphotic layer) was averaged in space in the main Mediterranean sub-domains and then climatologically averaged for the 1994-2012 years of simulation. In the table A.2 the MITgcm-BFM model-derived results are displayed in the first column, in comparison with the coupled model used in Lazzari et al. [2012] (second one), other models (third one), satellite data (fouth and fith ones) and in situ data (sixth one), with references in the caption. With respect to the sub-domains indicated in fig. A.6, the marginal seas (Adriatic Sea and Aegean Sea) were excluded from the statistics and from the definition of the MED domain, that is the Mediterranean Sea, and of the EAS sub-domain, that is the Eastern sub-basin; WES indicates the Western sub-basin. In the first two columns and in the fourth one also the intra-annual and the inter-annual variabilities are listed. In each sub-domain, the inter-annual variability was

computed as the standard deviation of the overall climatological mean, whereas the intra-annual variability as the mean of the 19 annual standard deviations. The MITgcm-BFM variabilities (first column) confirm that the seasonal cycle is the dominant component of variation in the Mediterranean production, as in the Lazzari et al. [2012] model and in the satellite cases (second and fourth columns, respectively).

The overall MITgcm-BFM climatological mean over the Mediterranean domain is about 104±3 $gC \cdot m^{-2} \cdot y^{-}1$, with higher values in the Western sub-domain with respect to the Eastern one (120±5 and 97±5 $gC \cdot m^{-2} \cdot y^{-}1$, respectively). This gradient is generally reproduced by all the other models and by the observations. Considering the single sub-domains, the ones belonging to the western part are in good agreement with the Lazzari et al. [2012] model and the satellite , despite the case of the Alboran Sea, whose integrated net primary production is underestimated by the MITgcm-BFM model, and the Tyrrenian Sea, whose values are overestimated; in the eastern sub-basin, both the Ionian Sea and the Levantine Sea display MITgcm-BFM values of integrated production overestimated, and this reflects on the global EAS mean. However, in these cases other models (third column) provide mean integrated productions with large deviations that comprise the MITgcm-BFM values. On the other hand, results from other satellites display globally higher values of productvity (fifth column) in all the Mediterranean areas, contrary to results from available in situ data (sixth column), for which the mean Mediterranean productivity is about 80-90 $gC \cdot m^{-2} \cdot y^{-}1$. Considering also the large variability associated to all the models and data used as reference, the capacity of the MITgcm-BFM to reproduce the integrated net primary production in the Mediterrean Sea was considered satisfactory.

	MITgcm BFM	OPATM BFM [a]	Other models	Satellite [e]	Other sat.	In situ
MED	104 (±63/±3)	98 (±82/±5)	x	90 (±48/±3)	135[f]	80-90[g]
WES	120 (±65/±5)	131 (±98/±6)	120[b]	112 (±65/±7)	163[f]	x
EAS	97 (±51/±5)	76 (±60/±5)	56[b]	76 (±20/±2)	121[f]	x
ALB	151 (±94/±7)	274 (±155/±11)	24-207[c]	179 (±116/±13)	x	x
SWW	125 (±51/±7)	160 (±89/±8)	24-207[c]	113 (±43/±6)	x	x
SWE	116 (±40/±6)	118 (±70/±13)	x	102 (±38/±4)	x	x
NWM	120 (±58/±7)	116 (±79/±6)	32-273[c]	115 (±67/±8)	x	86-232[h] 140-150[i]
TYR	109 (±40/±7)	92 (±63/±5)	x	90 (±35/±7)	x	x
ION	99 (±48/±6)	77 (±58/±4)	27-153[c]	79 (±23/±2)	x	62[l]
LEV	94 (±47/±7)	76 (±61/±5)	97[d] 36-158[c]	72 (±21/±2)	x	x

Table A.2. Horizontal averages of the vertical integrated net primary production (in units of $gC \cdot m^{-2} \cdot y^{-}1$) as annual climatologies computed in the different Mediterranean sub-domains, according to the MITgcm-BFM model (first column) and other models and reference data, as reported in Lazzari et al. [2012]. In parentheses there are the intra-annual and inter-annual variabilities, expressed as the mean over the analysed years of the standard deviations referred to the single years and the standard deviation of the final mean, respectively. References: a) Lazzari et al. [2012], b) Crispi et al. [2002], c) Allen et al. [2002], d) Napolitano et al. [2000], e) Colella [2007], f) Bosc et al. [2004], g) Sournia [1973], h) Marty and Chiavérini [2002], i) Conan et al. [1998], l) Boldrin et al. [2002].

Acknowledgements

This PhD thesis was developed in collaboration with the OGS - Istituto Nazionale di Oceanografia e di Geofisica Sperimentale (Trieste).

The research was co-sponsored by the Ministry of Education, University and Research (MIUR) under its extraordinary contribute for the Italian participation to activities related to the international infrastructure PRACE - The Partnership for Advanced Computing in Europe. The thesis work has been partially sponsored by OGS and CINECA under the HPC-TRES program award number 2016-04.

The Mediterranean configuration of the MITgcm used in this study was provided by Dr. Gianmaria Sannino (ENEA research center, Rome). I am thankful to him for his technical support in the first phase of the research project. The comparison with ESA-CCI data has been conducted using E.U. Copernicus Marine Service Information (`http://marine.copernicus.eu/`).

I would like to express my sincere gratitude mostly to my supervisor, Dr. Stefano Salon. His expertise, attention and encouragement were fundamental in all the time of research and writing of this thesis.

I am grateful also to Dr. Gianpiero Cossarini, for the great support that he gave to the project in all its parts, and to Dr. Cosimo Solidoro, for the insightful discussions and suggestions about the guidelines of the work. Finally, I would like to thank Dr. Stefano Querin and Dr. Paolo Lazzari that introduced me to the use of MITgcm and BFM models, Dr. Giorgio Bolzon and Eric Pascolo for their expert advice about parallel programming and Dr. Marco Reale for the discussions about the coupled model corroboration.

Bibliography

Allan, R. and Soden, B. (2008). Atmospheric warming and the amplification of precipitation extremes. *Science*, 321:1481–1484.

Allen, J., Somerfield, P., and Siddorn, J. (2002). Primary and bacterial production in the mediterranean sea: a modelling study. *Journal of Marine Systems*, 33:473–495.

Anderson, D. M., Glibert, P. M., and Burkholder, J. M. (2002). Harmful algal blooms and eutrophication: nutrient sources, composition, and consequences. *Estuaries*, 25(4):704–726.

Azam, F., Fenchel, T., Field, J. G., Gray, J., Meyer-Reil, L., and Thingstad, F. (1983). The ecological role of water-column microbes in the sea. *Estuaries*, 50(2).

Barale, V. (2003). Environmental remote sensing of the mediterranean sea. *Journal of Environmental Science and Health, Part A*, 38(8):1681–1688.

Barale, V., Jaquet, J.-M., and Ndiaye, M. (2008). Algal blooming patterns and anomalies in the mediterranean sea as derived from the seawifs data set (1998–2003). *Remote Sensing of Environment*, 112(8):3300–3313.

Bessières, L., Rio, M. H., Dufau, C., Boone, C., and Pujol, M. I. (2013). Ocean state indicators from myocean altimeter products. *Ocean Science*, 9(3):545–560.

Bethoux, J., Gentili, B., Morin, P., Nicolas, E., Pierre, C., and Ruiz-Pino, D. (1999). The mediterranean sea: a miniature ocean for climatic and environmental studies and a key for the climatic functioning of the north atlantic. *Progress in Oceanography*, 44(1):131–146.

Bethoux, J., Morin, P., Chaumery, C., Connan, O., Gentili, B., and Ruiz-Pino, D. (1998). Nutrients in the mediterranean sea, mass balance and statistical analysis of concentrations with respect to environmental change. *Marine Chemistry*, 63(1):155–169.

Bianchi, C. and Morri, C. (2000). Marine biodiversity of the mediterranean sea: Situation, problems and prospects for future research. *Marine Pollution Bulletin*, 40(5):367 – 376.

Bignami, F., Böhm, E., D'Acunzo, E., D'Archino, R., and Salusti, E. (2008). On the dynamics of surface cold filaments in the mediterranean sea. *Journal of Marine Systems*, 74(1–2):429 – 442.

Boldrin, A., Miserocchi, S., Rabitti, S., Turchetto, M., Balboni, V., and Socal, G. (2002). Particulate matter in the southern adriatic and ionian sea: characterisation and downward fluxes. *Journal of Marine Systems*, 33:389–410.

Bonanno, A., Placenti, F., Basilone, G., Mifsud, R., Genovese, S., Patti, B., Di Bitetto, M., Aronica, S., Barra, M., Giacalone, G., et al. (2014). Variability of water mass properties in the strait of sicily in summer period of 1998–2013. *Ocean Science*, 10(5):759–770.

Bosc, E., Bricaud, A., and Antoine, D. (2004). Seasonal and interannual variability in algal biomass and primary production in the mediterranean sea, as derived from 4 years of seawifs observations. *Global Biogeochemical Cycles*, 18(1).

Britton, C. and Dodd, J. (1976). Relationships of photosynthetically active radiation and shortwave irradiance. *Agricultural Meteorology*, 17(1):1–7.

Civitarese, G., Gačić, M., Lipizer, M., and Eusebi Borzelli, G. (2010). On the impact of the bimodal oscillating system (bios) on the biogeochemistry and biology of the adriatic and ionian seas (eastern mediterranean). *Biogeosciences*, 7(12):3987–3997.

Civitarese, G., Gačić, M., Vetrano, A., Boldrin, A., Bregant, D., Rabitti, S., and Souvermezoglou, E. (1998). Biogeochemical fluxes through the strait of otranto (eastern mediterranean). *Continental Shelf Research*, 18(7):773 – 789.

Colella, S. (2007). *La produzione primaria nel Mar Mediterraneo da satellite: sviluppo di un modello regionale e sua applicazione ai dati SeaWiFS, MODIS e MERIS*. PhD thesis, Università degli Studi di Napoli Federico II.

Colella, S., Falcini, F., Rinaldi, E., Sammartino, M., and Santoleri, R. (2016). Mediterranean ocean colour chlorophyll trends. *PLoS ONE*, 11.

Coll, M., Piroddi, C., Steenbeek, J., Kaschner, K., Lasram, F. B. R., Aguzzi, J., Ballesteros, E., Bianchi, C. N., Corbera, J., Dailianis, T., et al. (2010). The biodiversity of the mediterranean sea: estimates, patterns, and threats. *PloS one*, 5(8):e11842.

Conan, P., Pujo-Pay, M., Raimbault, P., and Leveau, M. (1998). Hydrological and biological variability in the gulf of lions. ii. productivity on the inner edge of the north mediterranean current. *Oceanologica Acta*, 6(21):767–782.

Conversi, A., Peluso, T., and Fonda-Umani, S. (2009). Gulf of trieste: A changing ecosystem. *Journal of Geophysical Research: Oceans*, 114(C3):n/a–n/a. C03S90.

Cossarini, G., Querin, S., Solidoro, C., Sannino, G., Lazzari, P., Di Biagio, V., and Bolzon, G. (2017a). Development of bfmcoupler (v1.0), the coupling scheme that links the mitgcm and bfm models for ocean biogeochemistry simulations. *Geoscientific Model Development*, 10(4):1423–1445.

Cossarini, G., Salon, S., Bolzon, G., Lazzari, P., and Clementi, E. (2017b). Mediterranean sea production centre medsea reanalysis bio 006-008 quality information document, copernicus marine environment monitoring service.

Crisci, C., Bensoussan, N., Romano, J.-C., and Garrabou, J. (2011). Temperature anomalies and mortality events in marine communities: insights on factors behind differential mortality impacts in the nw mediterranean. *PLoS One*, 6(9):e23814.

Crise, A., Allen, J., Baretta, J., Crispi, G., Mosetti, R., and Solidoro, C. (1999). The mediterranean pelagic ecosystem response to physical forcing. *Progress in Oceanography*, 44(1):219–243.

Crise, A., Solidoro, C., and Tomini, I. (2003). Preparation of initial conditions for the coupled model ogcm and initial parameters setting. *MFSTEP report WP11, subtask*, 11310:2003.

Crispi, G., Crise, A., and Solidoro, C. (2002). Coupled mediterranean ecomodel of the phosphorus and nitrogen cycles. *Journal of Marine Systems*, 33:497–521.

Dafner, E., González-Dávila, M., Santana-Casiano, J. M., and Sempéré, R. (2001a). Total organic and inorganic carbon exchange through the strait of gibraltar in september 1997. *Deep Sea Research Part I: Oceanographic Research Papers*, 48(5):1217–1235.

Dafner, E. V., Sempéré, R., and Bryden, H. L. (2001b). Total organic carbon distribution and budget through the strait of gibraltar in april 1998. *Marine Chemistry*, 73(3):233–252.

Delaunay, D. (1988). Extreme wind speed distributions for tropical cyclones. *Journal of Wind Engineering and Industrial Aerodynamic*, 28:61–68.

Demirov, E. K. and Pinardi, N. (2007). On the relationship between the water mass pathways and eddy variability in the western mediterranean sea. *Journal of Geophysical Research: Oceans*, 112(C2):n/a–n/a. C02024.

D'Ortenzio, F., Iudicone, D., de Boyer Montegut, C., Testor, P., Antoine, D., Marullo, S., Santoleri, R., and Madec, G. (2005). Seasonal variability of the

mixed layer depth in the mediterranean sea as derived from in situ profiles. *Geophysical Research Letters*, 32(12).

D'Ortenzio, F. and Ribera D'Alcalà, M. (2009). On the trophic regimes of the mediterranean sea: a satellite analysis. *Biogeosciences*, 6:139–148.

EEA (2015). European environment agency: Chlorophyll in transitional, coastal and marine waters. *http://www.eea.europa.eu/data-and-maps/indicators/chlorophyll-in-transitional-coastal-and-2*.

Efrati, S., Lehahn, Y., Rahav, E., Kress, N., Herut, B., Gertman, I., Goldman, R., Ozer, T., Lazar, M., and Heifetz, E. (2013). Intrusion of coastal waters into the pelagic eastern mediterranean: in situ and satellite-based characterization. *Biogeosciences*, 10(5):3349–3357.

Estrada, M. (1996). Primary production in the northwestern mediterranean. *Scientia Marina*, 60(2):55–64.

Estrada, M., Varela, R. A., Salat, J., Cruzado, A., and Arias, E. (1999). Spatio-temporal variability of the winter phytoplankton distribution across the catalan and north balearic fronts(nw mediterranean). *Journal of Plankton Research*, 21(1):1–20.

Estrada, M., Vives, F., and Alcaraz, M. (1985). Life and the productivity of the open sea. *Western Mediterranean. Pergamon Press, Oxford*, 148197.

Field, C. B. (2012). *Managing the risks of extreme events and disasters to advance climate change adaptation: special report of the intergovernmental panel on climate change*. Cambridge University Press.

Garcia Lafuente, J., Sanchez Román, A., Diaz del Rio, G., Sannino, G., and Sánchez Garrido, J. C. (2007). Recent observations of seasonal variability of the mediterranean outflow in the strait of gibraltar. *Journal of Geophysical Research: Oceans*, 112(C10):n/a–n/a. C10005.

Gascard, J. and Richez, C. (1985). Water masses and circulation in the western alboran sea and in the straits of gibraltar. *Progress in Oceanography*, 15(3):157–216.

Gačić, M., Borzelli, G. L. E., Civitarese, G., Cardin, V., and Yari, S. (2010). Can internal processes sustain reversals of the ocean upper circulation? the ionian sea example. *Geophysical Research Letters*, 37(9):n/a–n/a. L09608.

Gačić, M., Civitarese, G., Kovačević, V., Ursella, L., Bensi, M., Menna, M., Cardin, V., Poulain, P.-M., Cosoli, S., Notarstefano, G., and Pizzi, C. (2014). Extreme winter 2012 in the adriatic: an example of climatic effect on the bios rhythm. *Ocean Science*, 10(3):513–522.

Gertmann, I., Ovchinnikov, I., and Popv, Y. I. (1994). Deep convection in the eastern basin of the mediterranean sea. *Oceanology*, 34(1):19–25.

Ghil, M., Yiou, P., Hallegatte, S., Malamud, B., Naveau, P., Soloviev, A., Friederichs, P., Keilis-Borok, V., Kondrashov, D., Kossobokov, V., et al. (2011). Extreme events: dynamics, statistics and prediction. *Nonlinear Processes in Geophysics*, 18(3):295–350.

Gohin, F., Saulquin, B., Oger-Jeanneret, H., Lozac'h, L., Lampert, L., Lefebvre, A., Riou, P., and Bruchon, F. (2008). Towards a better assessment of the ecological status of coastal waters using satellite-derived chlorophyll-a concentrations. *Remote Sensing of Environment*, 112(8):3329–3340.

Green, J. and Stigebrandt, A. (2003). Statistical models and distributions of current velocities with application to the prediction of extreme events. *Estuarine, Coastal and Shelf Science*, 58:601–609.

Hansom, J. D., Switzer, A. D., and Pile, J. (2014). Extreme waves: causes, characteristics, and impact on coastal environments and society. *Coastal and Marine Hazards, Risks, and Disasters*, page 307.

Harzallah, A., Jordà, G., Dubois, C., Sannino, G., Carillo, A., Li, L., Arsouze, T., Cavicchia, L., Beuvier, J., and Akhtar, N. (2016). Long term evolution of heat budget in the mediterranean sea from med-cordex forced and coupled simulations. *Climate Dynamics*, pages 1–21.

Hauri, C., Gruber, N., McDonnell, A., and Vogt, M. (2013). The intensity, duration, and severity of low aragonite saturation state events on the california continental shelf. *Geophysical Research Letters*, 40(13):3424–3428.

Hobday, A. J., Alexander, L. V., Perkins, S. E., Smale, D. A., Straub, S. C., Oliver, E. C., Benthuysen, J. A., Burrows, M. T., Donat, M. G., Feng, M., et al. (2016). A hierarchical approach to defining marine heatwaves. *Progress in Oceanography*, 141:227–238.

Hopkins, T. (1978). Physical processes in the mediterranean basins. *Estuarine transport processes*, pages 269–310.

Huertas, I. E., Ríos, A. F., García-Lafuente, J., Makaoui, A., Rodríguez-Gálvez, S., Sánchez-Román, A., Orbi, A., Ruíz, J., and Pérez, F. F. (2009). Anthropogenic and natural co_2 exchange through the strait of gibraltar. *Biogeosciences*, 6(4):647–662.

Huertas, I. E., Ríos, A. F., García-Lafuente, J., Navarro, G., Makaoui, A., Sánchez-Román, A., Rodriguez-Galvez, S., Orbi, A., Ruíz, J., and Pérez, F. F. (2012). Atlantic forcing of the mediterranean oligotrophy. *Global Biogeochemical Cycles*, 26(2):n/a–n/a. GB2022.

Ignatiades, L., Gotsis-Skretas, O., Pagou, K., and Krasakopoulou, E. (2009). Diversification of phytoplankton community structure and related parameters along a large-scale longitudinal east–west transect of the mediterranean sea. *Journal of Plankton Research*, 31(4):411–428.

Katz, R. (1999). Extreme value theory for precipitation: sensitivity analysis for climate change. *Advances in Water Resources*, 23(2):133–139.

Korres, G., Pinardi, N., and Lascaratos, A. (2000). The ocean response to low-frequency interannual atmospheric variability in the mediterranean sea. part ii: Empirical orthogonal functions analysis. *Journal of Climate*, 13(4):732–745.

Kress, N. and Herut, B. (2001). Spatial and seasonal evolution of dissolved oxygen and nutrients in the southern levantine basin (eastern mediterranean sea): chemical characterization of the water masses and inferences on the n: P ratios. *Deep Sea Research Part I: Oceanographic Research Papers*, 48(11):2347–2372.

Krom, M., Emeis, K., and Van Cappellen, P. (2010). Why is the eastern mediterranean phosphorus limited? *Progress in Oceanography*, 85(3):236–244.

Krom, M., Kress, N., Brenner, S., and Gordon, L. (1991). Phosphorus limitation of primary productivity in the eastern mediterranean sea. *Limnology and Oceanography*, 36(3):424–432.

Larnicol, G., Ayoub, N., and Le Traon, P.-Y. (2002). Major changes in mediterranean sea level variability from 7 years of topex/poseidon and ers-1/2 data. *Journal of Marine Systems*, 33:63–89.

Lascaratos (1993). A mixed-layer study of the formation of levantine intermediate water. *Journal of Geophysical Research*, 98:14 739–14 749.

Lavigne, H., D'ortenzio, F., d'Alcalà, M. R., Claustre, H., Sauzède, R., and Gacic, M. (2015). On the vertical distribution of the chlorophyll a concentration in the mediterranean sea: a basin-scale and seasonal approach. *Biogeosciences*, 12(16):5021–5039.

Lazzari, P., Solidoro, C., Ibello, V., Salon, S., Teruzzi, A., Béranger, K., Colella, S., and Crise, A. (2012). Seasonal and inter-annual variability of plankton chlorophyll and primary production in the mediterranean sea: a modelling approach. *Biogeosciences*, 9(1):217.

Lazzari, P., Solidoro, C., Salon, S., and Bolzon, G. (2016). Spatial variability of phosphate and nitrate in the mediterranean sea: A modeling approach. *Deep Sea Research Part I: Oceanographic Research Papers*, 108:39–52.

Le Quéré, C., Moriarty, R., Andrew, R. M., Peters, G. P., Ciais, P., Friedlingstein, P., Jones, S., Sitch, S., Tans, P., Arneth, A., et al. (2015). Global carbon budget 2014.

Leaman, K. D. (1994). The formation of western mediterranean deep water. *Seasonal and Interannual Variability of the Western Mediterranean Sea*, pages 227–248.

Legendre, L., Rivkin, R. B., Weinbauer, M. G., Guidi, L., and Uitz, J. (2015). The microbial carbon pump concept: potential biogeochemical significance in the globally changing ocean. *Progress in Oceanography*, 134:432–450.

Levitus, S. (1982). Climatological atlas of the world ocean. *NOAA Prof. Pap.*, 13.

Lindeman, R. L. (1941). Seasonal food-cycle dynamics in a senescent lake. *American Midland Naturalist*, pages 636–673.

Lindeman, R. L. (1942). The trophic-dynamic aspect of ecology. *Ecology*, 23(4):399–417.

Lionello, P. (2012). *The climate of the Mediterranean region: from the past to the future*. Elsevier.

Llasses, J., Jordà, G., Gomis, D., Adloff, F., Macías, D., Harzallah, A., Arsouze, T., Akthar, N., Li, L., Elizalde, A., et al. (2016). Heat and salt redistribution within the mediterranean sea in the med-cordex model ensemble. *Climate Dynamics*, pages 1–25.

Longhurst, A. (1998). Ecology geography of the sea.

Ludwig, W., Dumont, E., Meybeck, M., and Heussner, S. (2009). River discharges of water and nutrients to the mediterranean and black sea: major drivers for ecosystem changes during past and future decades? *Progress in Oceanography*, 80(3):199–217.

Ludwig, W., Probst, J.-L., and Kempe, S. (1996). Predicting the oceanic input of organic carbon by continental erosion. *Global Biogeochemical Cycles*, 10(1):23–41.

Luterbacher, J., Dietrich, D., Xoplaki, E., Grosjean, M., and Wanner, H. (2004). European seasonal and annual temperature variability, trends, and extremes since 1500. *Science*, 303(5663):1499–1503.

Macías, D., Navarro, G., Bartual, A., Echevarría, F., and Huertas, I. E. (2009). Primary production in the strait of gibraltar: Carbon fixation rates in relation to hydrodynamic and phytoplankton dynamics. *Estuarine, Coastal and Shelf Science*, 83(2):197–210.

Manca, B., Burca, M., Giorgetti, A., Coatanoan, C., Garcia, M.-J., and Iona, A. (2004). Physical and biochemical averaged vertical profiles in the mediterranean regions: an important tool to trace the climatology of water masses and to validate incoming data from operational oceanography. *Journal of Marine Systems*, 48(1):83–116.

Maneesha, K., Sarma, V., Reddy, N., Sadhuram, Y., Murty, T. R., Sarma, V., and Kumar, M. D. (2011). Meso-scale atmospheric events promote phytoplankton blooms in the coastal bay of bengal. *Journal of earth system science*, 120(4):773–782.

Mann, K. and Lazier, J. (2006). *Dynamics of Marine Ecosystems*. Blackwell Publishing Ltd.

Markaki, Z., Loÿe-Pilot, M., Violaki, K., Benyahya, L., and Mihalopoulos, N. (2010). Variability of atmospheric deposition of dissolved nitrogen and phosphorus in the mediterranean and possible link to the anomalous seawater n/p ratio. *Marine Chemistry*, 120(1):187–194.

Marty, J. and Chiavérini, J. (2010). Hydrological changes in the ligurian sea (nw mediterranean, dyfamed site) during 1995–2007 and biogeochemical consequences. *Biogeosciences*, 7(7):2117–2128.

Marty, J.-C. and Chiavérini, J. (2002). Seasonal and interannual variations in phytoplankton production at dyfamed time-series station, northwestern mediterranean sea. *Deep Sea Research Part II: Topical Studies in Oceanography*, 49(11):2017–2030.

Mayot, N., D'Ortenzio, F., Ribera d'Alcalà, M., Lavigne, H., and Claustre, H. (2016). Interannual variability of the mediterranean trophic regimes from ocean color satellites. *Biogeosciences*, 13(6):1901–1917.

Miquel, J., Fowler, S., Rosa, J. L., and Buat-Menard, P. (1994). Dynamics of the downward flux of particles and carbon in the open northwestern mediterranean sea. *Deep Sea Research Part I: Oceanographic Research Papers*, 41(2):243 – 261.

Morel, A. and André, J.-M. (1991). Pigment distribution and primary production in the western mediterranean as derived and modeled from coastal zone color scanner observations. *Journal of Geophysical Research: Oceans*, 96(C7):12685–12698.

Moutin, T. and Raimbault, P. (2002). Primary production, carbon export and nutrients availability in western and eastern mediterranean sea in early summer 1996 (minos cruise). *Journal of marine systems*, 33:273–288.

Napolitano, E., Oguz, T., Malanotte-Rizzoli, P., Yilmaz, A., and Sansone, E. (2000). Simulations of biological production in the rhodes and ionian basins of the eastern mediterranean. *Journal of Marine Systems*, 24(3):277–298.

Okaichi, T. (2004). *Red tides*, volume 4. Springer Science & Business Media.

Oubelkheir, K., Ford, P. W., Clementson, L. A., Cherukuru, N., Fry, G., and Steven, A. D. (2014). Impact of an extreme flood event on optical and biogeochemical properties in a subtropical coastal periurban embayment (eastern australia). *Journal of Geophysical Research: Oceans*, 119(9):6024–6045.

Passow, U. and Carlson, C. A. (2012). The biological pump in a high co2 world. *Marine Ecology Progress Series*, 470:249–271.

Pinardi, N., Korres, G., Lascaratos, A., Roussenov, V., and Stanev, E. (1997). Numerical simulation of the interannual variability of the mediterranean sea upper ocean circulation. *Geophysical Research Letters*, 24(4):425–428.

Pinardi, N., Zavatarelli, M., Adani, M., Coppini, G., Fratianni, C., Oddo, P., Simoncelli, S., Tonani, M., Lyubartsev, V., Dobricic, S., et al. (2015). Mediterranean sea large-scale low-frequency ocean variability and water mass formation rates from 1987 to 2007: A retrospective analysis. *Progress in Oceanography*, 132:318–332.

Pujol, M.-I. and Larnicol, G. (2005). Mediterranean sea eddy kinetic energy variability from 11 years of altimetric data. *Journal of Marine Systems*, 58(3–4):121 – 142.

Reale, M., Crise, A., Farneti, R., and Mosetti, R. (2016). A process study of the adriatic-ionian system baroclinic dynamics. *Journal of Geophysical Research: Oceans*, 121(8):5872–5887.

Redfield, A. C. (1934). *On the proportions of organic derivatives in sea water and their relation to the composition of plankton*. University Press of Liverpool James Johnstone memorial volume.

Ribera d'Alcalà, M., Civitarese, G., Conversano, F., and Lavezza, R. (2003). Nutrient ratios and fluxes hint at overlooked processes in the mediterranean sea. *Journal of Geophysical Research: Oceans*, 108(C9).

Rixen, M., Beckers, J.-M., Levitus, S., Antonov, J., Boyer, T., Maillard, C., Fichaut, M., Balopoulos, E., Iona, S., Dooley, H., et al. (2005). The western mediterranean deep water: a proxy for climate change. *Geophysical Research Letters*, 32(12).

Robinson, A. R., Leslie, W. G., Theocharis, A., and Lascaratos, A. (2001). Mediterranean sea circulation. *Ocean currents: a derivative of the Encyclopedia of Ocean Sciences*, pages 1689–1705.

Roether, W., Klein, B., Manca, B. B., Theocharis, A., and Kioroglou, S. (2007). Transient eastern mediterranean deep waters in response to the massive

dense-water output of the aegean sea in the 1990s. *Progress in Oceanography*, 74(4):540–571.

Roether, W., Manca, B. B., Klein, B., Bregant, D., et al. (1996). Recent changes in eastern mediterranean deep waters. *Science*, 271(5247):333.

Schroeder, K., Chiggiato, J., Bryden, H., Borghini, M., and Ismail, S. B. (2016). Abrupt climate shift in the western mediterranean sea. *Scientific reports*, 6.

Schroeder, K., Josey, S., Herrmann, M., Grignon, L., Gasparini, G., and Bryden, H. (2010). Abrupt warming and salting of the western mediterranean deep water after 2005: atmospheric forcings and lateral advection. *Journal of Geophysical Research: Oceans*, 115(C8).

Segura-Noguera, M., Cruzado, A., and Blasco, D. (2016). The biogeochemistry of nutrients, dissolved oxygen and chlorophyll a in the catalan sea (nw mediterranean sea). *Scientia Marina*, 80:39–56.

Siokou-Frangou, I., Christaki, U., Mazzocchi, M., Montresor, M., Ribera d'Alcalà, M., Vaqué, D., and Zingone, A. (2010). Plankton in the open mediterranean sea: a review. *Biogeosciences*, 7(5):1543–1586.

Smith, R. O., Bryden, H., and Stansfield, K. (2008). Observations of new western mediterranean deep water formation using argo floats 2004–2006. *Ocean Science*, 4(2):133–149.

Sournia, A. (1973). *La production primaire planctonique en Méditerranée; essai de mise à jour*. Cooperative Investigations in the Mediterranean, International Coordinator and Operational Unit; Étude en commun de la Méditerranée, Coordonnateur international et Unité opérationnelle.

Stommel, H., Bryden, H., and Mangelsdorf, P. (1973). Does some of the mediterranean outflow come from great depth? *pure and applied geophysics*, 105(1):879–889.

Stommel, H. and Farmer, H. (1953). Control of salinity in an estuary by a transition. *J. Mar. Res.*, 12:13–20.

Tansley, A. G. (1935). The use and abuse of vegetational concepts and terms. *Ecology*, 16(3):284–307.

Theocharis, A., Krokos, G., Velaoras, D., and Korres, G. (2014). An internal mechanism driving the alternation of the eastern mediterranean dense/deep water sources. In *The Mediterranean Sea: Temporal Variability and Spatial Patterns*. John Wiley & Sons, Inc., Oxford.

Thienemann, A. (1926). Der nahrungskreislauf im wasser. *Verb. deutsch. Zool. Ges.*, 31:29–79.

Thingstad, T. F. and Rassoulzadegan, F. (1999). Conceptual models for the biogeochemical role of the photic zone microbial food web, with particular reference to the mediterranean sea. *Progress in Oceanography*, 44(1):271–286.

Tramblay, Y., Amoussou, E., Dorigo, W., and Mahé, G. (2014). Flood risk under future climate in data sparse regions: Linking extreme value models and flood generating processes. *Journal of Hydrology*, 519:549–558.

Tsimplis, M., Velegrakis, A., Drakopoulos, P., Theocharis, A., and Collins, M. (1999). Cretan deep water outflow into the eastern mediterranean. *Progress in oceanography*, 44(4):531–551.

Van Cappellen, P., Powley, H., Emeis, K.-C., and Krom, M. (2014). A biogeochemical model for phosphorus and nitrogen cycling in the eastern mediterranean sea: Part 1. model development, initialization and sensitivity. *Journal of Marine Systems*, 139:460–471.

Vichi, M., Lovato, T., Lazzari, P., Cossarini, G., Mlot, E. G., Mattia, G., McKiver, W., Masina, S., Pinardi, N., Solidoro, C., et al. (2015). The biogeochemical flux model (bfm): Equation description and user manual, bfm version 5.1. *BFM Rep. Ser*, 1:104.

Volpe, G., Pitarch, J., Colella, S., Brando, V. E., and Forneris, V. (2017). Quality information document: Ocean colour mediterranean and black sea observation product.

Walsh, K. J., McInnes, K. L., and McBride, J. L. (2012). Climate change impacts on tropical cyclones and extreme sea levels in the south pacificâĂŤa regional assessment. *Global and Planetary Change*, 80:149–164.

Zhang, H. and Sheng, J. (2015). Examination of extreme sea levels due to storm surges and tides over the northwest pacific ocean. *Continental Shelf Research*, 93:81–97.

ERRATA CORRIGE

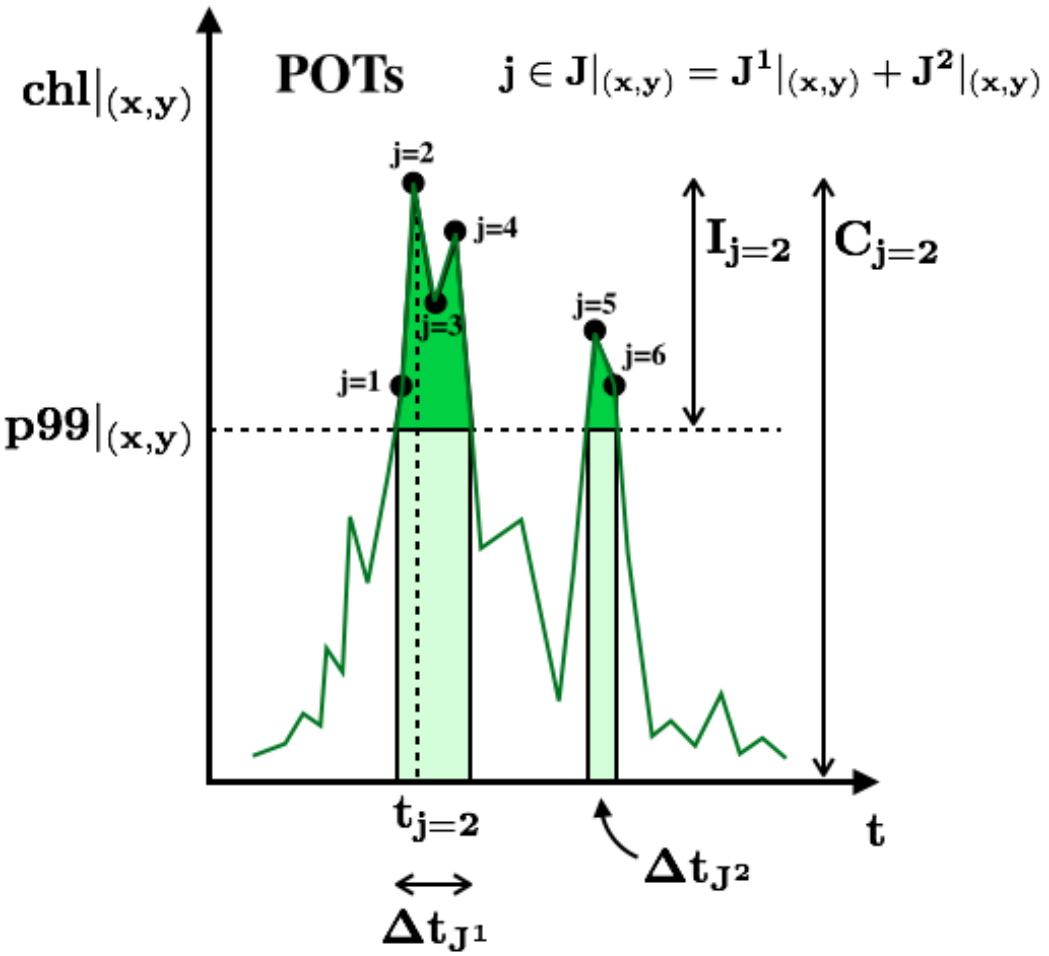

Figure 3.2. Schematics of the local metrics of the chlorophyll extremes. The horizontal dashed line indicates the 99th percentile threshold computed at the grid point. The daily chlorophyll values above the threshold are represented by the POTs (black circles), in the number of 6, as an example, grouped in two local extremes, with POTs indexes $J^1|_{(x,y)} = \{1, 2, 3, 4\}$ and $J^2|_{(x,y)} = \{5, 6\}$, respectively. The value of chlorophyll concentration C_j and the intensity I_j related to one POT, as well as the duration of the two local extremes, defined in the text, are also shown.